Entrance and Exit Effects on Flow through Metallic Foams

ALI M. MOSTAFID

A Thesis

in

The Department

of

Mechanical and Industrial Engineering

Presented in Partial Fulfillment of the Requirements
for the Degree of Master of Applied Science (Mechanical Engineering) at
Concordia University
Montreal, Quebec, Canada.

June, 2007

Your file Votre référence
ISBN: 978-0-494-34447-7
Our file Notre référence
ISBN: 978-0-494-34447-7

ABSTRACT

Entrance and Exit Effects on Flow through Metallic Foams

Ali M. Mostafid

Metallic foams have diverse industrial applications due to their unique properties such as high porosity and high surface to volume ratio. To improve and modify the design of such applications, understanding of the foam characteristics such as unit pressure drop is required. Because of the complex microstructure of metallic foams, it is difficult to predict their characteristics by mathematical modeling analysis. Therefore, experimental studies have been suggested to discover the effect of microstructure on the pressure drop of metallic foams.

Wide range of metallic foams having different thicknesses (2 to 63 mm), densities (83 to 91%), and pore sizes (0.4 to 2.3 mm) were tested in the present study. The unit pressure drop of same grade foam having different thicknesses was found to reduce with increasing the thickness. This effect results in different Darcian and non-Darcian permeability coefficients for the same foam which is unexpected, because these properties should be thickness independent and constant for each material. Consequently, experiments were conducted to validate that the pressure drop can be divided into two components of bulk and entrance pressure drops and found that, bulk contribution can be normalized by the thickness; however, entrance contribution cannot. After a certain thickness, which depends on the foam microstructure, the entrance contribution becomes constant. It was also observed that, entrance effect contributes more to the pressure drop for thin samples and at high velocities.

Tests were also performed to non-destructively examine the homogeneity of the metallic foams and found that, heterogeneity can be detected if it is either located at the foam sides or inside the foam but with pores finer than the bulk foam.

ACKNOWLEDGEMENT

This thesis is not just the result of my work, but an evidence of the kind and unlimited support of many who were with me along the way. I would like to take a moment to acknowledge their important contributions.

First of all my supervisor, Dr. Medraj, who gave me the opportunity to be a graduate student at Concordia University, and provided me with all the support needed to perform and complete this research under his supervision. I would like to express my deep appreciation to him.

I would also like to take this opportunity to extend my sincere thanks to Eric Baril and Louise-Philippe Lefebvre, the researchers at the Industrial Materials Institute of the National Research Council Canada, Boucherville, for their sincere assistance and valuable guidance. I am very pleased that I had the chance to perform this research with them.

I want to thank Mr. Verduyn, from Recemat International, for providing the required samples. It would have been difficult, if not unfeasible, to complete this experimental research without his support.

No word could express my gratitude to my parents who have been consistently supporting me with their well and endless wishes.

My wife, Elaheh, not only was very supportive and patient, but also helped me a great deal in organizing and finishing this work. I would like to express my love and thanks to her.

And finally, I am thankful to the productive criticism and support I received from my research group members. They helped me to improve my research and presentation abilities a great deal.

When modern man builds large load bearing structures, he uses dense solids; steel, concrete, glass. When nature does the same, she generally uses cellular materials; wood, bone, coral.

There must be good reasons for it!

Prof. M. F. Ashby, University of Cambridge

TABLE OF CONTENTS

LIST OF FIGURES

LIST OF TABLES

NOMENCLATURE

a	microscopic pore scale
A	cross section surface area
b	unit bulk pressure drop
d	foam average pore diameter
C	non-Darcian permeability coefficient
D_C	form force in Equation 2.6
D_μ	viscous force in Equation 2.6
E	modulus of elasticity
k	hydraulic conductivity in Equation 2.1
K	Darcian permeability coefficient
L	macroscopic length scale
P	pressure
P_i	pressure at foam inlet
P_o	pressure at foam outlet
ΔP	pressure drop
Q	fluid flow rate
Re	Reynolds number
S	absolute entrance effect
s	normalized entrance effect
t	foam thickness
V	fluid velocity

Greek Letters

α	empirical parameter in Equation 2.3
β	empirical parameter in Equation 2.3
ε	porosity
$\mathbf{e}$	strain

μ	fluid viscosity
ρ	fluid density
σ	stress

Recemat Foams

NC	nickel chromium
NCX	nickel chromium extra strong

CHAPTER 1: INTRODUCTION

Porous materials are known for their physical and mechanical properties, such as high stiffness in combination with very low specific weight or high gas permeability joined with high thermal conductivity. These characteristics are most probably the reasons why nature frequently uses cellular materials for constructional or functional purposes such as wood, coral, and bone.

Man has made use of natural cellular materials for centuries. The pyramids of Egypt have yielded wooden artifacts at least 5000 years old, and cork was used for bungs in wine bottles in Roman times (Horace, 27 BC) [1]. More recently man has made his own cellular solids. At the simplest level, there are honeycomb-like materials, made up of parallel, prismatic cells, which have been used for lightweight structural components. Another famous example is the polymeric foam used in disposable coffee cups.

Metallic foams are a relatively new group of materials with low densities and novel physical, mechanical, thermal, electrical and audio properties. They offer potentials for thermal management, lightweight structures, energy absorption, flame and spark arrestors, filters for separating solids from liquids and gases, and medical purposes.

In the first two chapters of this work, a brief description of metallic foams, their manufacturing methods and applications together with a review of the literature related to the flow through the porous materials is presented. In the next chapters, the experimental procedure and results along with their analysis which led to proposing a new model for predicting the pressure drop through metallic foams are presented. Subsequently, based on this analysis, some attempts to detect heterogeneity in metallic foams are presented.

1.1. Definition of Metallic Foam

Metallic foam has become a very popular phrase which is now used for almost any kind of metallic material which has voids; therefore it is difficult to find a comprehensive definition of metallic foams. These kinds of materials have been sometimes called as cellular metal, porous metal, metallic foam, or metal sponge [2]. Banhart [3] defined foams as uniform dispersions of gas in either liquid or solid; however, when speaking of metallic foams, it generally means solid foams. The liquid metallic foam is merely a stage that occurs during the fabrication of the material. Figures 1.1 to 1.5 show some materials which contain voids, but the structure shown in Figure 1.1 is very much similar to what we call *open cell metallic foam* which can have very high porosity.

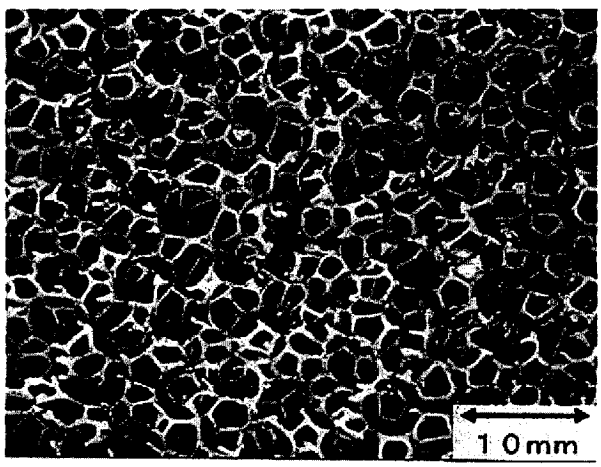

Figure 1.1: *Structure of super cellular magnesium alloy [4].*

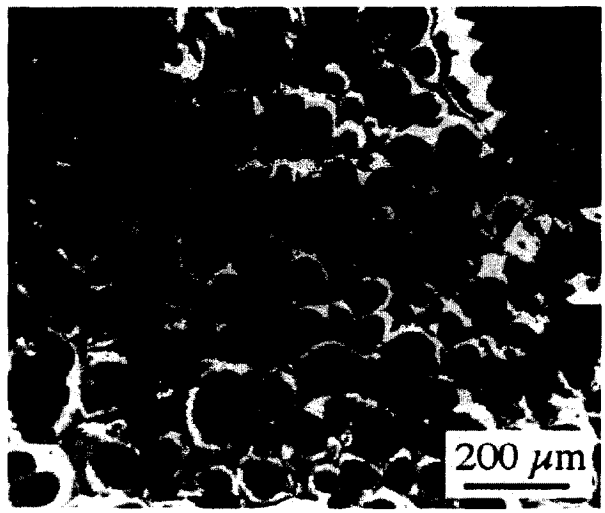

Figure 1.2: *Optical micrograph of a fracture surface from a typical foam. The fracture surface is normal to the direction of pore alignment [5].*

Figure 1.3: *Sintered spherical bronze (100X, 45-100 micrometer powder particles) [6].*

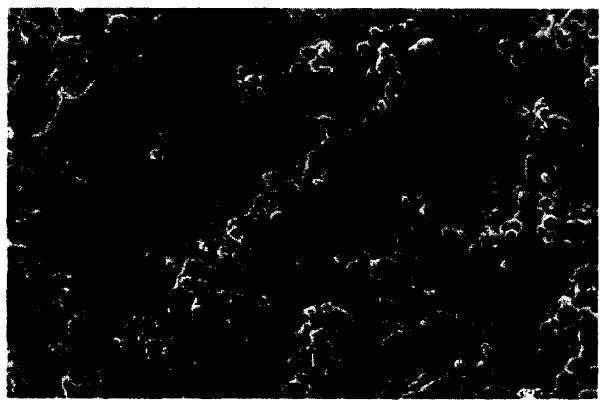

Figure 1.4: *Sintered nickel powder (2000X, 2-4 micrometer powder particles) [6].*

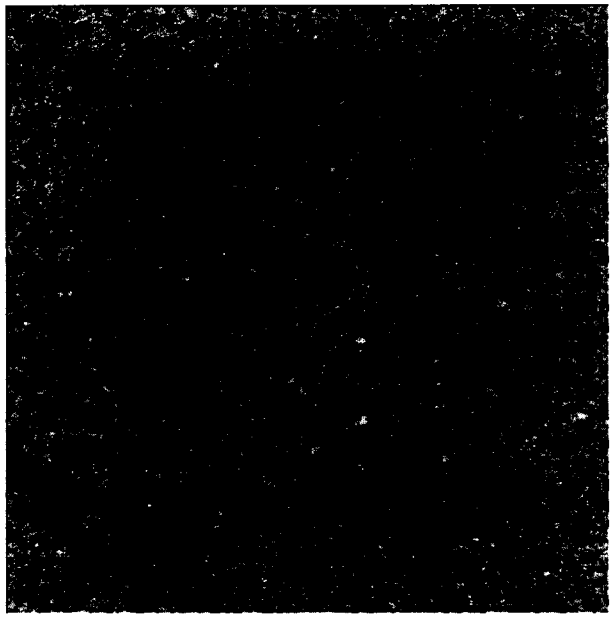

Figure 1.5: *Pore structure of aluminum foamed by adding TiH_2. Section shown is 80x80 mm^2 in size [2].*

Although metal foaming technology is relatively advanced now, the properties of metallic foams and the physics of metallic foam production and development are just starting to be characterized. At present, metallic foams are not completely characterized and the processes to make them are poorly controlled. These reasons cause variability in properties. Two parallel but interconnected works are being done to solve these problems. First, improving the manufacturing methods of making metallic foams, and second, testing the produced foams to find their characteristics and apply this information for the improvement of the manufacturing methods [2,7-10].

1.2. Production Methods of Metallic Foams

Some of the techniques that exist for foaming metals, ceramics and glasses as well as polymers, are specially designed to take advantage of characteristic properties of metals such as their sintering activity or the fact that they can be electrically deposited. Some

methods produce open-cell foams, other produce foams in which the majority of the cells are closed [11]. Different methods can be classified according to the state during which the metal is processed which defines four families of processes as, *liquid metal, solid metal in powdered form, metal ion solution, metal vapor or gaseous metallic compounds* [12]. Metallic foams are produced either by introducing voids into an initially pore-free liquid (molten) metal or by collecting subdivided material in a way that the assembly becomes highly porous [5].

1.2.1. Liquid Metal Production Methods

In order to effectively foam a melt to produce a useful material, gas must be introduced in a way that a solid with a relatively high void content is achieved. One group of processes creates the cellular structure from the liquid metal. The molten metal is processed into a porous material by directly foaming it, using an indirect method by means of a polymer foam, or by casting the liquid metal around solid space holding filler materials which reserve space for what becomes the pore space after processing.

1.2.1.1. Foaming by Gas Injection into Liquid Metal

Foaming by gas injection into liquid metal is probably one of the oldest methods for foaming aluminum and aluminum alloys [12]. The first step in this process is to prepare a homogeneous melt containing some viscosity-increasing particles. Then, specially designed rotating impellers or vibrating nozzles, as shown in Figure 1.6, is used to inject gases such as air, nitrogen or argon into the molten metal. The resultant viscous mixture of bubbles and metal melt floats up to the liquid surface, where it turns into a fairly dry liquid foam as the liquid metal drains out. It can then be pulled off the liquid surface with

a conveyor belt, and allowed to cool down and solidify. Before solidification, the semisolid foam can be flattened by means of one or more top-mounted rolls or belts to yield a foam slab with closed and fairly even upper and lower skins [13].

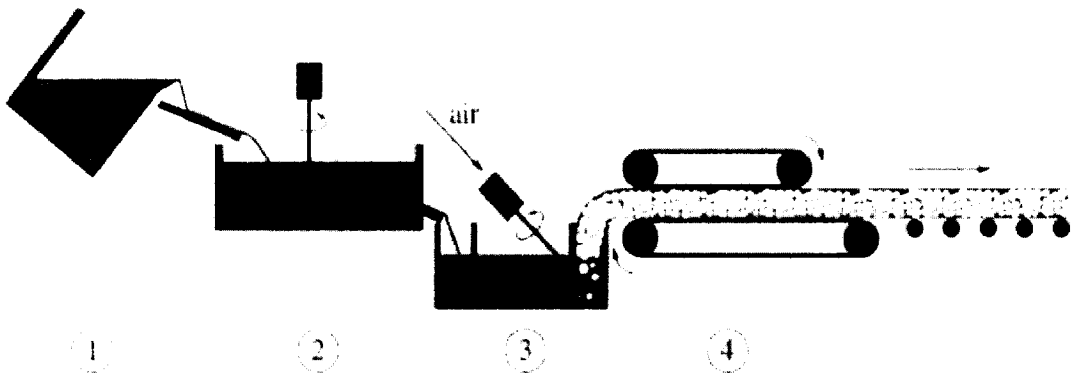

Figure 1.6: *Schematic depiction of the continuous foam process developed by Alcan for production of flat panels. The components of the system illustrated are: 1.melting furnace, 2.holding furnace, 3.foaming box, 4.twin-belt caster [5].*

The resulting solid foam in principal can be 10 cm thick [12]. Figure 1.7 shows two different samples manufactured by gas injection into melt method. The porosities of aluminum foams produced this way range from 80 to 98%, which corresponds to

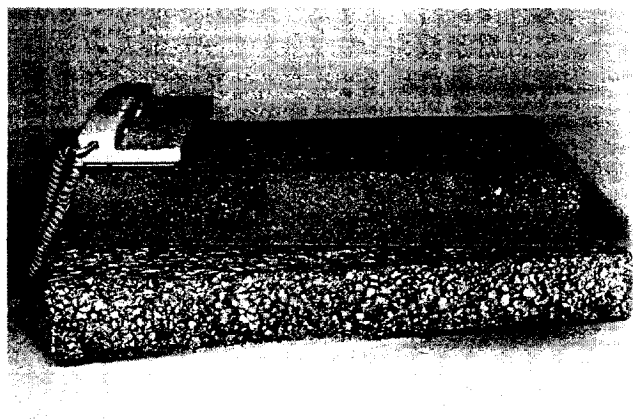

Figure 1.7: *Foam slabs of two different densities and cell sizes produced by the gas injection method (sample: Hydro Aluminum, Norway) [12].*

densities between 0.069 and 0.54 g/cm^3, average pore sizes from 3 to 25 mm, and wall thicknesses from 50 to 85 μm [14,15].

Advantages of the direct foaming process can be the large volume of foam which can be continuously produced and the low densities which can be achieved. A possible disadvantage of the direct foaming process is the necessity to cut the foam, which results in opening the cells. Thus, efforts for making shaped parts by casting the semi-liquid foam into moulds [16], or by shaping the emerging foam with rolls [17] have been carried out.

1.2.1.2. Foaming of Melt with Blowing Agents

Another method for foaming melts is to introduce a blowing agent into the melt instead of blowing gas into it. The blowing agent decomposes under the influence of heat and releases gas which then propels the foaming process. Figure 1.8 shows schematics for producing foam through this method. In this technique, calcium metal is added to metal

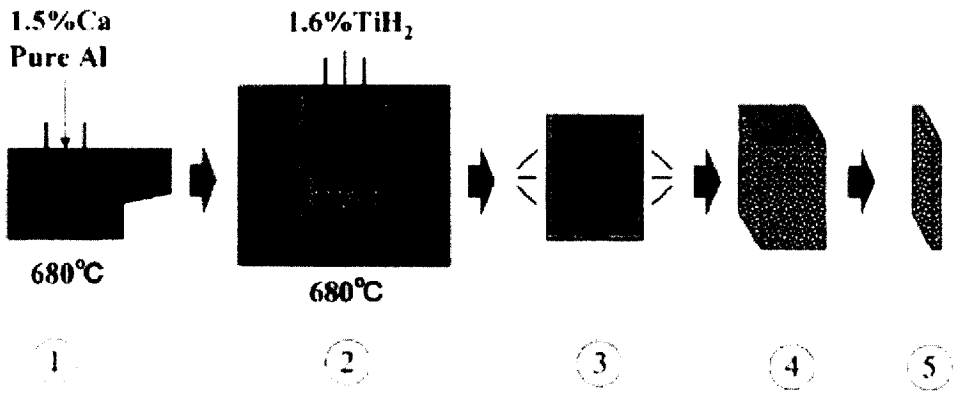

Figure 1.8: *Schematic depiction of the direct foaming of melts with blowing agents foam production. The stages of the process are: 1. melt thickening, 2. melt foaming, 3. cooling (solidification), 4. foamed block, 5. foam slicing [12].*

melt such as aluminum. Due to the formation of calcium oxide (CaO), calcium–aluminum oxide ($CaAl_2O_4$) or perhaps even Al-Ca intermetallics which thicken the liquid metal [18] during the several minutes of stirring, the melt viscosity continuously increases by a factor of up to five [19]. After the viscosity has reached the desired value, titanium hydride (TiH_2) is added which serves as a blowing agent by releasing hydrogen gas in the hot viscous liquid. The melt shortly and slowly begins to expand and gradually fills the foaming vessel. The foaming occurs at constant pressure. Then the vessel cools down below the melting point of the alloy, and subsequently the liquid foam becomes solid aluminum foam and can be removed for further processing [12]. The whole foaming procedure can take 15 min for a typical large batch [19]. The pore morphology of such foams is shown in Figure1.9.

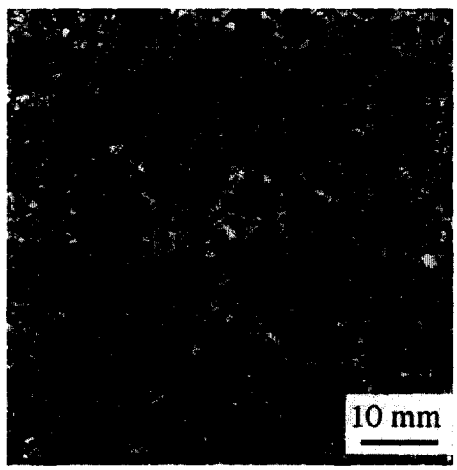

Figure 1.9: *Optical micrograph of a section through typical Alporas aluminum foam [5].*

In the literature, zirconium hydride (ZrH_2) has also been recommended as a blowing agent for the production of aluminum foams. It has been claimed that even ferrous alloys can be foamed in a way similar to aluminum and other low melting alloys by injecting a mixture of a blowing agent and a foam stabilizer, such as tungsten powder,

into a ferrous melt [20]. This method was patented by the Shinko Wire Company Ltd., Amagasaki, Japan [5]. This foam is now in relatively wide industrial use under the trade name *Alporas*.

1.2.1.3. Investment Casting with Polymer Foams

Foams can be manufactured from molten metal without directly foaming the metal. This is shown in Figure 1.10. According to this process, a polymer foam, such as polyurethane foam, is used as a starting point. If the polymer foam has closed pores, it has to be transformed into an open porous one by a reticulation treatment. The resulting polymer foam with open cells is then filled with a slurry of sufficiently heat resistant material, e.g. a mixture of mullite, phenolic resin and calcium carbonate or simple plaster [21]. After curing, the polymer foam is removed by thermal treatment and molten metal is cast into the resulting open voids, which replicate the original polymer foam structure. Application of pressure and heating of the mould may be necessary if no filling of the narrow cavities with the liquid metal can be achieved in simple gravity casting. After removal of the

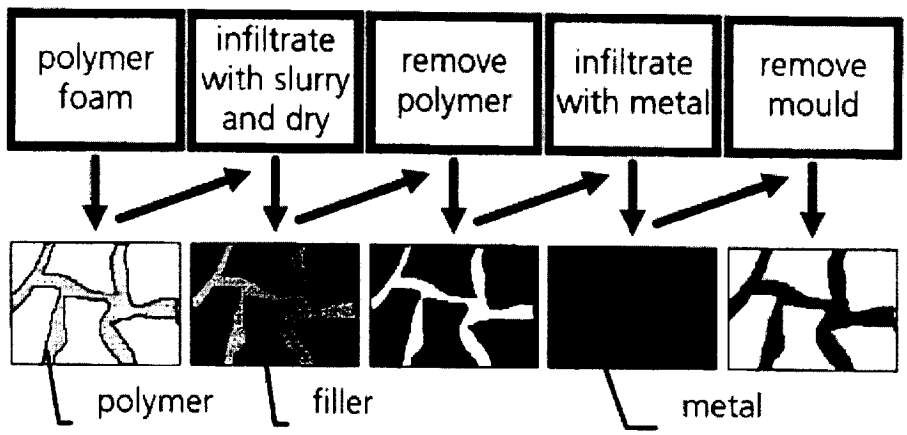

Figure 1.10: *Production of cellular metals by investment casting [2].*

mould material, e.g. by pressurized water, a metallic structure is obtained which is an exact replicate of the original polymer foam.

Difficulties in this process include achieving a complete filling of the pore walls, controlling the directional solidification, and removing the mould material without damaging the fine structure too much [12]. By preforming the polymer foam complex shaped parts can also be fabricated. The densities and foam morphologies of the final metal product are determined by the polymer and typically range from 80 to 97% [12].

1.2.2. Solid Metal Particles Production Methods

Instead of a molten metal, solid metal in powder form can be used for making cellular metallic structures. The powder remains solid during the entire process and merely goes through a sintering treatment or other solid state operations.

1.2.2.1. Gas-Releasing Particle Decomposition in Semi-Solids

In this process, foaming agents are introduced into metals in the solid state by mixing the combined powders. A schematic diagram of the manufacturing sequence is shown in the Figure 1.11. It begins by combining particles of a foaming agent (TiH_2) with metal, e.g. aluminum powder. Then the ingredients get completely mixed, cold compacted and extruded into a bar or plate of near theoretical density. This material is chopped into small pieces, placed inside a sealed split mold, and heated to a slightly above the solidus temperature of the alloy. By inserting the material into a hollow mold and expanding it by heating, near net shaped parts can be obtained [11,12].

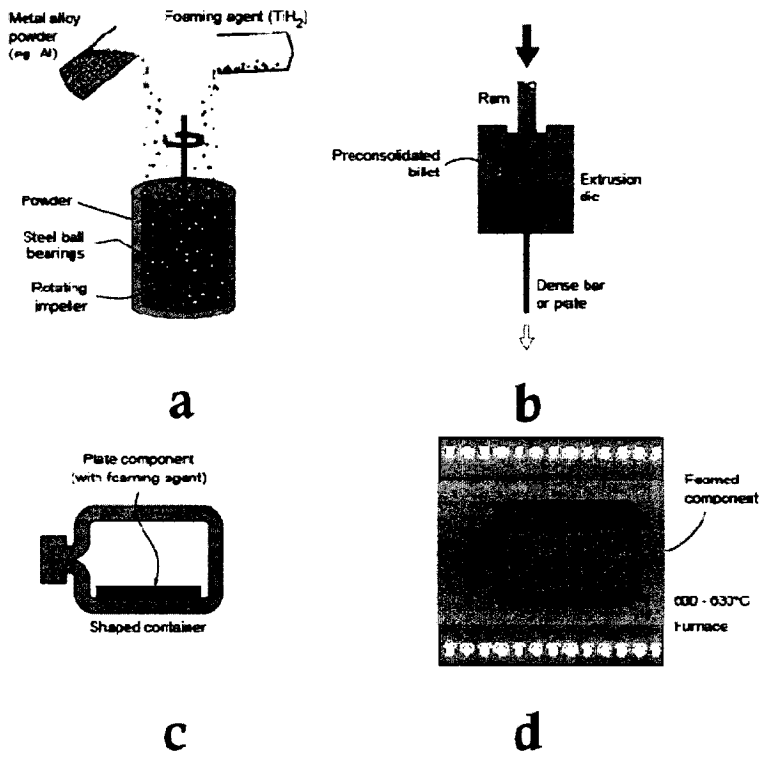

Figure 1.11: *Powder metallurgy steps used to manufacturing metallic foams by gas releasing particles in semi-solids. a. select and mix ingredients b. warm extrusion c. shaped mold d. foaming [22].*

1.2.2.2. Sintering of Metal Powders and Fibers

Porous metallic products are being mass produced for a multitude of applications. A large variety of metals is used, including titanium or superalloys, although bronze and stainless steel account for most market applications [12]. In general, the production of porous structures consists of various steps: powder fractioning and preparation, compaction or moulding, and sintering [23].

1.2.2.3. Production of Cellular Metals Based on Space Holding Fillers

In this method, fine metal powder is filled into the bulk of space holding material. The space holding can be a dry bulk of fillers [24] or a suitable solvent [25]. An organic

binder [12] may also be used to mix the space holders and the metal powders. Ceramic particles, polymer grains, salts or even metals can be used as space holders. The filled bulk is then either simply compacted at room temperature, or if the space holders are heat resistant, pressed at elevated temperatures to improve compaction and to start sintering processes between the metal powder particles. In both cases, a composite is obtained which consists of a metal matrix with surrounded filler granules. It is possible to remove the space holder material almost completely, if the metal content is sufficiently low. This can be done by thermal treatment, leaching, or by an aqueous solvent. A final sintering step can be applied to increase the density of the porous metallic network. Figure 1.12 shows a schematic of this method.

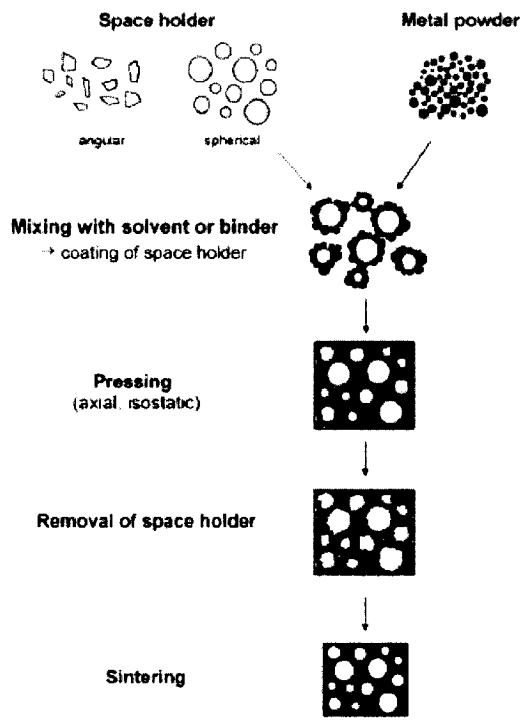

Figure 1.12: *Space holder technique for making porous metallic structures from metal powders [25].*

1.2.2.4. Metal Powder-Binder Method

Metal powders and polymer binders can be mixed, pressed, and then heat treated to produce porous materials. Even though no space holding fillers are used, it is possible to achieve porosities of up to 50% [12]. Also, materials with oriented pores can be made with bars having diameters ranging from several microns to several millimeters in a similar way for a variety of metals and alloys.

1.2.2.6. Metallic Foam Production Method at NRC-IMI

At the Industrial Materials Institute of the National Research Council of Canada (NRC-IMI) a technique has been recently developed to produce foamed metallic structures from dry powder blends containing a metallic powder, a polymeric binder, and a foaming agent. This procedure consists of forming polymer foams highly charged with metallic particles, eliminating the polymer by thermal decomposition, and consolidating the particles by sintering. The metallic powder, solid polymer binder, and chemical foaming agent are dry-mixed, and heat-treated in a three-step process including foaming, debinding, and sintering. The schematic of this method is shown in Figure 1.13. During sintering, solid-state diffusion results in metallurgical contacts between the metallic particles, which improve the mechanical properties. Higher sintering temperature improves mechanical properties at the expense of surface area [26].

1.2.3. Electro-Deposition Technique

This process has superior control on the cell size because preformed structure determines the foam microstructure. The material is very open and has a tight pore size distribution. This process is similar to the investment casting, which was described earlier, because the

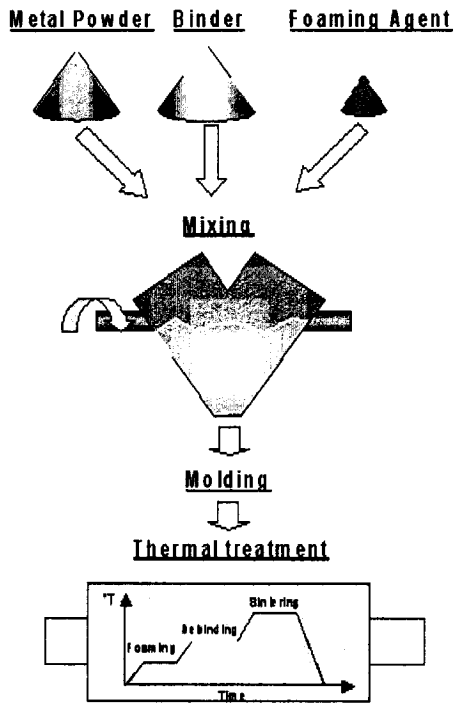

Figure 1.13: *Producing IMI metallic foams using powder metallurgy approach [27].*

actual foaming does not occur on the molten or solid metal and an open cell polymeric foam is used, which is replaced by metal during the process. In this method, the deposition starts from the ionic state of metals, such as solution of ions in an electrolyte. In order for the polymeric preform to become electrically conductive, it can be dipped into an electrically conductive slurry based on graphite or carbon black, immersed into an electroless plating solution, or coated with a thin conductive layer by cathode sputtering [28,29]. The polymeric foam is removed after the metal gets electrically deposited onto the foam by thermal treatment. Usually the manufactured foams in this method have hollow struts [12]. Figure 1.14 shows schematic of this process.

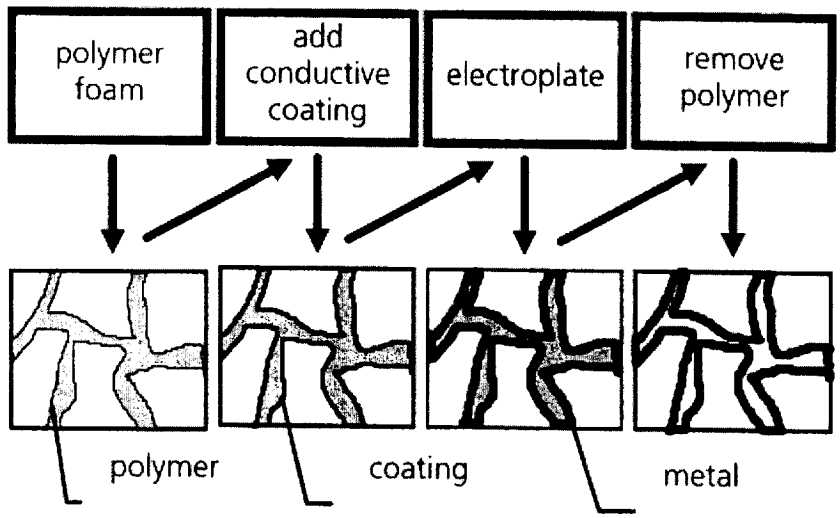

Figure1.14: *Electro-deposition technique for making metallic foam [12].*

Foams of various grades can be fabricated ranging from 2.5 to 30 cells/cm (about 6–70 ppi) with the cell size between 3.2 and 0.5 mm, and the surface areas ranging from 500 to 7500 m^2/m^3 [30]. The preferred metals are nickel or nickel–chromium alloys but copper foams can also be made. Nickel–chromium foams are manufactured by making alternate coatings of nickel and chromium, then a heat treatment creates an alloy by thermally induced diffusion of the two metals [12]. Some companies that manufacture metallic foams by this method are Retimet (GB), Celmet (Japan) [30], Recemat (The Netherlands) [31] and probably a Belorussian company called ECOSOT [32]. Sheets with thicknesses between 1.6 and 20 mm [31] are available for nickel or nickel–chromium foams. The density of such foams has been found to be virtually independent of the average pore size [31].

1.3. Applications of Metallic Foams

Cellular metallic materials have very vast range of applications. Selection of the suitable porous metal or metallic foam for a given problem depends on factors such as morphology, metallurgy, processing, and economy [12].

Morphology is one of the main important factors in selecting the right material for different applications. Some applications require that a medium passes through the cells, which results in open cell structures, while some other applications may need completely closed cells. There might be a need for various degrees of *openness*, ranging from very open, for high rate fluid flow, to completely closed, for load-bearing structural applications [12]. Another consideration is whether the application is functional or structural. Figure 1.15 shows what type of porosity is used for each type of application.

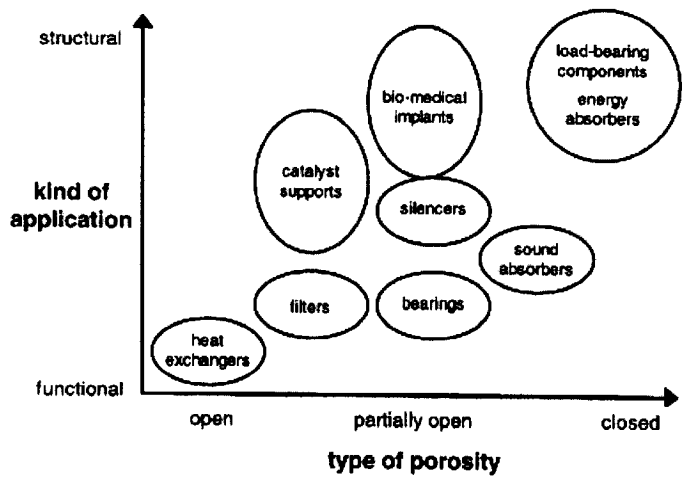

Figure 1.15: *Applications of cellular metals grouped according to the degree of "openness" needed and whether the application is more functional or structural [12].*

Generally, open cell metallic foams are used in functional applications while structural applications are made of closed cell foams. Selecting the right material is

another issue. For example, aluminum, magnesium or titanium foams, or porous metals are preferred for light weight structural applications; titanium, tantalum and their alloys are useful in medical devices because of their excellent bio-compatibility; and stainless steel or titanium is required for applications where aggressive media or high temperatures are involved.

1.3.1. Structural Applications

Metallic foams are used in different structural applications. Some of these applications are briefly listed here.

- Automotive industry
- Light-weight construction
- Energy absorption
- Acoustic and thermal control
- Aerospace industry
- Foams as cores for castings
- Railway and building industries
- Machine construction
- Sporting equipment
- Decoration and arts

Figures 1.16 to 1.19 show some of these applications.

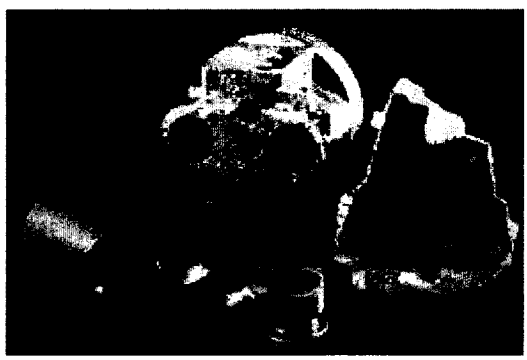

Figure 1.16: *Applications of metallic foams in manufacturing automobile parts such as gear box case or pipe connectors [33].*

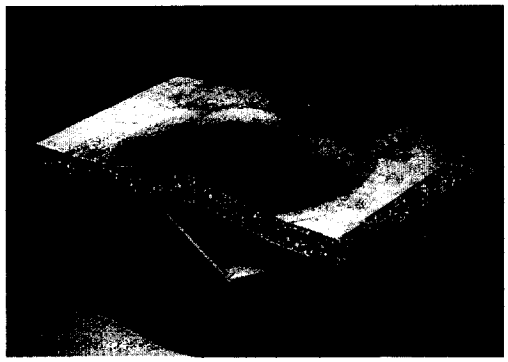

Figure 1.17: *Sandwich panel having an aluminum foam core (thickness 12 mm) and two steel face sheets (courtesy of Fraunhofer and Studiengesellschaft Stahlanwendungen).*

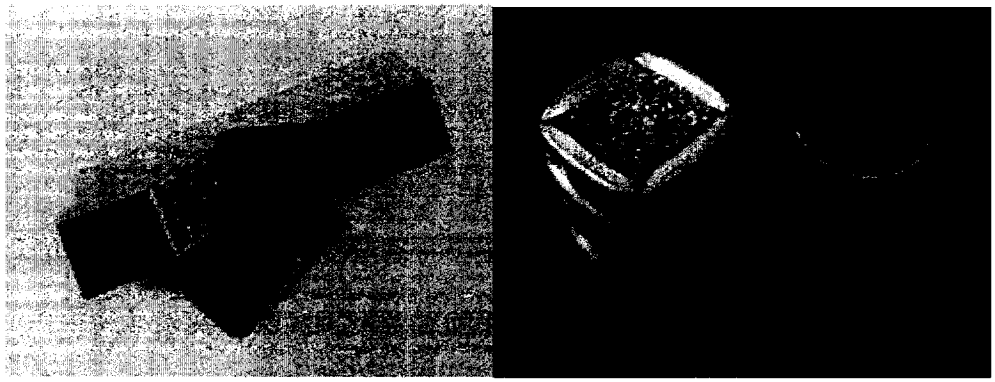

Figure 1.18: *Metallic foam as a core of a beam (left) [34], and prototypes of crash absorbers based on aluminum extrusions with a filling of Cymat aluminum foam (courtesy of Cymat).*

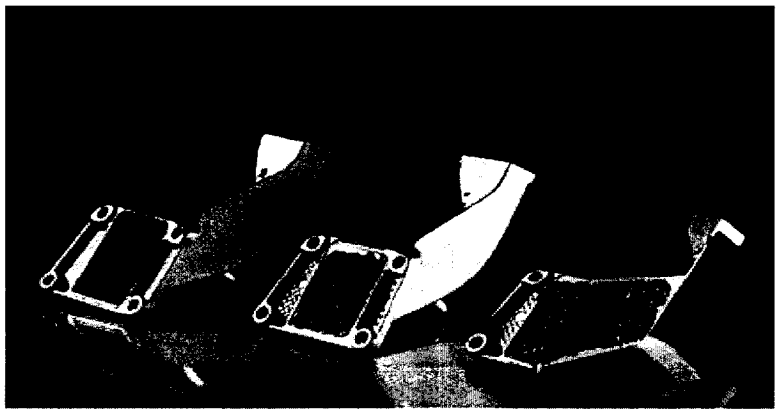

Figure 1.19: *Prototype of a BMW engine mounting bracket manufactured by LKR Ranshofen (Austria). From left to right: empty casting, entire composite part consisting of foam core and cast shell, section through composite part (courtesy of LKR).*

1.3.2. Functional Applications

Metallic foams, usually open cell foams, have different functional applications, ranging from heat exchangers and filters to biomedical applications. Due to the high-speed growth in the electronics industry and high needs for cooling the electronic components, this field is one of the interesting areas for researchers [35,36]. Some metallic foam due to their unique structure, corrosion resistance, biocompatibility, and mechanical properties are attractive for tissue attachment, because defects in bone are usually filled with artificial tissue grafts that, in the ideal case, should have properties similar to those of the natural bone [37]. Titanium or cobalt–chromium alloys are used for prostheses or dental implants, because of their bio-compatibility [12].

NRC-IMI's unique open-cell structure titanium foam has become attractive for the fabrication of biomedical implants [38]. As opposed to the solid titanium currently used in orthopedic and dental applications, the mechanical properties of the titanium foams are very close to those of bones,. Table 1.1 summarizes these properties.

Table 1.1: *Comparative compressive mechanical properties of solid and foamed titanium and trabecular bone [38].*

Materials	**E** (Gpa)	**σ** (MPa)	**e** (%)
Ti foams	0.6 – 2.2	10-50	2-5
Solid Ti	110	175	-
Trabecular bones	0.4 – 2	5 - 15	2 - 5

Some other functional applications for metallic foams are listed bellow, and Figures 1.20 to1.22 show some of these applications.

- Flame and sparkle arresters
- Filtration and separation
- Supports for catalysts
- Fluid flow control
- Heat exchangers and cooling machines
- Storage and transfer of liquids
- Acoustic control and sound absorber
- Silencers
- Battery electrodes
- Electrochemical applications
- Water purification

Figure 1.20: *Two heat exchangers made of open-cell aluminum foam (courtesy of ERG Aerospace).*

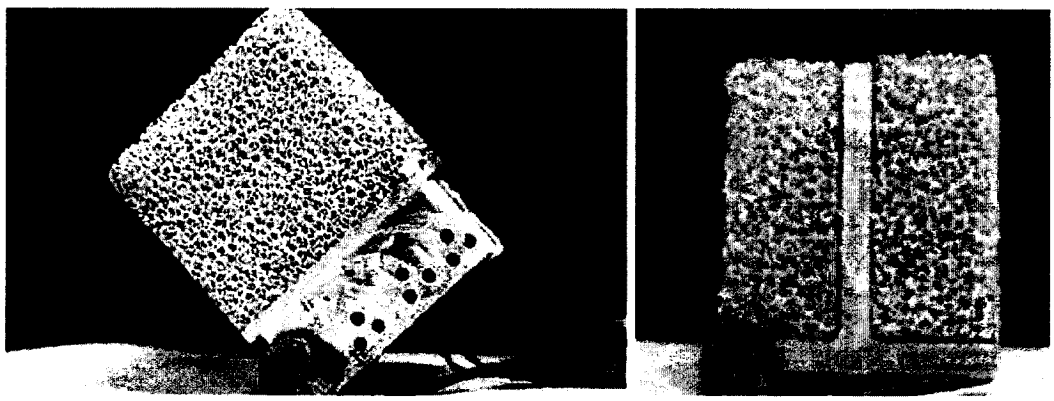

Figure 1.21: *Metallic foam application for cooling electronic devices [35,36].*

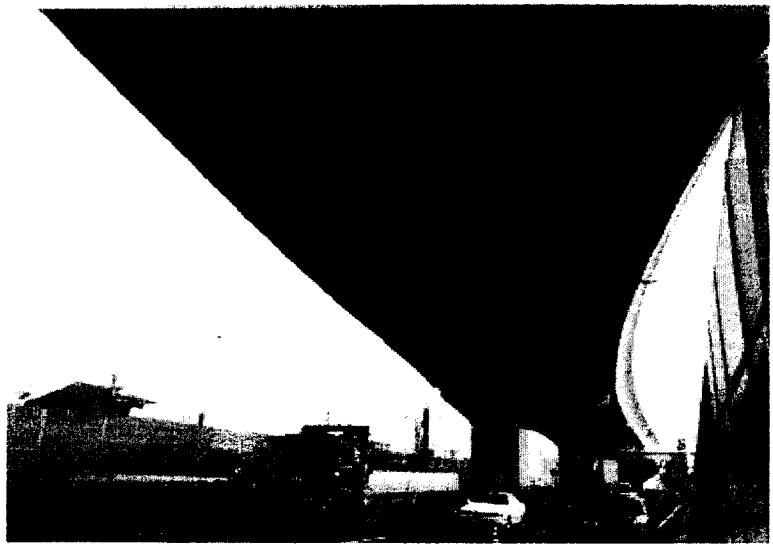

Figure 1.22: *Sound absorbing structure on the under-side of an elevated viaduct [39].*

CHAPTER 2: LITERATURE REVIEW

Diverse properties of metallic foams have made them interesting for different applications, as mentioned in the previous chapter. For better understanding of the properties and usages of these materials, researchers have studied them, probably, since their innovation. But more work is needed in order to completely understand their structure-property relationships. A summary of the concepts, related researches and experimental works on determining the physical properties, especially the permeability, of metallic foams is discussed in this chapter.

There are two approaches to look at a cellular material: from *microscopic* and from *macroscopic* viewpoints. From the microscopic viewpoint, a cellular material is a construction consisting of multitudes of struts, membranes or other elements which themselves have the mechanical properties of some bulk metal. But according to the macroscopic viewpoint, whole elements which form the foam are considered as one bulk material and tests result in the bulk material properties. According to this viewpoint, it is possible to treat the cellular structure as a homogeneous medium which is represented by effective or averaged material parameters. Therefore it is important to make sure that the material is homogeneous. Moreover, some critical applications, such as tissue attachments, need that each specimen gets individually tested before placing inside the patient body. This means that the homogeneity tests should be non-destructive.

2.1. Non-Destructive Testing

In general, methods for testing materials can be divided into destructive and non-destructive. If the material is permanently deformed or changed, the process is destructive, and if the material remains unchanged, or only minimally affected during characterization, it is called non-destructive. The Non-Destructive Testing (NDT) plays a critical role in assuring that structural components and systems perform their functions in a reliable and cost effective fashion. Some important and related methods are briefly discussed in the following sections.

2.1.1. Applicable Test Methods

There are several methods to non-destructively test the specimens but not all of them are applicable to metallic foams. Also just a few of these methods are applicable for studying the internal structure of materials. Since detecting the heterogeneity in the metallic foam structure will be attempted in this work, some of the methods which have already been used in the industry and research are described here.

2.1.1.1. Visual Testing

In visual testing, the inspector uses his eyes to look for defects, surface structure, or other physical properties. Special tools such as magnifying glasses, mirrors, microscopes, or borescopes might be used to have access and more closely inspect the subject area. For instance, Loya [40] used scanning electron microscope to inspect the microstructure of metallic foams. On the other hand, Zhou *et al.* [41] stated that investigating the

macrostructure and microstructure of aluminum foam using microscopy caused the cells to appear elongated.

2.1.1.2. X-ray Radiography and Radioscopy

In this method, an X-ray beam is directed through a sample and its attenuation is measured. The averages over a certain area, and scans over two dimensions result in obtaining a 2D attenuation map for the foam. If thin slices of foam are investigated, for instance pieces with a thickness in the order of the average pore diameter, the individual pores and map of the pore morphology can be visualized. However, if the slices are much thicker, single pores are not further distinguishable. This method is more favorable for the thin slices of foam or for foams with low densities. Banhart *et al.* [42] used synchrotron radioscopy to evaluate metallic foams of thickness of 10 mm. Burzer *et al.* [43] also monitored the densification of aluminum foams by measuring the X-ray attenuation perpendicular to the surface.

2.1.1.3. Computer Tomography and Microfocus Computer Tomography

Computer tomography is a technique to visualize the internal features of an object and has recently become an important tool to examine the porous media [44]. In this method, a small slice of the object is irradiated with X-rays at a series of angles. Figure 2.1 shows the principle of the X-ray computed tomography. The X-rays which are transmitted in the direction of the incident beam by each column of the object element get recorded by a detector. The absorption at each point in the slice can be calculated from measurements at many angles using Fourier transformation algorithms [45]. Three-dimensional pictures can be obtained in X-ray computer tomography [46].

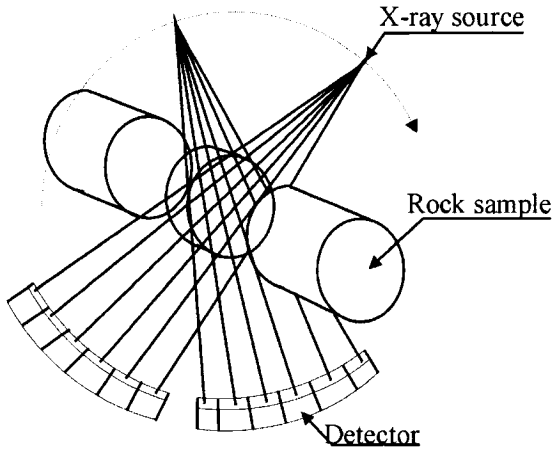

Figure 2.1: *Principle of computer tomography scanning [44].*

Microfocus computer tomography (MCT) is similar to the computer tomography, but for studying the materials, the X-ray source is smaller than the computer tomography, which increases the sharpness of the projection, and also rotates around the object, which reduces the vibration and enhances the resolution. This makes it possible to put the object near the X-ray-source and to increase the primary enlargement of the object, which again enhances the resolution [44]. Figure 2.2 shows sample pictures taken using X-ray microfocus computer tomography.

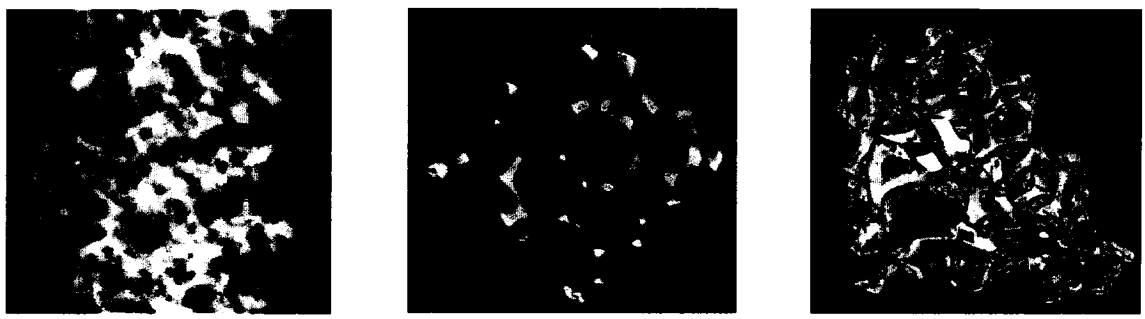

Figure 2.2: *Microfocus computer tomography investigation of open Al-foam; left: X-ray-shadow image, middle: Reconstructed cross-sectional image, right: 3D model, created from the set of reconstructed cross-sections [46].*

Researchers such as Cornelis *et al.* [47] investigated the wide potentials of micro computed tomography to generate two and three dimensional images of foam structure. Sassov *et al.* [48] also showed that micro-computed tomography gives wide opportunity for non-destructive tests to determine the microstructure and internal morphology of foams.

X-ray computed tomography and MCT provide novel opportunities to study the 3D pore structure of porous materials in order to construct the flow models and compare their results with those obtained by experimental investigations. Wildenschild *et al.* [49] used the combination of experimental techniques and mathematical analysis to characterize the pore geometry and distribution in porous media using X-ray computed tomography. Kriszt *et al.* [50] used MCT to generate the density map and used it as an input to finite element modeling. Also Nakashima *et al.* [51] studied the transport properties of porous media by microfocus X-ray computed tomography and found that the results for porosity, surface to volume ratio, and diffusion coefficient were within 5–8% of the actual measured values.

This method has sometimes been claimed inappropriate. In 2002, Olurin *et al.* [48] used X-ray computed tomography and indicated that the method to precisely characterize the microstructure and the internal architecture of the foam was unclear. They also stated that, as long as the measured size is considerably larger than the measurement resolution, parameters, such as resolution, very little affect the foam morphometric parameters.

Although NDT field is very important in different industries, the applicable NDT methods for homogeneity tests on metallic foams are relatively expensive and not always

applicable and accurate. As a result, other easier, more accessible, and less expensive methods are preferred for homogeneity tests on metallic foams.

2.1.1.4. Permeametry

Permeametry is based on the study of a gas or liquid flow through a porous medium. Pressure drop is measured across the foam and fluid velocity can be calculated by measuring the fluid flow rate. Having these two parameters and knowing the fluid viscosity and density, permeability and non-Darcian permeability coefficients of metallic foam can be calculated. Considering that the friction is related to the internal surface area of the pore volume, estimation can be done to obtain the foam specific surface area [12]. Khayargoli *et al.* [52] determined the permeability of metallic foams by applying the measured pressure drop across the metallic foam into the quadratic model of Hazen-Dupuit-Darcy and found that the pressure drop across the specimens strongly depends on the structure of the material.

2.2. Pressure Drop across Porous Media

Henry Philibert Gaspard Darcy (1803–1858) was a French scientist who made an important contribution to hydraulics. In 1856, he conducted column experiments to describe the flow through sand and established what has become known as Darcy's law, which is generalized to a variety of situations and is in extensive use today. The unit of fluid permeability, darcy, is named in honor of his work.

Considering the volumetric flow rate, Q, and the average fluid speed $V=Q/A$, where A is the filter cross-section surface area, Darcy presented his experimental results in terms of V and the pressure difference across the filter, Δp. He found a coefficient k

called hydraulic conductivity, and related it to the filter height, t, pressure-drop, and the average fluid speed as:

$$\frac{\Delta p}{t} = \frac{1}{k} V \tag{2.1}$$

It should be noted that the above mentioned empirical hydraulic equation, called *Darcy's equation*, is different from the following equation which is presented in most textbooks as *Darcy's Law*,

$$\frac{\Delta p}{t} = \frac{\mu}{K} V \tag{2.2}$$

Since his experiments were only with water, Darcy did not make any reference to the fluid viscosity. Couple of years later, Hazen indirectly observed the effect of fluid viscosity by changing the temperature of the fluid flowing through a filter [53]. After that, the fluid viscosity appeared as an individual parameter in Darcy's equation. Equation 2.2 is now mainly called *Hazen-Darcy equation* and should be distinguished from Darcy's equation. The hydraulic conductivity k of the original Equation 2.1 was substituted by K/μ in Equation 2.2, where K is called specific permeability, a hydraulic parameter independent of the fluid properties, and μ is the fluid dynamic viscosity. Equation 2.2 states that the pressure drop per unit length for a flow through a porous medium is proportional to the product of velocity and the dynamic viscosity of the fluid [54]. These two equations are macroscopic equations and do not explain the interactions between the fluid and the solid which takes place in the porous media.

Darcy's equation is applicable only when velocity is sufficiently small, which means that the Reynolds number of the flow is around unity or smaller [55]. Davis and

Olague [56] have shown from their analysis that experimental datasets published by Darcy for higher velocity range $V > 4 \times 10^{-3}$ m/s fits quadratic model better than linear model. As the velocity increases, the influences of inertia and turbulence become more significant and the results depart from this simple model. This departure eventually causes that the pressure-drop across a porous medium be governed by the form drag, which depends on the fluid density and quadratic velocity, V^2. This phenomenon is known as the non-Darcy flow behavior.

According to Lage [54], Darcy likely did not compare his work with Poiseuille's work which was based on straight tubes since Darcy worked with sand. Lage also mentioned that Kozeny provided an explanation for the fluid viscosity dependency and obtained a formula similar to Equation 2.2 by assuming uniform pressure drop and solving Poiseuille's partial differential equations along a discrete capillary length. Later Prony mentioned that the shear resistance should be a polynomial function of the fluid velocity at the solid surface, which he verified experimentally and found that quadratic polynomial is a good fit [54]. Later, as mentioned by Lage and Antohe [57], Dupuit, and not Forchheimer, as believed by many, modified the Equation 2.2 by proposing the following polynomial equation for predicting the steady flow through a homogeneous permeable medium based on the fact that the large flow resistance imposed by each small pore, being uniformly distributed, would induce a uniform fluid velocity as,

$$0 = \frac{\Delta p}{t} - \alpha V - \beta V^2 \qquad (2.3)$$

The responsible physical phenomenon for the quadratic term in Equation 2.3 is assumed to be the form force imposed to the fluid by any solid surface obstructing the flow path.

Newton in his book [58] proposed that this resistivity to the unidirectional flow force is proportional to the fluid density and the average fluid velocity square. Using this concept and Equation 2.2, Equation 2.3 can be rewritten as the *Hazen-Dupuit-Darcy equation*,

$$0 = \frac{\Delta p}{t} - \frac{\mu}{K} V - C\rho V^2 \qquad (2.4)$$

where, C is a form coefficient related to the geometry of the porous media and ρ is the medium density. The form drag, C, varies with changing the medium porosity. The last two terms in Equation 2.4 represent the lumped viscous drag and the lumped form drag, respectively, imposed by the solid porous matrix to the flowing fluid [55,57,59]. These two effects are always present in the flow, but the viscous effect will predominate at low enough fluid speeds. Equation 2.4 could be called as a *macroscopic momentum balance equation* of fluid flow through a porous medium [57,60].

Later on, Ward [61] proposed the idea to replace the form parameter C in the Equation 2.4 by $c/K^{1/2}$, where c is a dimensionless universal constant with the value of approximately 0.55 [55]. This suggestion was based on his assumption that the pressure drop versus fluid speed relationship depends only on V, K, ρ, and μ. Hence, the form coefficient C, where form is defined as the variation of the cross section area of the solid matrix, would depend on the permeability of the medium which is not correct [57], because:

1. Permeability is actually linked to the viscous drag and is related to the effective surface area of the solid porous matrix.
2. The form coefficient C depends on the form of the solid matrix not the extent of the surface.

Studies from Antohe *et al.* [62] and Beavers *et al.* [63] found that c is not a constant. Thus this replacement may not have practical benefit.

2.3. Inertia Effect

Newton presented some important definitions in his book [58]. Two of them are the *definition of quantity of motion*, and the definition of *inertial force*, which is the force that measures the difficulty to change the quantity of motion of a body. Based on these two definitions and the Newton's second law, it can be said that, the change in quantity of motion is identical to the inertial force, which is equal to the resultant of the entire forces act on the body.

Considering Equation 2.4, it can be concluded that a unidirectional steady flow passing through a permeable medium with uniform cross section retains its momentum or quantity of motion. This means that, the fluid has zero macroscopic inertial force. In this equation, which is a macroscopic equation, the right side represents all the forces acting on the fluid. The *form force* term, $C\rho V^2$, is usually referred as the *inertia force* or *inertia term* [57]. This expression is not correct because when there is a constant macroscopic momentum, the flow does not exert any inertial force. Also, if the microscopic scale, or pore level, is considered, the microscopic inertial force of the fluid should be equal to the resultant of all forces act on the fluid. But it is not the only force that affects the change of the inertial force of the fluid because the viscous force also contributes to that. According to Lage and Antohe [57], this confusion is created because the form force is proportional to V^2, and also sometimes the fluid inertial force or the time rate of change of momentum is written as velocity square. The term $C\rho V^2$ in Equation 2.4 represents a

force that varies with V^2 and is inertia related. Another evidence is that, in general, the inertial force is proportional to the fluid viscosity, while the form force is not.

This issue has been one of the critical problems influencing many scientists and generating misconceptions. For example, some of the researchers [61,63] incorrectly related the quadratic velocity term in Hazen-Dupuit-Darcy equation to turbulence. In another typical misconception, the permeability based Reynolds number, Equation 2.5,

$$\mathrm{Re}_K = \frac{\rho V K^{1/2}}{\mu} \tag{2.5}$$

where K is the permeability coefficient of the medium, has been used in some studies [61,64] to indicate the departure from linear equation in the fully developed steady flow. Firdaouss *et al.* [65] presented a definition of Reynolds number in term of fluid pressure drop as:

$$\mathrm{Re}_{\Delta P} = \frac{\Delta P a^3 \rho}{L \mu^2} \tag{2.6}$$

where a and L are microscopic pore scale and macroscopic length scales of the medium. But at high fluid speed, in which Reynolds number becomes proportional to V^2, this definition becomes inconsistent with the usual definition of Reynolds number.

Actually because the fully developed unidirectional steady flow has no inertia, this Reynolds numbers have no meaning and should not be used to estimate the transition from Hazen-Darcy (viscous dominated) to Hazen-Dupuit-Darcy equation (form dominated flow regime). According to Lage and Antohe [57], if the macroscopic Reynolds number is used to infer the transition from linear to quadratic regime, the pore-scale information would be ignored. Therefore, in macroscopic scale, lack of physical

meaning and pore information hinder the use of Reynolds number to predict this transition. To overcome this issue, Lage [54] suggested using the physical and meaningful ratio of the form force D_C to the viscous force $D\mu$ to determine the departure from linear flow regime, as presented in Equation 2.7. This equation has no ambiguity in

$$\frac{D_C}{D_\mu} = \frac{C\rho V^2}{\left(\frac{\mu}{K}\right)V} = \frac{C\rho K}{\mu}V \tag{2.7}$$

the definition of force ratio and requires knowledge of form factor C of the medium, which is an obvious factor to determine the time that the form force becomes major. Based on this definition, the transition from linear to quadratic regime, opposite to what has been believed by others, is media specific. Lage and Antohe [57] believed that, the transition is due to the switch of the drag force from linear to quadratic with the fluid velocity, and the drag depends on the shape and extent of the fluid solid in the porous media or the internal structure of porous media.

2.4. Permeability Studies

The behavior of fluid through the porous media has been one of the interesting subjects for researchers. There are lots of experimental and modeling studies; however, due to the nature of the present work, more focus will be directed towards experimental studies, especially the permeability related subjects. Some researchers also performed both to check their model accuracy. For instance Du Plessis *et al.* [66] in 1994 analyzed the experimental results for isothermal Newtonian flow through metallic foams in comparison with a theoretical model. Their model was based on a rectangular

representative unit cell to predict the pressure gradients for both Darcian and non-Darcian flows. In both regimes, their results showed promise for the accurate theoretical prediction of fluid dynamic phenomenon in foams like porous materials of very high porosity. They also validated their model using water and a glycerol solution in foams with porosity of about 97%. Later in 2001, Bhattacharya *et al.* [67] modified Du Plessis model to incorporate a correction for the tortuosity of metallic foam and showed that it is in reasonable agreement with the measured data. Furthermore they proposed an analytical model to predict inertial coefficient based on the theory of flow over bluff bodies and found that it is in excellent agreement with the experimental data. Further, Fourie and Du Plessis [68] in 2002 presented a theoretical model to predict the pressure drop in a Newtonian fluid flowing through highly porous isotropic metallic foams. Their experimental results for flow through isotropic, highly porous, cellular metallic foam showed that their model is capable of accurately predicting the hydrodynamic conditions in both Darcy and Forchheimer regimes.

Due to their wide range of applications, the behaviors of heat transfer and pressure drop have been very popular subjects for researchers. For instance, Huang and Vafaei [69] in 1993 studied the fluid flow and heat transfer in a composite system made of multiple porous block structure. They analyzed the changes in the flow pattern and heat transfer characteristics, and study the effects of several governing dimensionless parameters, such as the Darcy and Reynolds numbers as well as the inertia parameters. Kim *et al.* [70] also studied the impact of porous fins on the pressure drop and heat transfer characteristics of in-plate-fin heat exchangers. They tested porous aluminum foam fins with different permeabilities and porosities and compared the performance

between the porous fins and the conventional louvered fins. Their experimental results indicated that the friction and heat transfer rates are significantly affected by permeability and porosity of the porous fins and mentioned that for compactness of the heat exchanger, the porous fins with high pore density and low porosity are preferable. In another effort in 1998, Bastawros [71] studied the effectiveness of metallic foams in forced convection heat removal. Their model was based on a bank of cylinders in cross-flow to understand the effect of various foam morphologies. They experimentally analyzed the hydraulic and thermal characteristics of cellular metals subject to transverse airflow and found that a power law was followed when pressure versus velocity plots were recorded.

The form coefficient, viscous and form drags have also been important key subjects in the porous material study. For example, Zhang *et al.* [72] studied and reported the contributions of viscous and form drags to the total pressure drop, and Liu *et al.* [73] indicated that the form coefficient decreases as the flow velocity increases. Hwang *et al.* [74] also studied the effects of heat transfer and friction drag in a filled porous duct and showed that both the friction factor and the volumetric heat transfer coefficient increase with decreasing the foam porosity at a fixed Reynolds number.

Kaviany [75] in 1995 found that at low pressure and small pore size, a velocity slip can occur. This slippage effect reveals as an increase in the flow rate as the pressure gradient was decreased which leads to an apparent higher permeability. Lage *et al.* [76] also experimentally observed that by increasing the fluid speed through a porous medium, a transition from one quadratic to another quadratic regime with different form coefficient happens. They suggested adding a cubic function of fluid speed to the

quadratic Hazen-Dupuit-Darcy equation to represent their experimental data. Actually this extension was already suggested by Forchheimer [54] but with no physical reason and was purely empirical. In addition, they found that, contrary to the experimental results with water and packed bed of spheres, the results with air and aluminum porous medium layers yielded an increase in static pressure gradient as velocity was increased. They considered internal versus external incompressible viscous flow to justify this distinct behavior. Antohe *et al.* [62] also observed that at high flow speeds, the pressure drop is more sensitive to changes in compression ratio. They found that the permeability of their foams decreases with an increase in foam density and increase of its compression ratio. They also found that, to calculate the permeability of a medium, its regime, i.e. Darcian or non-Darcian, should be known. Later, in 1998, Seguin *et al.* [77] experimentally characterized the flow regimes for various porous samples and found that, the flow regime transition is gradual from laminar to turbulent in the entire bed, and is characterized with the pore Reynolds number.

Paek *et al.* [78] in 2000 conducted experiments on high porous aluminum foams with different porosities of higher than 89%. Considering that at a fixed porosity, decreasing the cell size increases the surface area to volume ratio, which increases the flow resistance by lowering the permeability and increasing the pressure drop, they inferred that the permeability was influenced significantly by both the porosity and the cell size. They also found that the friction factor was correlated with the permeability based Reynolds number. In a similar work, Boomsma and Poulikakos [79] conducted some research on aluminum foams with water as the working fluid. They reported that increasing the compression factor decreases the permeability by regular reduction

amounts, and holding the porosity constant while decreasing the pore diameter decreases the permeability. Finally, they mentioned that changing the velocity regime results in different values for the flow parameters.

Bhattacharya *et al.* [80] presented a comprehensive analytical and experimental investigation for determination of the effective thermal conductivity, permeability and internal coefficient of high porosity metallic foams. Their results showed that permeability increases with pore diameter and porosity of the medium, and the inertia coefficient depends only on porosity. Later in 2004, Khayargoli *et al.* [52] found that by increasing the pore size, the permeability increases and the inertia coefficient decreases, but no clear relation with the porosity was observed. They used different samples with the porosity ranging from 83 to 90%, and studied the effect of the microstructure on the permeability of metallic foams. Furthermore they found that as the pore size decreases, the surface area increases which creates additional flow resistance. Crosnier *et al.* [81] also performed some experimental work on aluminum and steel samples with porosities greater than 90%. It was revealed that as the pore diameter increased, the permeability increased. Also, as the pore size decreased, the surface area increased, resulting in higher mechanical energy dissipation and lower permeability. They define the term passability as the ratio of the inertia coefficient to the square root of the permeability coefficient, and found that as the pore size increases, there was more variation in the permeability than the passability. This indicates that the permeability scales well with the square root of the pore size while the passability scales well with the pore size. Also, it was found that permeability and passability were functions of the porosity, pore size, the surface area and the solid structure of the foam. In another work, Tradrist *et al.* [82] experimentally

determined the permeability and inertia coefficient of aluminum metallic foams used for compact heat exchanger with porosities greater than 90%.

Recently, in 2006, Wilson *et al.* [83] performed experiments with two different velocity profiles of what they called plug flow (PF) and fully developed flow (FDF). They create the PF by a generator before entering the test samples and found that, to determine the K and C, a PF profile should be formed at the inlet of the test section; however, if the PF has not been generated before entering the test sample, the test section should have a sufficient length for the inlet velocity profile to develop into the plug flow before the exit. They also found that by altering the inlet velocity profile, the form drag, which is dependant on the velocity square, is affected more than the viscous drag.

2.5. Objectives of the Present Work

The pressure drop of metallic foam, as stated before, depends on its microstructure which is characterized by parameters such as morphology of the ligaments that form the network of pores, pore size, pore shape, and porosity, as well as the viscosity, density and flow rate of the fluid.

According to Khayargoli *et al.* [52] and Zhou *et al.* [41], due to the complex structures of metallic foams, the main difficulty to model the flow through them is to accurately determine the structural characteristics of the foam. This task can become much more difficult if the foam is heterogeneous, or is compressed to decrease its porosity when the cells become significantly deformed. Therefore, the experimental data together with the empirical correlations can give the most accurate and reliable results.

In the present work, the experiments were carried out on a wide range of nickel-chromium open cell metallic foams having different thicknesses, densities, and pore sizes. The samples had well distributed and uniformed pore structure manufactured by the electro deposition technique. The objectives of this work are:

- to identify the effect of pore size and foam thickness on the pressure drop of metallic foams.
- to realize the effect of thickness on the total and unit pressure drop of metallic foams.
- to understand and determine the contributions of bulk and entrance effects on the pressure drop of metallic foam.
- to establish the relationship between the foam pressure drop, thickness, pore size, permeability and fluid velocity.
- to find out the effect of structure, location and thickness of heterogeneity on the foam pressure drop.

CHAPTER 3: SAMPLE PREPARATION AND EXPERIMENT PROCEDURE

3.1. Experimental Equipment

The experiments were conducted using the apparatus shown in Figure 3.1. This set-up

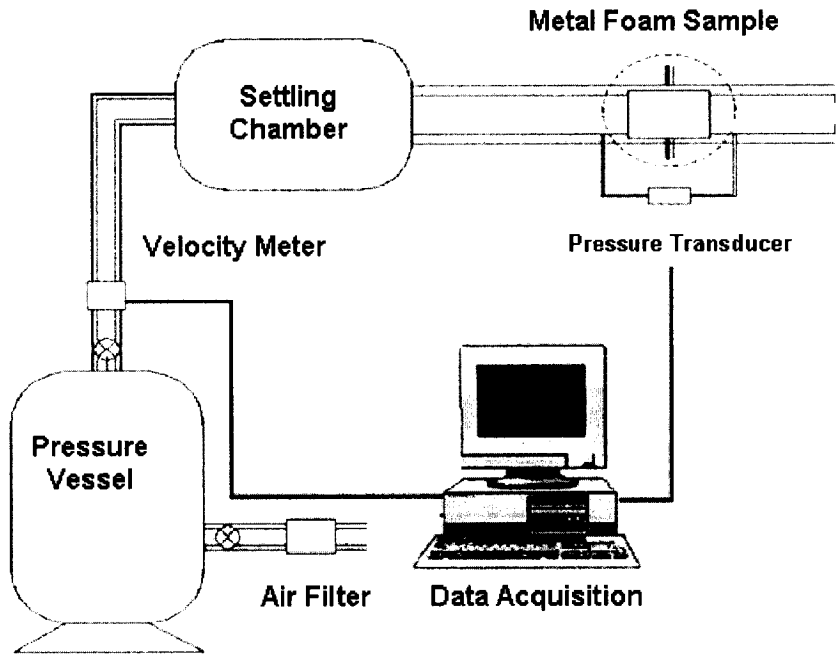

Figure 3.1: *Experimental Set-up [39].*

consists of three different middle flanges, a pressure transducer, a velocity meter, a pressure vessel and a settling chamber which are connected with galvanized steel pipes and fittings. This was designed and built by two former graduate students in our research group, P. Khayargoli and V. Loya, to obtain accurate determination of the flow velocity and pressure drop across the sample. The set-up was based on the experimental set-up used in Paek *et al.* [78] and ISO4022-1987-10-01 standard. The set-up was modified

slightly during the present work, e.g. extra mid flanges were added to accommodate thicker samples. In this set-up, compressed air was the flowing media and was allowed to fill the pressure vessel at the pressure of about 18 psi. The pressure was controlled by a manual pressure control-valve. Air filter was employed in line prior to the pressure vessel to absorb any impurities and foreign particles. Air was then allowed to pass through the settling chamber by means of 2 inch steel pipe and then entered a 1 inch steel pipe to reach the samples. The length of the 1 inch pipe was selected long enough in order to have the air flow completely developed before entering the samples for the entire velocity range. The settling chamber avoids any possible turbulence in the flow.

Metallic foam samples were securely assembled using different middle flanges, such as the one shown in Figure 3.2, and held in place by means of two standard (1"x4¼") flanges as shown in Figure 3.3. Three middle flanges were used; one has the thickness of 13 mm and the other two are 25 mm each. In order to have no metal to metal or no O-Ring to O-Ring contact, one of the 25 mm flanges has a flat metal surface at one side. Also, four different spacers (see Figure 3.4) with the thicknesses of 3, 8, 10, and 21 mm were used to fill up the gaps between the samples and the standard flanges when they are placed inside the middle flanges. This combination of different flanges and spacers gave the flexibility to test samples with different thicknesses ranging from 2 to 63 mm. Little pressure was used to push the samples in the middle flange and was done carefully to avoid any shearing or permanent deformation of the samples. Pressure tap was drilled on the pipe 80 mm from the sample, and one way valve was used to prevent air leakage. The pressure at downstream was atmospheric, which was confirmed by measurement. To this end, a small pipe with pressure gage was connected to the flange after the sample

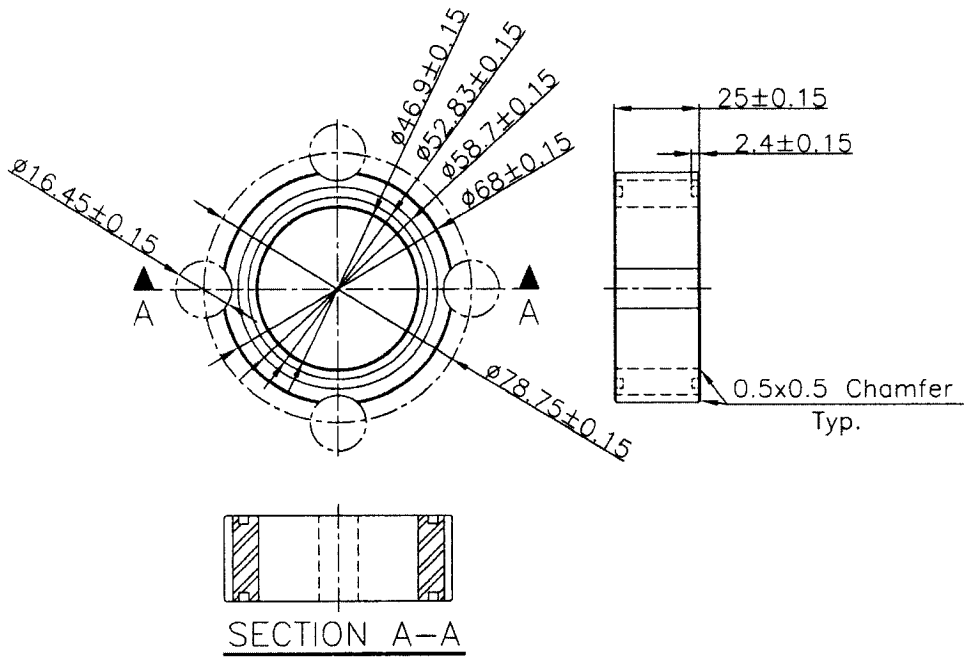

Figure 3.2: *Double O-ring flange.*

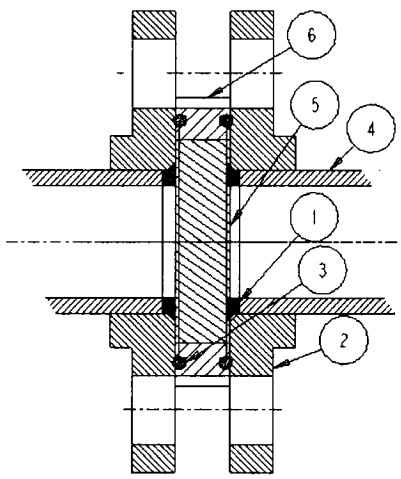

Id	Name	Qty
1	EPOXY	2
2	FLANGE	2
3	ORING56	2
4	PIPE	2
5	RECEMATSAMPLE	1
6	RECEMAT_FLANGE	1

Figure 3.3: *Flange assembly [39].*

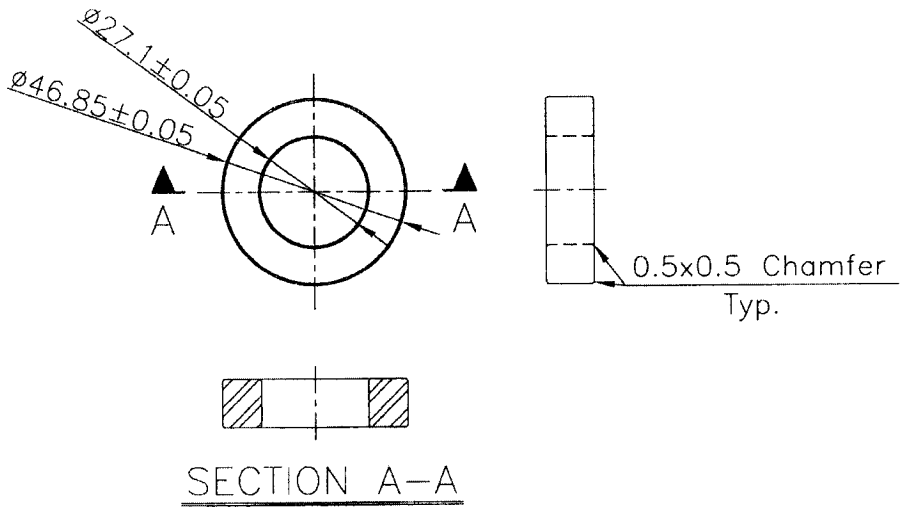

Figure 3.4: *Spacer.*

and pressure was measured before and after the sample. The result of this test showed that, when there is no connection after the sample, the pressure at the point exactly after the sample is equal to the atmospheric pressure. Thus, only the upstream pressure was measured using an OMEGA pressure transducer for pressure range of 0-25 psia with ±0.1% full scale accuracy. Flow velocity was measured using an OMEGA velocity meter for the flow velocity range of 10-1000 fpm with an accuracy of ±1% full scale. The velocity meter was calibrated and placed into the pipe at correct position using a flow meter. The signals from the velocity meter and pressure transducer were collected by a data acquisition device manufactured by OMEGA which was connected to the computer. InstaCal software, provided by OMEGA was installed to configure data acquisition device. Lab-view software was also used to program the required set-up, to read the sensors and finally to write the data into the output file. With this configuration, the pressure and flow velocity were viewed and recorded to the computer hard drive in real time. During a typical experimental run, the set-up was first tested for any leak. To minimize the experimental errors, for each condition, after the flow became stabilized,

100 data points were collected at 2 seconds and the average was used to plot the graphs. The diameter of the samples were 47 mm, however, the diameter of the effective area was just one inch.

3.2. Sample Preparation

Recemat metallic foam (RMF) is one of the commercially available metallic foams for several decades. It is an open cell polyurethane foam metallized using electro-deposition technique which has superior control on the cell size. The detailed process description is given in the section 1.2.3. Figure 3.5 shows a typical RMF microstructure. Nickel-chromium (NC) and nickel-chromium extra strong (NCX) metallic foams with thicknesses ranging from 1.6 to 20 mm and pore sizes from 0.4 to 2.3 mm were tested. In Table 3.1, the thickness availability for each material and grade is presented. Figures 3.6 and 3.7 show two of the actual foams used in this work. Discs of the required dimensions were cut from these sheets using wire EDM.

Figure 3.5: *A typical RMF microstructure [31].*

Table 3.1: *Sample availability.*

Grade	Nominal Thickness (mm)								
	1.6	2	3	4	5	7	10	13	20
NC 4753	■				■				
NC 3743					■				
NC 2733		■	■		■		■		
NCX 2733							■		
NCX 1723				■	■	■	■	■	
NCX 1116					■	■	■	■	■
NC 610							■		

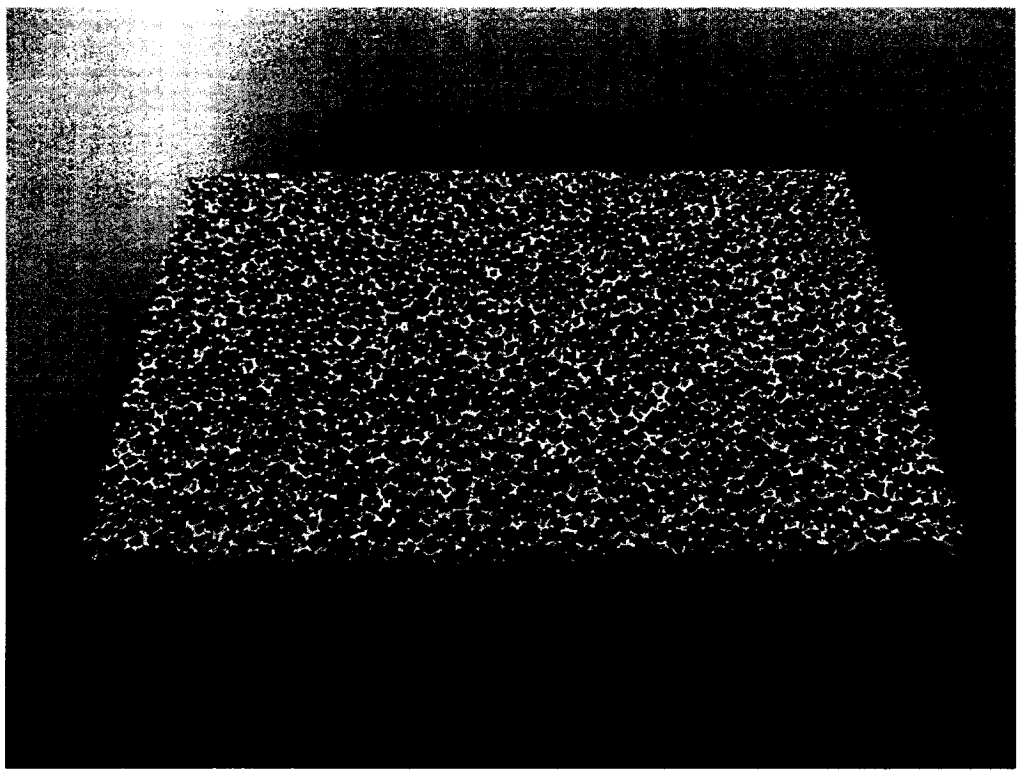

Figure 3.6: *A NCX1116 Recemat foam with dimensions 120x100x10 mm.*

Table 3.2 shows some of the RMF structural properties. The grade number relates to the range of pores, which is the approximate number of pores per linear inch (25.4 mm). The surface area to volume is also tabulated. Data in this table are provided by the

Recemat International [31], Netherlands based MF manufacturer. Recemat kindly provided us with the metallic foams used in this study.

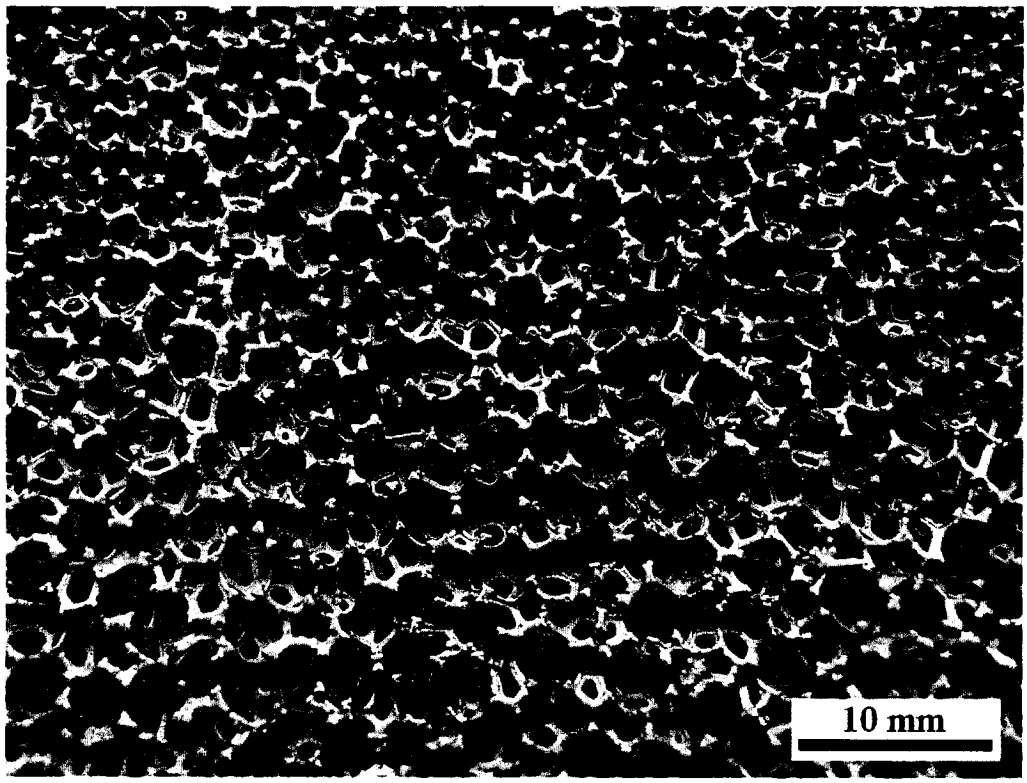

Figure 3.7: *Photograph of a NC610 Recemat foam.*

Table 3.2: *Recemat metallic foam structural properties [31].*

Grade Number	Range of Pores (pores / inch)	Estimated Average Pore Diameter (mm)	Estimated Specific Surface Area (m^2/m^3)
610	6 ... 10	2.3	500
1116	11 ... 16	1.4	1000
1723	17 ... 23	0.9	1600
2733	27 ... 33	0.6	2800
3743	37 ... 43	0.5	4000
4753	47 ... 53	0.4	5400

3.3. Porosity Measurements

Porosity of the metallic foam can be calculated by the equation:

$$\varepsilon = 1 - \frac{V_{solid}}{V_{foam}} \tag{3.1}$$

where, V_{solid} is the solid phase volume and V_{foam} is the total foam volume. Volume of the foam in Equation 3.1 can be measured easily by measuring the dimensions of the sample, but measuring the volume of the pores is complicated. The average density of the solid was measured by Loya [40] using ASTM-792-98 standard and is 5.16±0.20 g/cm^3. It can also be done by means of gas pycnometer. The volume of the solid was then calculated by weighing each individual sample and dividing by the solid average density. The actual sample (foam) thickness and volume were measured directly and are tabulated with the estimated porosity in the Table 3.3. One of the error sources in calculating the porosity is the tiny air gaps inside the strands, which had been formed during the manufacturing process, and cannot be accurately measured.

Table 3.3: *Volumetric Porosity of Recemat Metallic Foam.*

	Sample #	Thickness (dx)(mm)	Weight (g)	V_{foam} (mm^3)	V_{solid} (mm^3)	ε
NC4753-1.6, d=0.4mm, dx=1.6mm	1	1.69	2.38	2934	461	0.84
	2	1.69	2.44	2934	473	0.84
NC4753-5, d=0.4mm, dx=5mm	1	5.30	6.0	9 206	1 162	0.87
	2	5.31	6.3	9 220	1 220	0.87
	3	5.30	7.1	9 206	1 375	0.85
NC3743-5, d=0.5mm, dx= 5mm	1	5.10	7.6	8 852	1 472	0.83
	2	5.20	7.7	9 025	1 492	0.84
NC2733-2, d=0.6mm, dx=2mm	1	2.13	2.43	3810	471	0.88
	2	2.12	2.40	3793	465	0.88
NC2733-3, d=0.6mm, dx=3mm	1	3.21	3.99	5743	773	0.87
	2	3.22	3.76	5760	728	0.87
NC2733-5, d=0.6mm, dx=5mm	1	4.87	4.6	8 456	891	0.89
	2	5.10	4.6	8 859	910	0.90
	3	4.90	4.4	8 512	852	0.90
NC2733-10, d=0.6mm, dx=10mm	1	10.00	10.0	17 363	1 937	0.89
	2	10.20	9.4	17 704	1 821	0.90
	3	10.20	9.9	17 704	1 918	0.89
NCX2733-10, d=0.6mm, dx=10 mm Extra Strong	1	10.34	14.0	17 953	2 713	0.85
	2	10.40	14.7	18 051	2 848	0.84
	3	10.23	14.7	17 752	2 848	0.84
NCX1723-4, d=0.9mm, dx=4mm	1	4.30	4.80	7465	930	0.88
	2	4.30	4.91	7465	951	0.87
NCX1723-5, d=0.9mm, dx=5 mm Extra Strong	1	5.21	5.60	9044	1085	0.88
	2	5.23	5.45	9079	1056	0.88
	3	5.22	5.07	9062	982	0.89

Table 3.3: *Volumetric Porosity of Recemat Metallic Foam (Cnt'd).*

	Sample #	**Thickness (dx)(mm)**	**Weight (g)**	**V_{foam} (mm^3)**	**V_{solid} (mm^3)**	**ε**
NCX1723-7, d=0.9mm, dx=7mm, Ex. St.	1	7.28	9.03	13024	1749	0.87
	2	7.27	9.95	13006	1928	0.85
NCX1723-10, d=0.9mm, dx=10 mm Extra Strong	1	10.17	9.4	17 648	1 821	0.90
	2	10.40	11.1	18 051	2 151	0.88
	3	10.23	10.3	17 759	1 996	0.89
NCX1723-13, d=0.9mm, dx=13mm	1	13.35	14.97	23883	2900	0.88
	2	13.34	15.24	23865	2952	0.88
NC1116-5, d=1.4mm, dx=5mm	1	5.20	4.99	9027	967	0.89
	2	5.21	4.96	9044	961	0.89
NCX1116-7, d=1.4mm, dx=7mm	1	7.42	7.82	12881	1515	0.88
	2	7.44	7.62	12916	1476	0.89
NCX1116-10, d= 1.4mm, dx= 10mm	1	10.01	8.5	17 377	1 647	0.91
	2	10.00	8.7	17 356	1 686	0.90
	3	10.40	11.0	18 051	2 131	0.88
NCX1116-13, d=1.4mm, dx=13mm	1	13.23	15.4	22 966	2 984	0.87
	2	13.27	13.1	23 035	2 538	0.89
	3	13.24	12.9	22 980	2 500	0.89
NCX1116-20, d=1.4mm, dx=20mm	1	21.78	19.71	37809	3818	0.90
	2	21.81	19.52	37861	3781	0.90
NC610-10 d=2.3mm, dx=10mm	1	10.02	9.80	17394	1898	0.89
	2	10.03	8.72	17412	1689	0.90

CHAPTER 4: RESULTS AND DISCUSSION

4.1. Results

Pressure drop of porous media can be calculated using permeability, dimensions, and morphology of the porous media, as well as the fluid viscosity, density and flow rate. Most of the different models have shown that pressure drop is a function of the porous medium thickness and the fluid velocity.

The total pressure drop was measured for different grades of metallic foams having different thicknesses of 2 to 63 mm, depending on the thickness availability for each grade, at different air velocity ranging from 0 to 20 m/s. The flow was steady-state, unidirectional, and fully developed before entering the samples. Two or three replicas for each thickness of the same grade were tested and compared with each other to make sure their pressure drop curves are consistent. In Figure 4.1, the results for replicas of NCX1723 grade (d=0.9 mm) with 5 and 10 mm thicknesses are presented. This figure clearly shows the agreement between the replicas. The pressure drop results were also obtained after rotating the sample to switch the surface facing the flow. The results of the two tests were found identical indicating that, reversing these metallic foams has no effect on the pressure drop.

To obtain samples with thicknesses higher than any of the individual discs, combinations of discs of the same grade were used. The individual discs were selected randomly from the available replicas. Table 4.1 shows some of the individual disc combinations used for the NCX1723 grade.

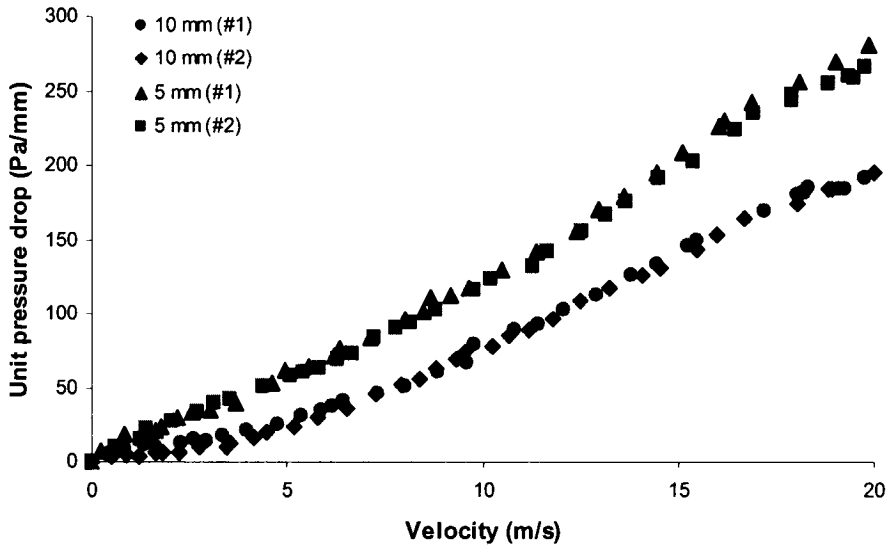

Figure 4.1: *Repeatability test results for NCX1723, (d=0.9 mm).*

Table 4.1: *Individual disc combinations for NCX1723.*

Replica Number		1	2	1	2	3	1	2	1	2	1	2
Nominal Thickness (mm)		4	4	5	5	5	7	7	10	10	13	13
Actual Thickness (mm)		4.30	4.30	5.21	5.23	5.22	7.28	7.27	10.17	10.40	13.35	13.34
Actual Composite Sample Thickness (mm)	4.30	■										
	7.27							■				
	13.34											■
	20.57								■	■		
	24.87	■							■	■		
	37.36	■		■			■		■	■		
	42.31					■				■	■	■
	45.78	■			■	■	■			■	■	
	54.54						■		■	■	■	■
	63.14	■	■				■		■	■	■	■

In order to verify this procedure, results of testing the metallic foams with certain thickness were compared with the results of the foams with the same thickness but made by combining discs of the same grade. Fore example, Figure 4.2 shows the results of the tests performed on a simple sample with nominal thickness of 10 mm, and a sample made from two individual discs of the same grade, each with 5 mm nominal thickness. This clearly shows that, the results of both tests are similar.

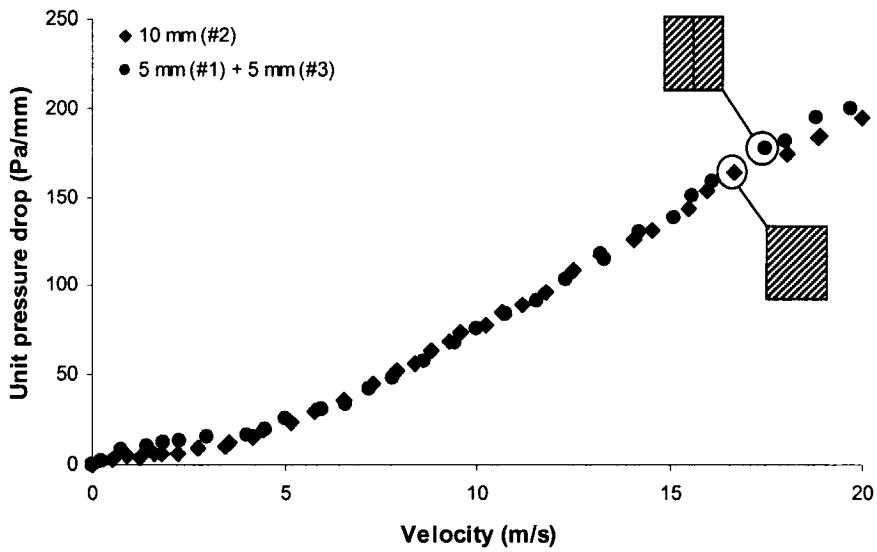

Figure 4.2: *Simple and combined foams pressure drop test results, NCX1723, d=0.9 mm.*

For compressible fluids (ideal gasses), the pressure drop term, ΔP, in Equation 2.4 should be calculated as:

$$\Delta P = \frac{P_i^2 - P_o^2}{2P_o} \tag{4.1}$$

where P_i and P_o are the absolute pressures at the foam inlet and outlet, respectively, and P_i is taken as the reference pressure for the density and viscosity of the flowing fluid [84].

The compressibility effect was checked using Equation 4.1 and was found to affect our results with less than 1% error, and thus assumed negligible.

To determine the permeability, K, and non-Darcian permeability coefficient, C, the unit pressure drop curve (pressure drop per unit length of the foam) for each grade should be determined. In order to do that, the unit pressure drop curve for each specimen was obtained using its total pressure drop and thickness. Equation 2.5 was used for curve fitting which is a widely accepted model by several researchers [39,85,86], and a least squares fit was performed to determine the values of α and β. K and C were also calculated using Equations 2.3 and 2.4 as:

$$K = \frac{\mu}{\alpha}, \quad C = \frac{\beta}{\rho} \tag{4.2}$$

where the dynamic viscosity and density of air are taken as 1.85×10^{-5} Pa.s and 1.225 kg/m^3, respectively.

4.2. Pressure Drop Contradictions

Contrary to what was expected, the unit pressure drop curves for samples with different thicknesses from the same grade did not collapse to one curve. Figure 4.3 and 4.4 show the total and unit pressure drop curves, respectively, for the NCX1723 grade with various thicknesses from 4 to 63 mm. As shown in Figure 4.3, increasing the thickness increases the total pressure drop. But, this increase is not linear with sample's thickness. Figure 4.4 shows that by increasing the thickness, the rate of decreasing the unit pressure drop decreases. This figure also shows that, for each different thickness, the unit pressure drop

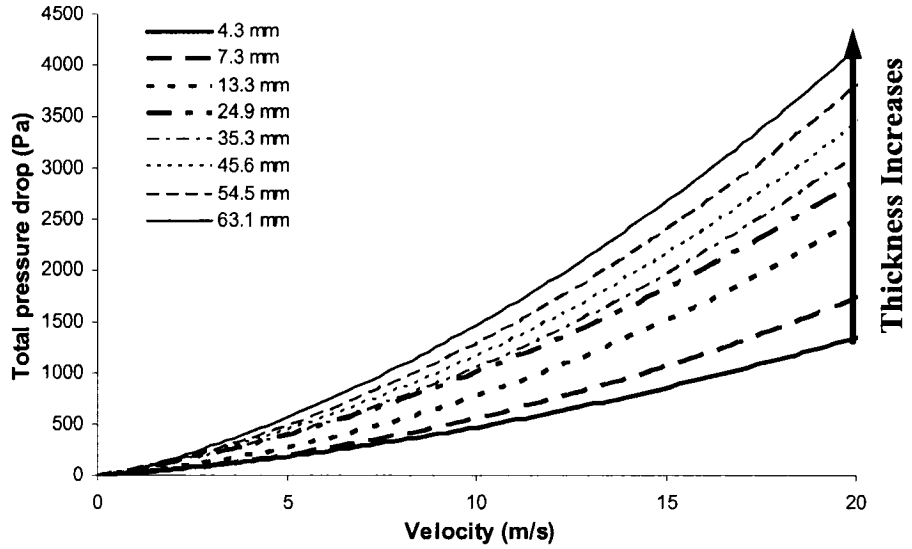

Figure 4.3: *Total pressure drop for NCX1723 with d=0.9 mm.*

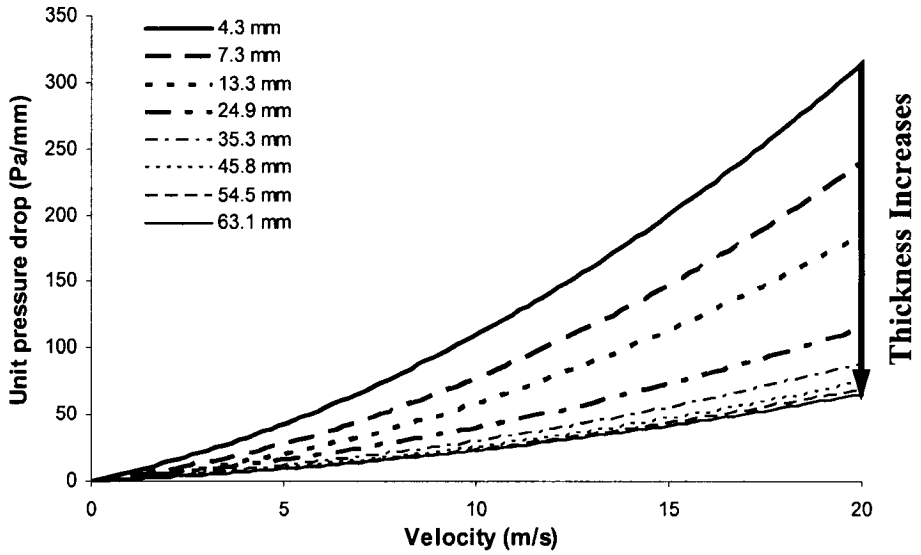

Figure 4.4: *Unit pressure drop for NCX1723 with d=0.9 mm.*

curve is different, which results in different Darcian and non-Darcian permeability coefficients for each thickness. This is contrary to what is expected; i.e. the permeability coefficients should be characteristic of the foam and not dependent on the thickness.

Figures 4.3 and 4.4 also show that, the effect of thickness on the total and unit pressure drop of the samples is completely opposite; while increasing the thickness increases the total pressure drop, it decreases the unit pressure drop. The total and unit pressure drop graphs for grades NC4753, NC2733, and NCX1116 with pore sizes of 0.4, 0.6, and 1.4 mm, respectively, are shown in Appendix A.

Table 4.2 presents the calculated K and C values using Equations 2.3 and 4.2, and clearly shows different values for K and C for metallic foams of the same grade but with different thicknesses. This result shows that, the total pressure drop simply divided by the medium thickness cannot be used in Equations 2.3 and 4.2 to describe the flow characteristic through metallic foams. The accurate relationship between pressure drop, thickness, and velocity will be realized in the current work.

Table 4.2: *Calculated K and C values based on unit pressure drop curve results, NCX1723, d=0.9 mm.*

Thickness (mm)	α	β	K (10^{-9}) (m^2)	C (10^3) (m^{-1})
4.3	6.27	0.47	2.95	0.39
7.27	3.54	0.42	5.23	0.34
13.34	2.41	0.34	7.69	0.28
24.87	2.39	0.17	7.74	0.14
35.29	1.56	0.14	11.86	0.12
45.78	1.37	0.12	13.54	0.10
54.54	1.24	0.11	14.95	0.09
63.14	1.19	0.11	15.58	0.09

Figures 4.5 and 4.6 show the three dimensional graphs of pressure drop versus thickness and velocity for NCX2733 grade which has an average pore size of 0.6 mm. These two graphs clearly show that, while the total pressure drop increases by increasing the thickness (Figure 4.5), the unit pressure drop decreases (Figure 4.6). Also, it can be

seen that the rate of this decrease in pressure drop diminishes and reaches a constant value after a certain thickness. This behavior is the same for all the grades studied in this thesis.

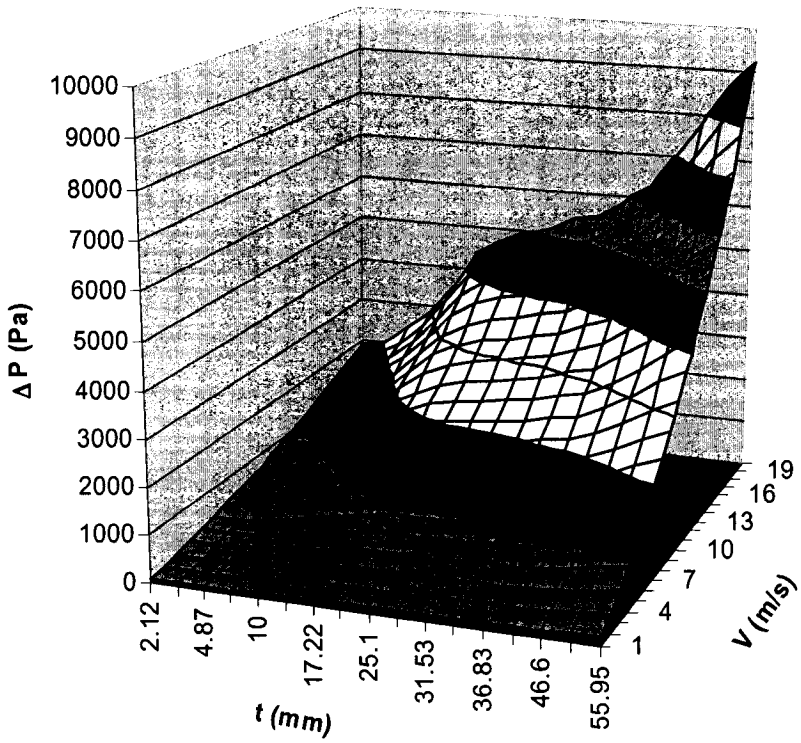

Figure 4.5: *3-D graph of total pressure drop for NC2733, d=0.6 mm.*

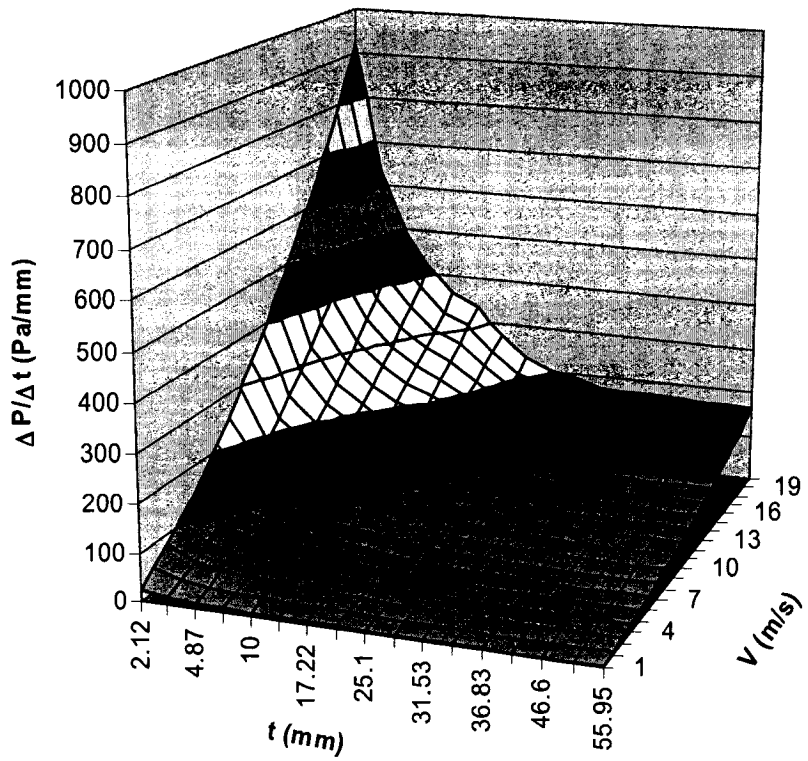

Figure 4.6: *3-D graph of unit pressure drop for NC2733, d=0.6 mm.*

4.3. Entrance Effect

Experimental test results show that the mathematical addition of the pressure drops of the individual components of a combined foam is not equal to the total pressure drop of the combined foam itself. As shown in Figure 4.7, and was observed for the other samples, this mathematical addition of the pressure drop of the two components of a combined foam is always higher than the experimental value for the pressure drop of the combined foam. For example, in Figure 4.7, the following relation can be observed:

$$\Delta P_{13(exp)} < \Delta P_{10(exp)} + \Delta P_{3(exp)} \tag{4.3}$$

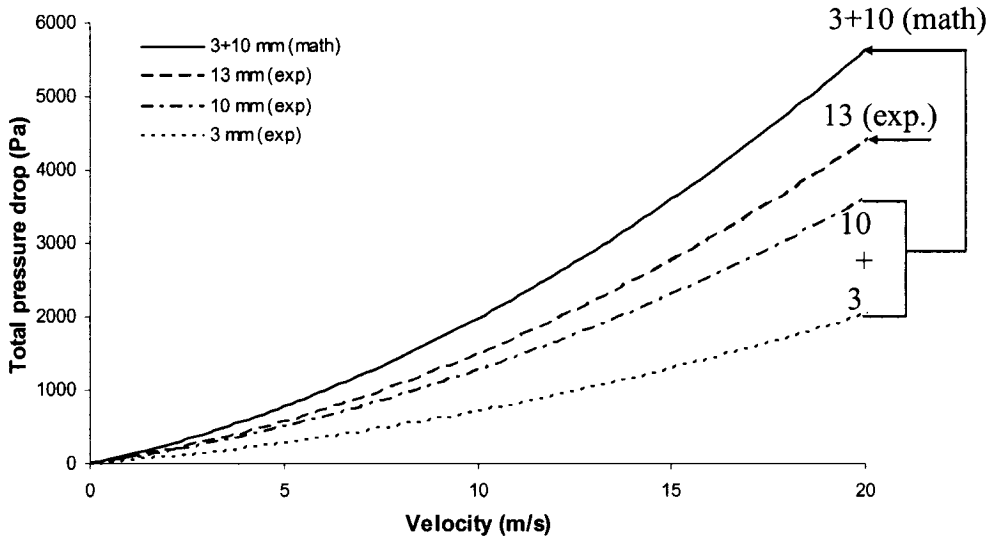

Figure 4.7: *Individual, experimental and mathematical additions of pressure drop curves for NC2733, d=0.6.*

Figure 4.7 is for samples composed of discs from the same grade. However when different grades were used, it was found that different surface facing the flow result in different pressure drop values. To prove this, a composite sample with the total thickness of 63 mm having two foams with different grades was tested. The two components are a 33 mm foam from grade NCX1723 with the pore size of 0.9 mm and a 30 mm foam from grade NC2733 with the pore size of 0.6 mm. This composite sample was tested in two different positions, as shown in Figure 4.8. In the first test, the disc with the smaller pore size and in the second test the one with the bigger pore size were facing the air before entering the foam. As shown in Figure 4.9, the pressure drop measured in test 1 is higher than the measured pressure drop in test 2. This figure also shows that the classical models are applicable at low fluid velocities in which the entrance effect is small.

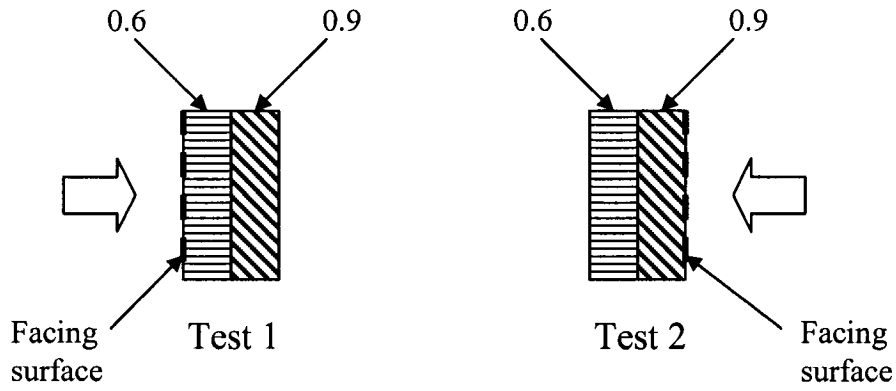

Figure 4.8: *Schematic drawing for the entrance effect tests.*

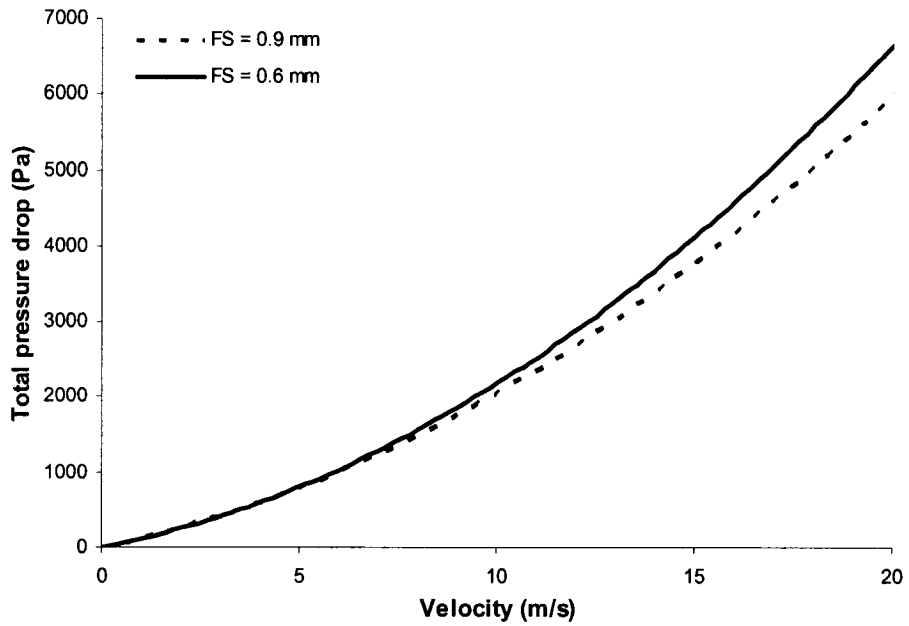

Figure 4.9: *Entrance effect test results.*

The entrance effect becomes more interesting when comparing the results of composite sample tests with the results of simple sample tests. Figure 4.10 shows the results for the effect of flow direction on the pressure drop of simple and composite specimens. As shown in this figure, the lowest curve is for the result of the test on a 5

mm sample with the pore size of 0.6 mm. The figure also shows that, a sample with the same thickness but with pore size of 0.4 mm has higher pressure drop values which is expected. However, it is interesting to compare these results with the results of the flow through 10 mm composite specimens made from these two different foams. Figure 4.10 shows clearly that the highest pressure drop curve is for the composite specimen with the foam of smaller pore size facing the flow. But, if in the composite, the foam with the bigger pore size faces the flow, the total pressure drop at higher velocities would be equal

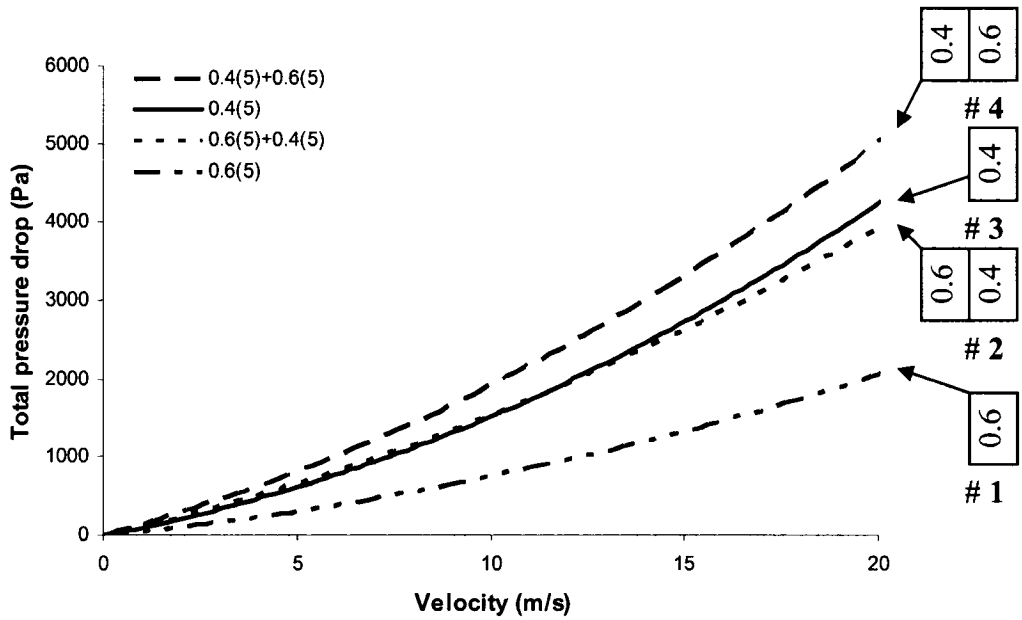

Figure 4.10: *Flow direction effect test results for composite samples, (d=0.4 & 0.6 mm, t=5, 10 mm).*

or even less than the pressure drop for the simple foam with smaller pore size. In this test, sample #2 has facing surface with bigger pores compared to sample #3. This means that the facing surface in sample #2 contributes less than the facing surface in sample #3 to the pressure drop, which results in lowering the total pressure drop of sample #2.

Various tests for different composite samples having different facing surfaces were performed. For example different arrangements of metallic foam samples, as shown

in Figure 4.11, were obtained using discs of two grades and different thicknesses. As shown, the sample with bigger pore size was located in different positions in the

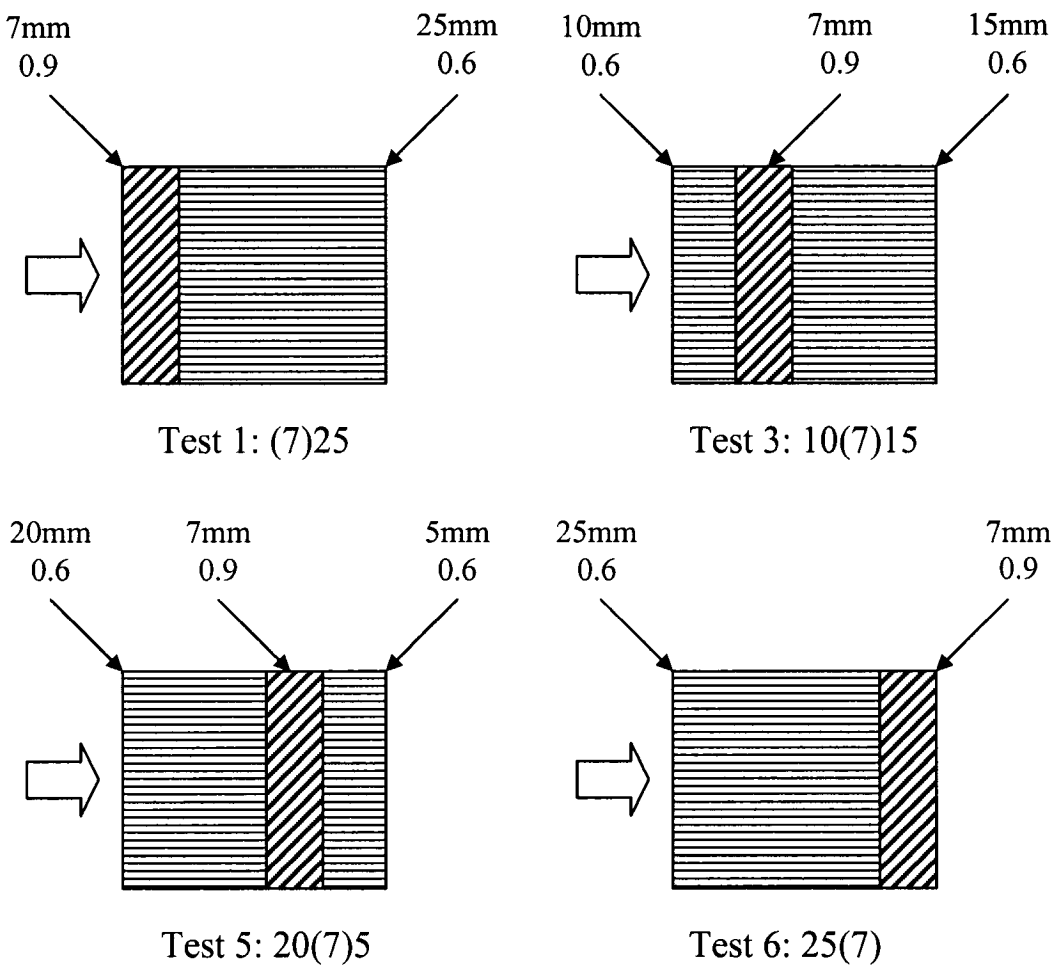

Figure 4.11: *Composite sample combinations schematic diagram.*

composite metallic foam. In the first test, the facing surface is made from the foam with bigger pore size and the rest of the sample is all from the smaller pore size foams. From test 2 to test 5, the sample with bigger pore size is located at different distances from the facing surface, but not completely at the end of the composite sample. Finally, in test 6, the bigger pore sample is located at the very end of the composite sample. The results in

Figure 4.12 show that, although the components of composite samples are exactly the

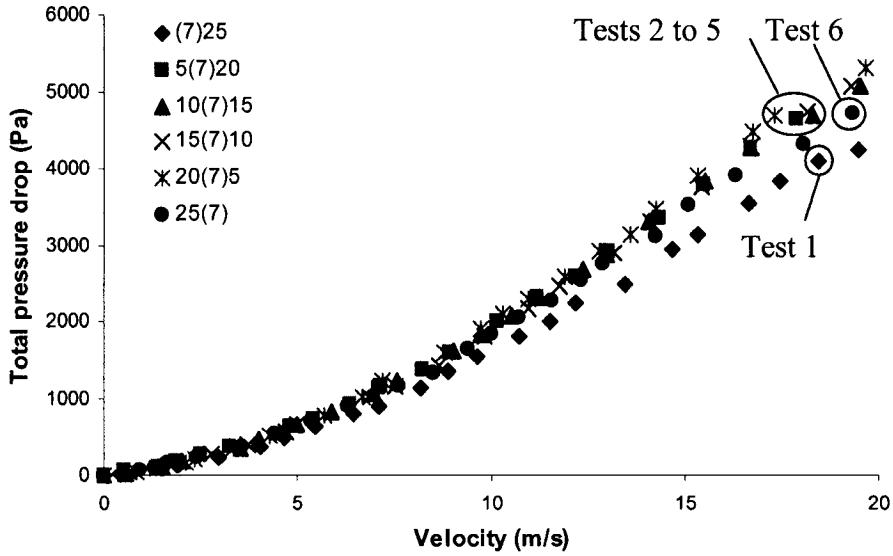

Figure 4.12: *Composite sample test results, 25 mm with d=0.6 mm and 7 mm with d=0.9 mm (The number in parenthesis states the foam thickness with d=0.9 mm, and the two side numbers are the foam thicknesses with d=0.6 mm at two sides).*

same in all the tests, when the facing surface is made of bigger pore foams, the measured total pressure drop is smaller. These results also show that:

- when the bigger pore sample is placed inside the composite, the pressure drop is not affected by the relative location of the bigger pore sample.
- when the bigger pore size sample is located at the very end of the composite, the pressure drop is a little smaller than when it is located at the middle of the composite, but not less than when located at the front.

In similar tests, the composite specimens with the total nominal thickness of 62 mm, made of NCX1723 foams with pore size of 0.9 mm and a 5 mm grade NC2733 foam with 0.6 mm pore size, were tested. Figure 4.13 shows the schematics for the location of

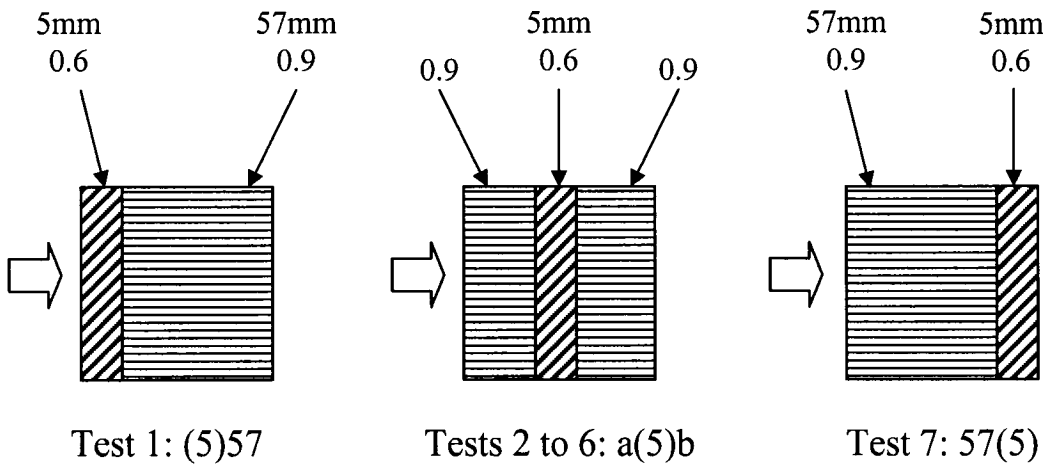

Figure 4.13: *Composite foam arrangements for the test results of Figure 4.14.*

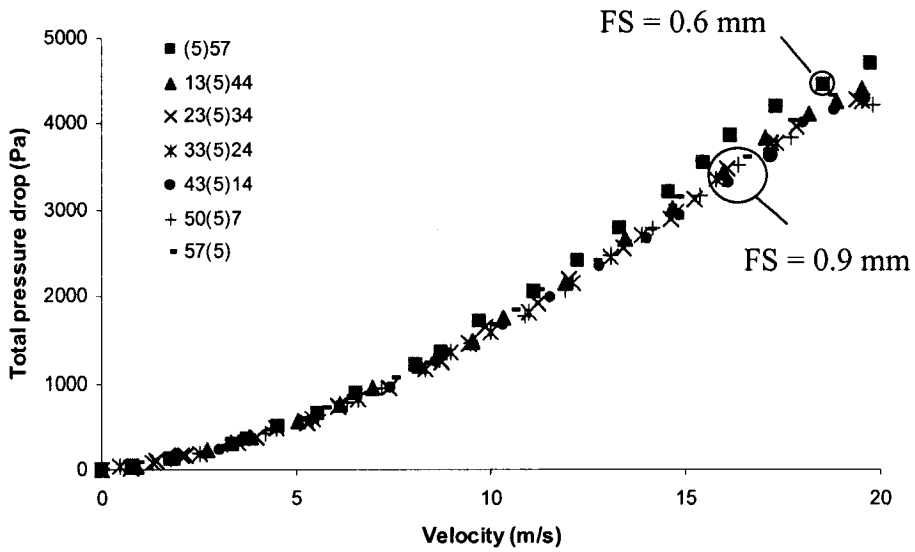

Figure 4.14: *Composite sample test results, 57 mm with d=0.9 mm and 5 mm with d=0.6 mm (The number in parenthesis states the foam thickness with d=0.6 mm, and the other number(s) states the foam thickness(es) with d=0.9 mm at the side(s)).*

the 5 mm sample with larger pore size inside the composite foam. The results in Figure 4.14 show that, when the facing surface is made from the foam with smaller pore size, test 1, the total pressure drop is higher than when the facing surface is made of foams with the bigger pores.

Two samples having the same thickness and from the same grade were tested in three different positions to demonstrate the entrance effect on the pressure drop of foams. Figure 4.15 shows the different relative positions of two foams to each other. In the first position, the two foams are completely touching and there is no gap between them. In the second and third positions, gaps of 3 and 8 mm, respectively, were placed between the two foams. The results in Figure 4.16 show that, when there is a gap between two foams, the pressure drop is higher than when there is no gap. This increase in pressure drop can be due to the turbulence created in the gap and also because of the additional entrance effect of the second foam. But, comparing the small increase in the pressure drop from the 3 mm-gap to the 8 mm-gap curves with the larger increase in the pressure drop from the no-gap to 3 mm-gap curves suggests that, this increase is mainly due to the additional entrance effect in the combined foam. This clearly shows that when the flowing fluid enters the foam, it creates some additional pressure drop that should be considered. If this additional pressure drop is not considered, different thicknesses of foam from the same grade will have different K and C values, indicating that these values are not characteristic of the material.

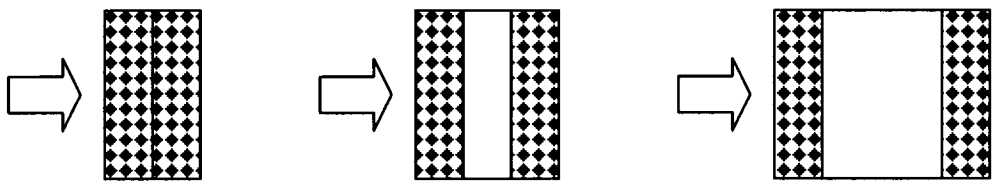

Figure 4.15: *Gap effect tests samples schematic depiction.*

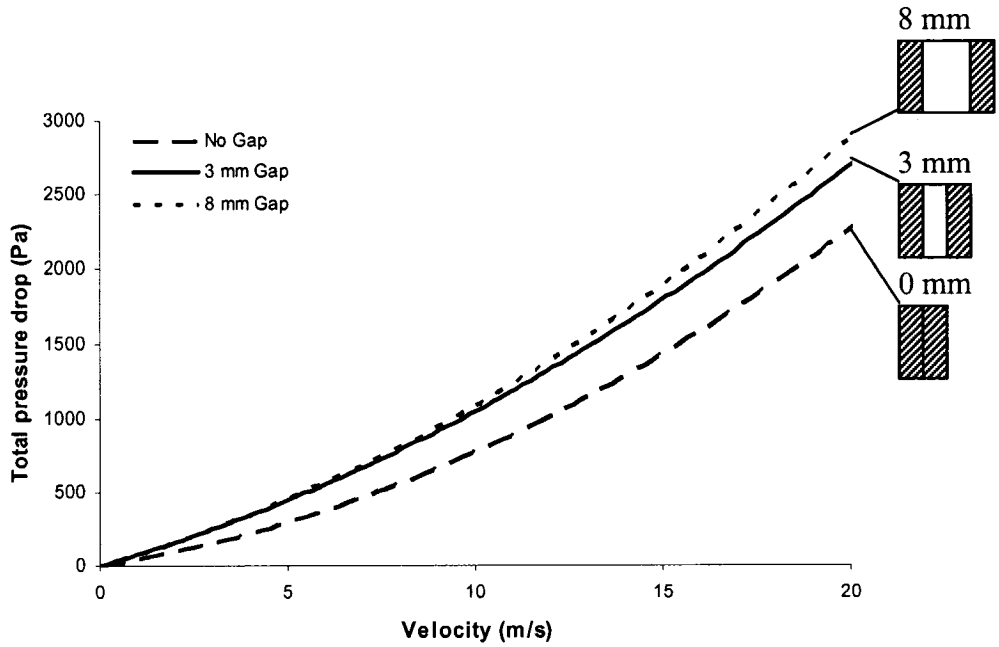

Figure 4.16: *Gap effect test results.*

All these results demonstrate that the foam facing surface affects the pressure drop value of porous media. Also, they demonstrate that, decreasing the pore size of the facing surface increases the pressure drop value.

4.4. Critical Thickness

The relation between the unit pressure drop and thickness for NC2733 at different velocities is presented in Figure 4.17. This graph clearly shows that the unit pressure drop decreases by increasing the thickness and the rate of this decrease becomes very small or reaches to zero at high thicknesses, which results in constant unit pressure drop. It can be understood from this figure that, the unit pressure drop decreases by increasing the

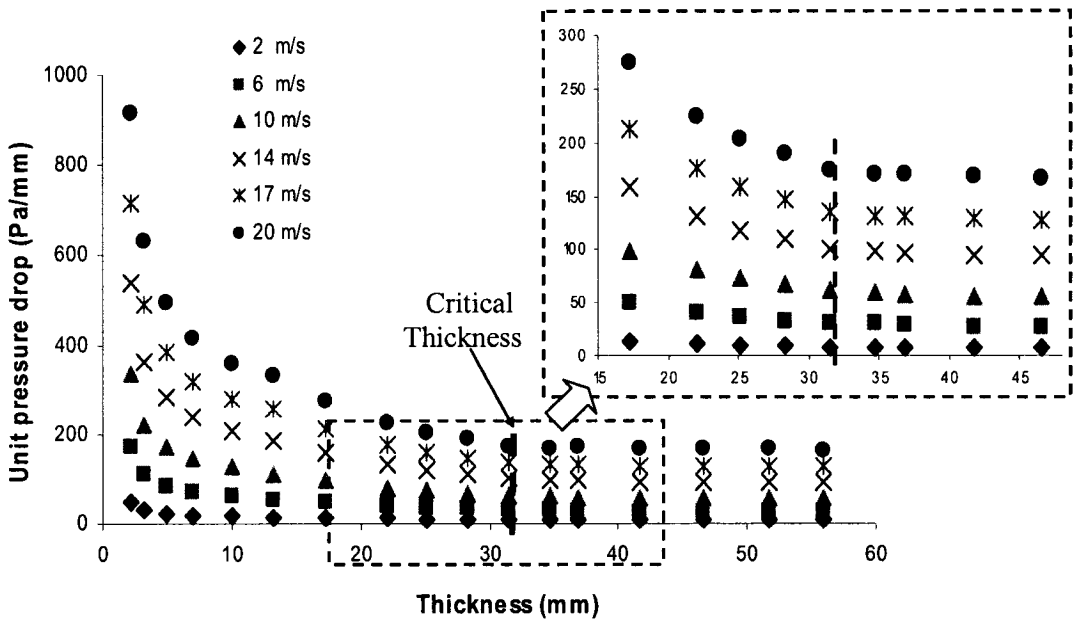

Figure 4.17: *Unit pressure drop vs. thickness at different velocities, NC2733, d=0.6 mm.*

thickness and after a certain thickness, which is called *critical thickness* in this work, the rate for the change of pressure drop becomes very small. Figure 4.18 shows the same graph for the foams of NCX1116 grade with the pore size of 1.4 mm. From this figure, the critical thickness for foams with pore size of 1.4 mm is around 60 mm while Figure 4.17 shows that this thickness is around 32 mm for foams with 0.6 mm pore size. Comparing the critical thickness for all grades declares that the critical thickness increases by increasing the pore size. Table 4.3 shows the critical thickness values for all grades in relation with the pore size.

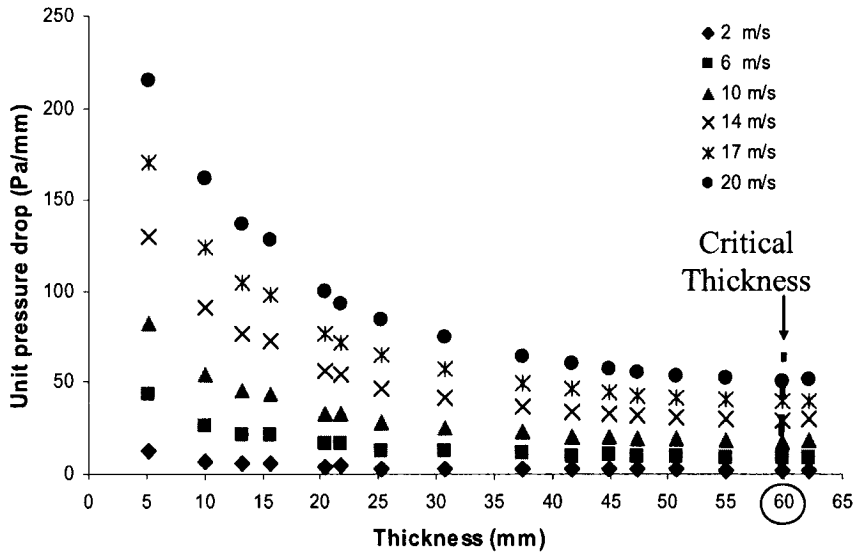

Figure 4.18: *Unit pressure drop vs. thickness at different velocities, NCX1116, d=1.4 mm.*

Table 4.3: *Critical thickness for different metallic foam grades.*

Grade	Pore Size (mm)	Critical Thickness (mm)
NC 4753	0.4	18
NC 2733	0.6	32
NCX 1723	0.9	50
NCX 1116	1.4	60

From the results in Figures 4.17 and 4.18, it can be stated that, at higher thicknesses of metallic foam, the unit pressure drop either becomes thickness independent, which follows Darcy's law, and can be modeled as:

$$\frac{\Delta P}{\Delta t} = Constant \tag{4.3}$$

or has a relation, such as linear with very small slope or hyperbolic, with the thickness.

This behavior suggests that there should be a parameter or individual term, either a constant or a variable, in the expression of the metallic foam pressure drop, which contributes less to the unit pressure drop or becomes negligible at higher thicknesses.

4.5. Lateral Effect

Another factor that can affect the permeability of metallic foams is the effect of fluid expansion and contraction while passing through the foam, which will be referred to as *lateral effect*. This can take place when the cross sections of the fluid inlet and outlet are different from the actual foam cross section. In order to check for this effect in our tests, the foams were impregnated with a non permeable material (paraffin) from the edge, leaving a permeable area equal to the fluid inlet cross section, as shown in Figure 4.19. Figures 4.20 and 4.21 show the unit pressure drop curves for the NCX1116 impregnated foams at different velocities and thicknesses. These results show that the expansion

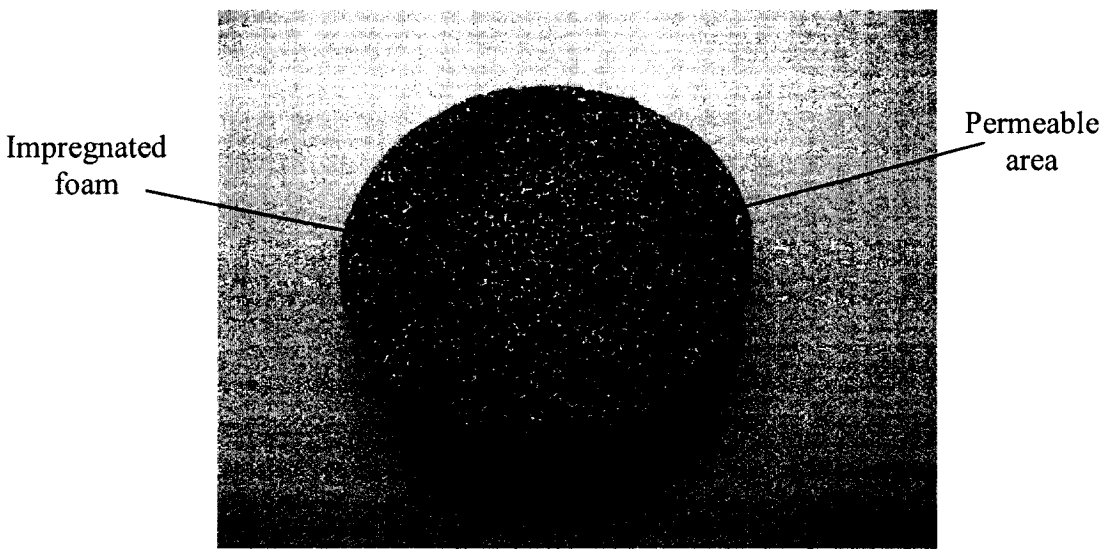

Figure 4.19: *A NCX1723 impregnated foam.*

does not change the general foam pressure drop behavior, and all the observations of this work, such as entrance effect and critical thickness, could be detected.

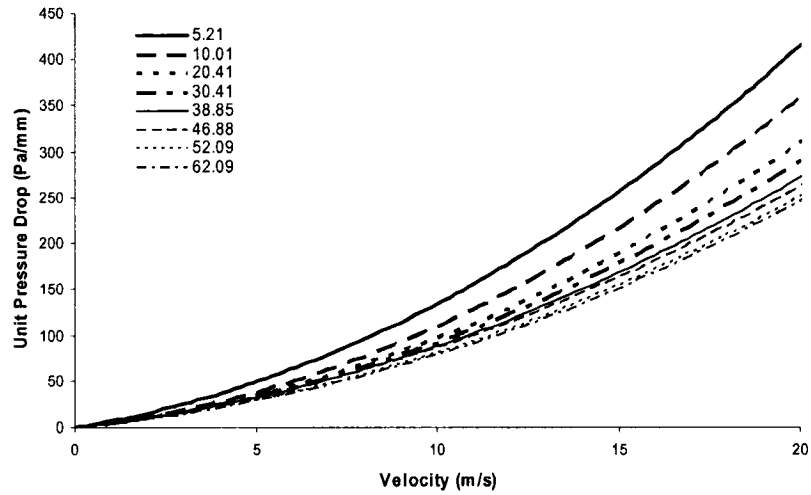

Figure 4.20: *Unit pressure drop for embedded NCX1116.*

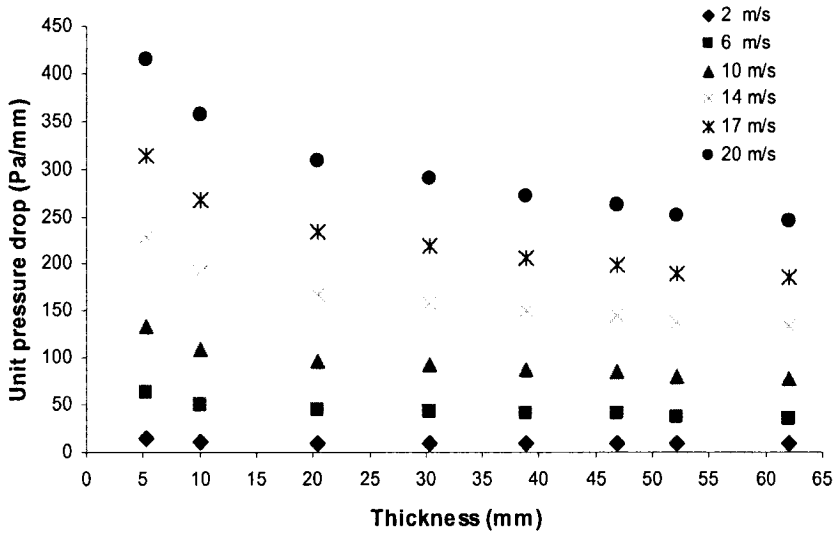

Figure 4.21: *Unit pressure drop vs. Thickness at different velocities for embedded NCX1116.*

A noticeable issue here is whether the lateral flow affects the entrance contribution or not. As shown in Figure 4.22, the entrance contribution is the same for

both situations and the observed difference between the two curves is actually a constant that represents the lateral effect. Since the entrance effect is constant for both tests, and knowing that the impregnated part of the foam with paraffin results in a cross sectional area that is not exactly identical to that of the inlet cross section which affects the accuracy of the measurements, all analyses and calculations in this work are performed on the non impregnated foams.

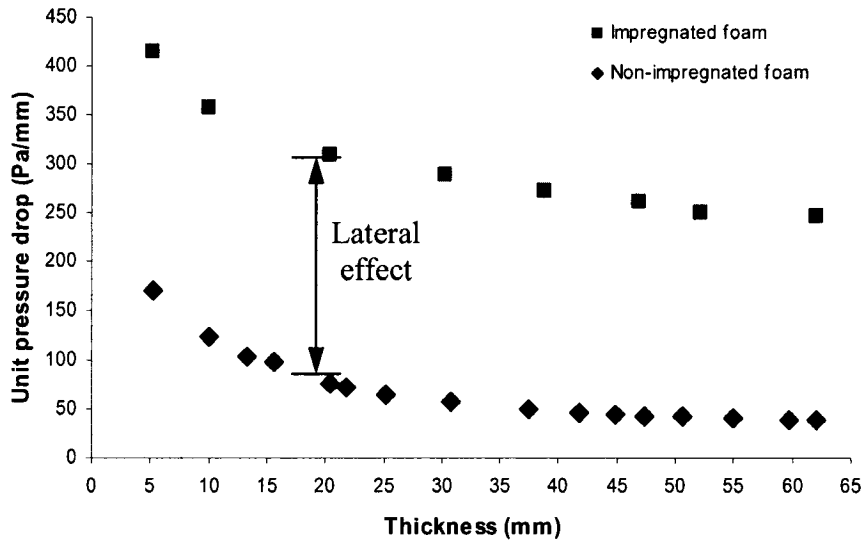

Figure 4.22: *Comparison between the unit pressure drop vs. thickness for embedded and non embedded NCX1116 foams at 20 m/s.*

4.6. Rough Prediction of C and K

One approach towards finding bulk material properties of metallic foams is to predict their parameters individually. As it is seen from Figure 4.23, which is the unit pressure drop for foams with 0.4 mm pore size, by increasing the foam thickness the unit pressure drop curves get close to each other. This infers that, at very high thicknesses all the unit pressure drop curves should collapse to one curve which results in unique K and C

values. This (imaginary) curve is shown with thick dashed line in Figure 4.23. Considering the unit pressure drop curves for different thicknesses of the same material, K and C values can be calculated from the imaginary curve. By drawing the curves of K and C versus thickness, as in Figures 4.24 and 4.25, it can be observed that, by increasing the thickness, K increases and C decreases; however, both curves reach a constant value

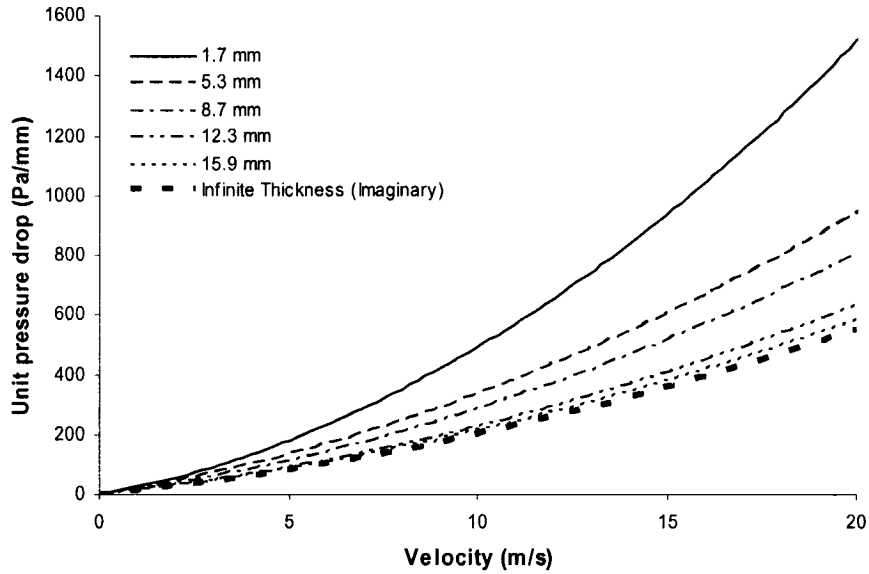

Figure 4.23: *Infinite thickness unit pressure drop curve for NC4753, d=0.4 mm.*

after a certain thickness. For instance, for foams with 0.4 mm pore diameter, C reaches to around $0.6\times10^{3}(m^{-1})$ (Figure 4.25) at around 18 mm, which has already been stated as the critical thickness for this grade (Table 4.3).

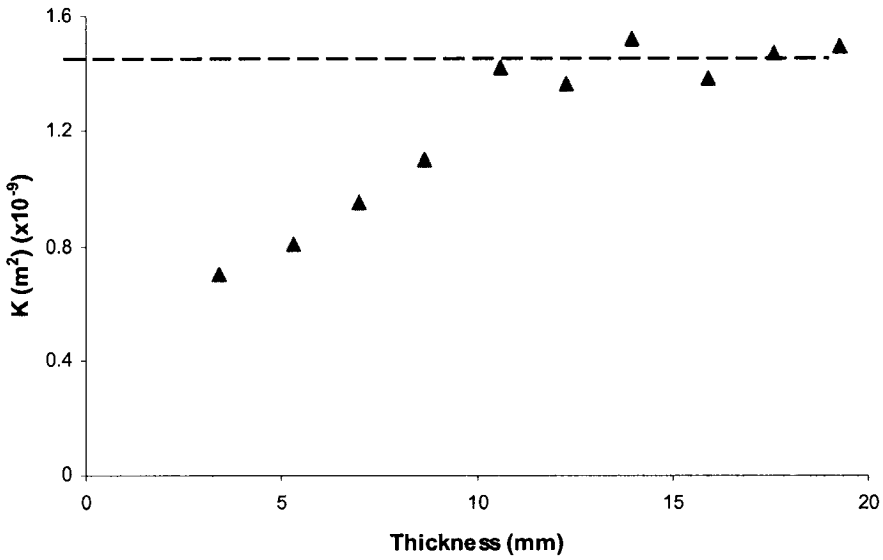

Figure 4.24: *Permeability coefficients for different thicknesses of NC4753, d=0.4 mm.*

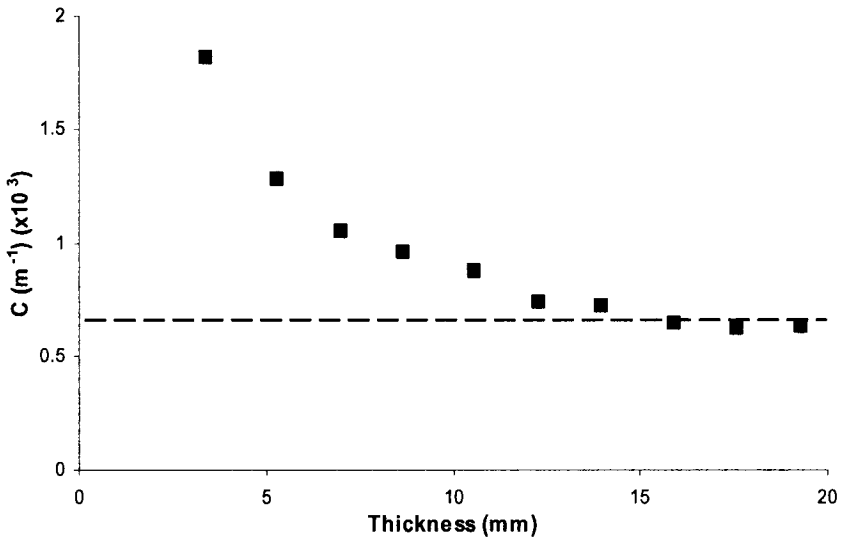

Figure 4.25: *Non-Darcian permeability coefficients for different thicknesses of NC4753, d=0.4 mm.*

The K and C values for the other grades were calculated in similar way and are provided as a function of pore diameter in Figures 4.26 and 4.27, respectively. Theses values show that by increasing the pore size, the foam permeability coefficient increases,

and the non-Darcian permeability coefficient decreases. This observation is similar to what other researchers such as Loya [40] obtained before.

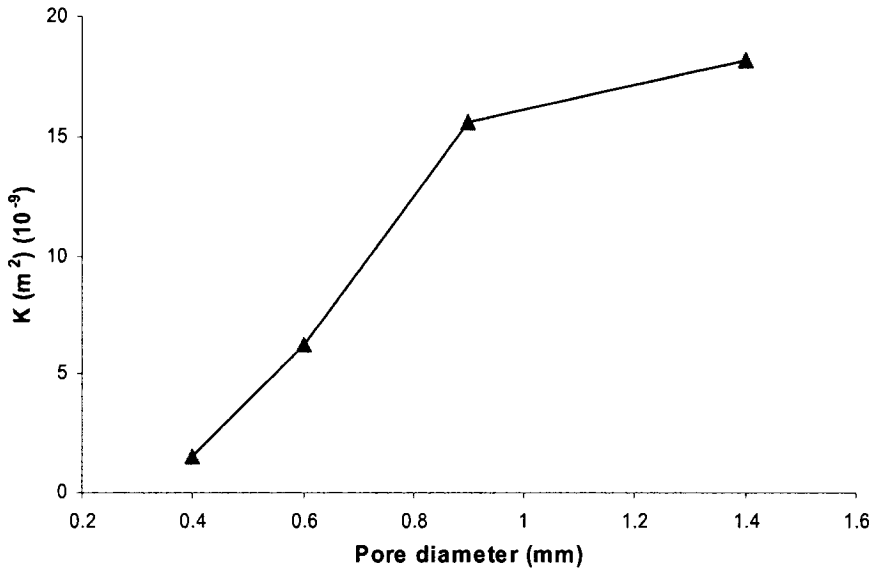

Figure 4.26: *Estimated permeability coefficients for different grades of Recemat metallic foams.*

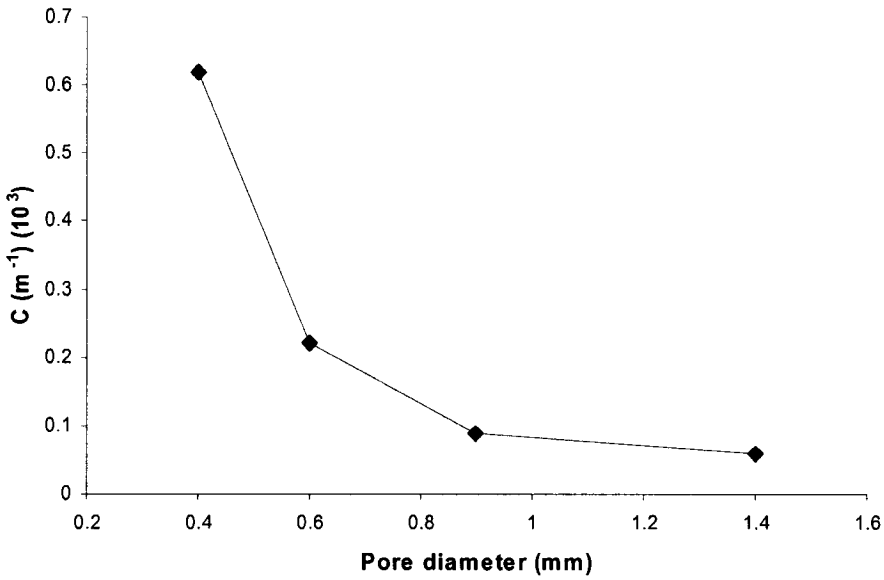

Figure 4.27: *Estimated non-Darcian permeability coefficients for different grades of Recemat metallic foams.*

4.7. Entrance Effect Contribution Analysis

Considering the relation between the unit pressure drop and thickness for foams with 0.4 mm pore diameter, as shown in Figure 4.28, it can be seen that the entrance contribution decreases by increasing the foam thickness. This behavior can be described by a hyperbolic function that reaches to a constant value.

Assuming that the total pressure drop is a combination of entrance and bulk effects, the total pressure drop can be written as:

$$\Delta P_{Total} = \Delta P_{Bulk} + \Delta P_{Surface} \tag{4.4}$$

Dividing both sides of Equation 4.4 by the foam thickness, assuming that the unit bulk pressure drop, that we will call here b, is thickness independent, and labeling the total entrance pressure drop effect as S, Equation 4.4 can be re-written as:

$$\frac{\Delta P_{TOTAL}}{\Delta t} = b + \frac{S}{\Delta t} \tag{4.5}$$

where t is the foam thickness. This equation clearly shows that, by increasing the foam thickness, the entrance effect contribution to the unit pressure drop should decrease. The rate of this decrease in pressure drop is similar to a hyperbolic function. But, the unit pressure drop will never become less than the bulk material unit pressure drop, b (there will always be bulk contribution).

The entrance effect contribution, S, was first assumed to be a constant value. Modifying the Hazen-Dupuit-Darcy equation, based on our assumption, results in the

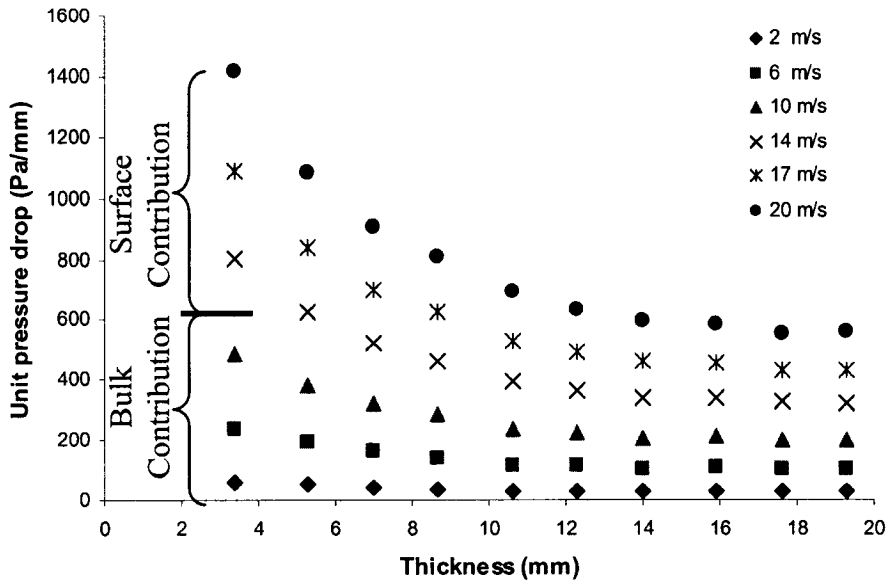

Figure 4.28: *Entrance and bulk effect contributions, NC4753, d=0.4 mm.*

following equation:

$$\Delta P_{TOTAL} = S + (\frac{\mu}{K} V + C\rho V^2) \cdot t \tag{4.6}$$

This equation means that, the entrance effect can be canceled out by subtracting the pressure drops of two different foams from the same grade but with different thicknesses as:

$$\Delta P_2 - \Delta P_1 = S_2 - S_1 + (\frac{\mu}{K} V + C\rho V^2) \cdot (t_2 - t_1) \tag{4.7}$$

in which $S_2 = S_1$ and results in,

$$\frac{\Delta P_2 - \Delta P_1}{\Delta t} = (\frac{\mu}{K} V + C\rho V^2) \tag{4.8}$$

This equation results in unique K and C for all thicknesses from the same grade.

Taking into consideration our tests on foams with 0.9 mm pore diameter, and assuming $\Delta P_1 = \Delta P_{@4.3mm}$ and ΔP_2 is the pressure drop of thicker foams, i.e. t = 5.2, 7.3, 10.17, ...63.1 mm, using Equation 4.8, the unit pressure drop curves were calculated and drawn in Figure 4.29. As shown in this figure, calculating the unit pressure drop, with the assumption of constant entrance effect, results in different unit pressure drop curves. Therefore, this assumption is not correct. Also, it can indirectly show that the entrance effect depends on the foam thickness.

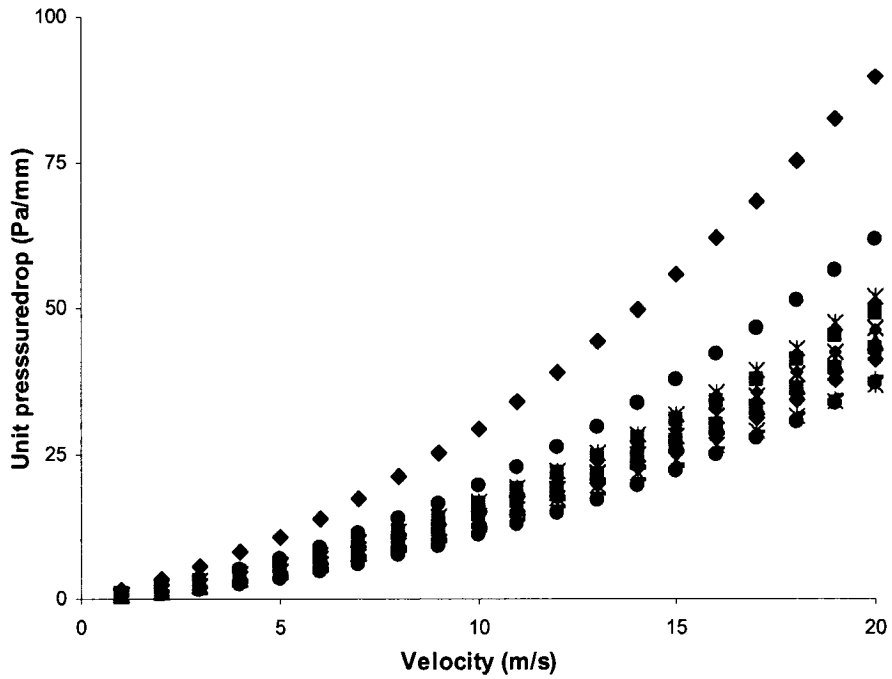

Figure 4.29: *Calculated curves of bulk pressure drop effect for NCX1723, d=0.9mm.*

Considering the graph of unit pressure drop versus thickness for NCX1723 grade which is shown in Figure 4.30, it can be observed that, the entrance effect contribution increases by increasing the fluid velocity. Assuming the pressure drop after the critical thickness is mainly bulk pressure drop, the entrance contribution at 20 m/s is much more

than its value at 10 m/s for the same sample (compare ΔP_1 and ΔP_2). Also, comparing the entrance effect at a constant velocity for two different thicknesses again proves that, the entrance effect is dependant on the medium thickness (compare ΔP_1 and ΔP_3).

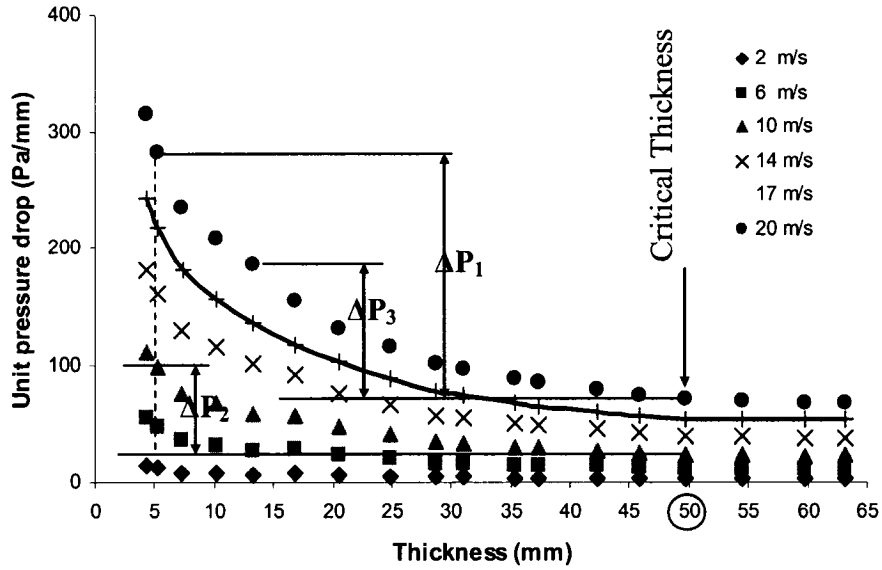

Figure 4.30: *Dependency of entrance effect to fluid velocity and foam thickness for NCX1723, d=0.9.*

All these discussions prove that, the entrance effect contribution depends on,

1. Fluid velocity.
2. Material thickness.
3. Permeability difference of material at the facing surface, which causes inertia change.

This means that the entrance effect can be stated as:

$$S = s(V,t,K)\cdot t \tag{4.9}$$

where $s(V,t,K)$ is the normalized foam entrance effect.

4.8. Entrance Effect Modeling

The results of previous sections proved that the pressure drop of porous media can be divided into two components of bulk and entrance effects. Thus, a good approach to calculate the entrance effect is to subtract the absolute bulk contribution from the total pressure drop. The total pressure drop was measured experimentally. Also because some researchers measured the pressure drop between two points inside the foam and found it in agreement with the classical models, it can be assumed that the total bulk pressure drop can be calculated using the K and C values from the discussion in section 4.5 and the following formula:

$$\Delta P_{BULK} = (\frac{\mu}{K} V + C\rho V^2) \cdot t \qquad (4.10)$$

and the total entrance contribution can be calculated using Equation 4.4. Figure 4.31 shows the relation between the absolute entrance contribution at different velocities and thicknesses for NCX1723 which is calculated using the above-mentioned approach. As shown here, the absolute entrance effect increases up to a thickness and after that decreases by increasing the thickness. But basically, the entrance effect is because the air molecules hit the foam surface before and while entering the foam and increasing the thickness cannot reduce the quantity of the molecules that hit the surface. Therefore, this approach, which leads to decreasing the entrance effect after a specific thickness, is not correct.

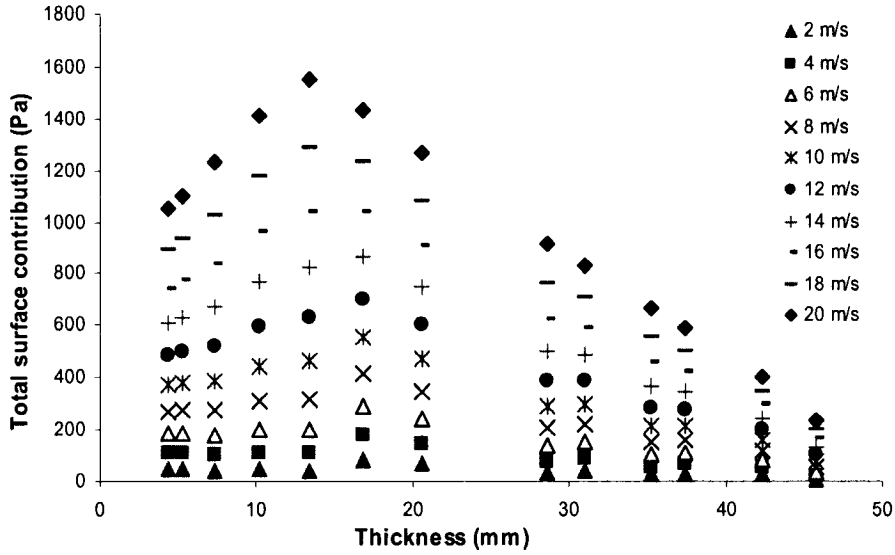

Figure 4.31: *Total entrance contribution based on the total bulk contribution calculated using Eq'n 4.10.*

By combining Equations 4.6 and 4.9, Equation 4.11 can be written as:

$$\Delta P_{TOTAL} = s(V,t,K)\cdot t + (\frac{\mu}{K}V + C\rho V^2)\cdot t \qquad (4.11)$$

But, the term $C\rho V^2$ in this equation is strongly related to the entrance contribution and can be combined with it. This means that the bulk contribution can be assumed merely related to the term $\frac{\mu}{K}V$ which results in Equation 4.12.

$$\Delta P_{TOTAL} = \Delta P_{SURFACE} + \frac{\mu}{K}\cdot V\cdot t \qquad (4.12)$$

It was also assumed that, the total entrance contribution reaches a constant value at a certain thickness and after that specific thickness, the absolute entrance contribution remains constant. To evaluate this assumption, the absolute entrance contribution at different thickness and velocity was calculated using Equation 4.12 and K value from section 4.5. Figure 4.32 shows the absolute entrance contribution for different thicknesses

and velocities for NCX1723. As shown in this figure, the total entrance contribution reaches a maximum limit and remains relatively constant. This is similar to an exponential model which rises to a maximum value. Therefore, the total entrance

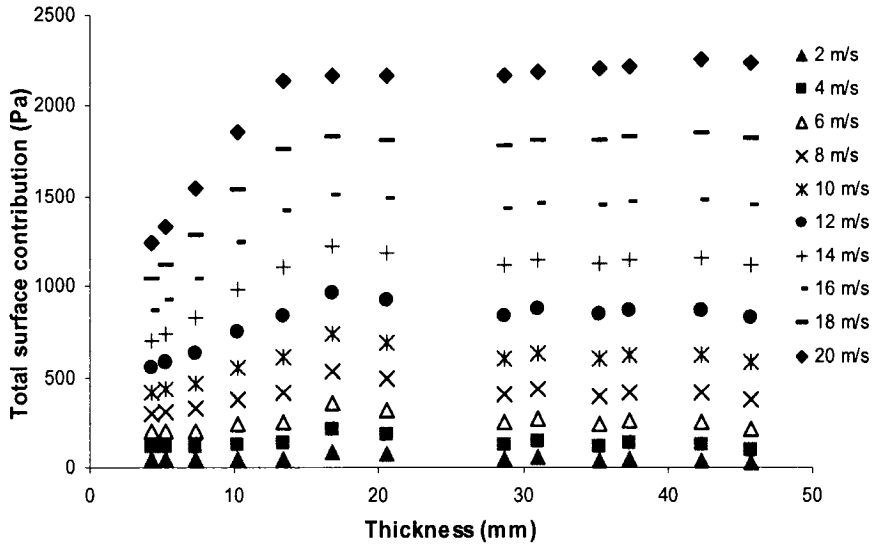

Figure 4.32: *Total entrance contribution based on Eq'n 5.12.*

contribution was modeled using nonlinear regression and the model presented in Equation 4.13, in which a and b are constant and are different for each grade.

$$S(t,K) = a \cdot (1 - b^{t}) \tag{4.13}$$

Equation 4.14 and Figure 4.33 show the results of this regression analysis for the absolute entrance contribution of different thicknesses for NCX1723 at 20 m/s. As

$$S = 2232(1 - 0.8354^{t}) \tag{4.14}$$

shown in this figure, the suggested model has good agreement with the experimental values. Based on these results, the total entrance contribution term as a function of t and V^2 can be modeled as:

$$S(V,t,K) = a \cdot (1 - b^t) \cdot V^2 \tag{4.15}$$

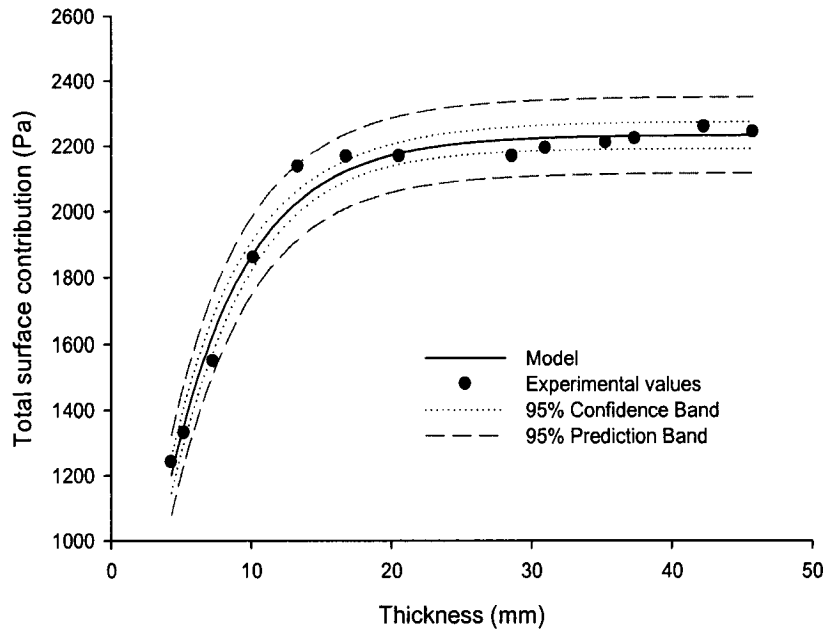

Figure 4.33: *Experimental and model values for NCX1723 at 20 m/s.*

Having observed this, a general equation that includes thickness as well as the flow velocity will be presented. Equation 4.16 and Figure 4.34 show the results of nonlinear regression analysis for the absolute entrance contribution for NCX1723 at different thicknesses and velocities. It should be mentioned that the suggested model has an acceptable coefficient of determination (R^2) of 99%.

$$S(V,t) = 5.8485(1 - 0.8327^t)V^2 \tag{4.16}$$

Similar analyses were performed for other grades and the results are summarized in Table 4.4. This model is an initial approach toward modeling the entrance effect contribution in metallic foams and is in good agreement with the experimental data at high velocities.

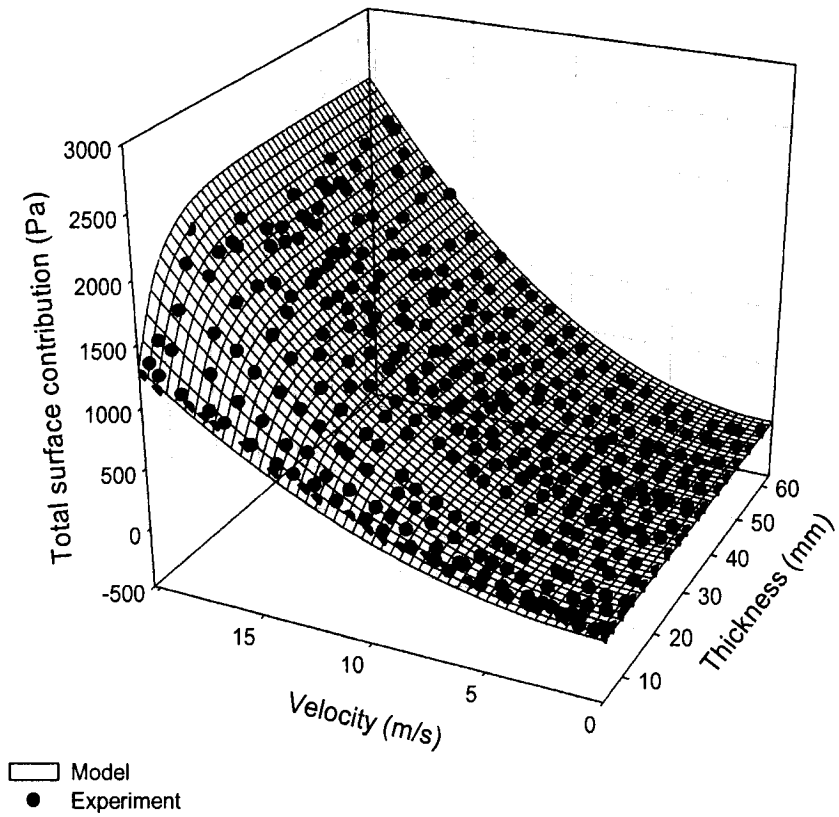

Figure 4.34: *Experimental values and model surface for NCX1723.*

Table 4.4: *Calculated model parameters for all grades of Recemat foams.*

d (mm)	a	b	R^2 (%)
0.4	12.7156	0.6618	98
0.6	10.9132	0.8636	94
0.9	5.8485	0.8327	99
1.4	4.2101	0.8286	98

4.9. Heterogeneity Detection Tests

Based on the results of previous discussions regarding the entrance and bulk pressure drop effects, several tests were performed in order to detect the thickness, location, and structure of the heterogeneity of porous media. As was previously shown in Figures 4.8

and 4.9, if the porous material has different structures at different sides, this kind and location of heterogeneity can be detected by testing the sample in different positions by switching the surface facing the flow. Comparing the results of the two tests, information regarding the structure of the facing surface relative to the bulk material can be obtained.

Detecting internal heterogeneity in terms of different pore size was attempted in this work. If the internal heterogeneity is due to the existence of pores that are smaller than the average pore size, it is obvious that this increases the pressure drop and in this case the thicker the heterogeneity the higher the pressure drop. Figure 4.35 shows the effect of heterogeneity with smaller pores on the total pressure drop. As shown in this figure, a thin 5 mm heterogeneity causes an increase of about 500 Pa at 20 m/s, which is about 13% of the total pressure drop at this velocity.

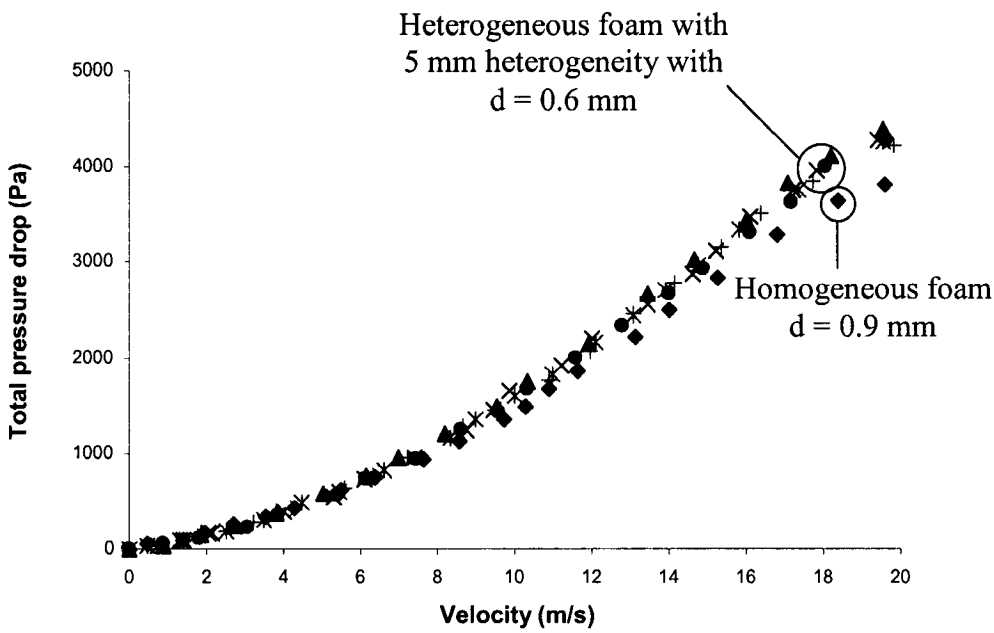

Figure 4.35: *Effect of heterogeneity with smaller pore size inside the foam on the total pressure drop of the porous media.*

Detecting the heterogeneity when bigger pores than the average pore diameter exist inside the foam is more complicated. As shown in Figure 4.36, the results of pressure drop tests, when this kind of heterogeneity is located inside the foam, is not distinguishable from the results of testing the homogeneous material. Because of the fact that, in this situation, each pore of heterogeneous material is open to more than one pore of bulk material, as shown in Figure 4.37 there is another entrance effect at the contact between the heterogeneity and bulk material. This additional pressure drop can compensate for the reduction in pressure drop due to the heterogeneity of bigger pore size, and even increases the total pressure drop of the heterogeneous material. On the other hand, if the heterogeneity is located at the end of the foam, as shown in Figure 4.36, there is no second entrance effect and the pressure drop decreases (triangles in Figure 4.36).

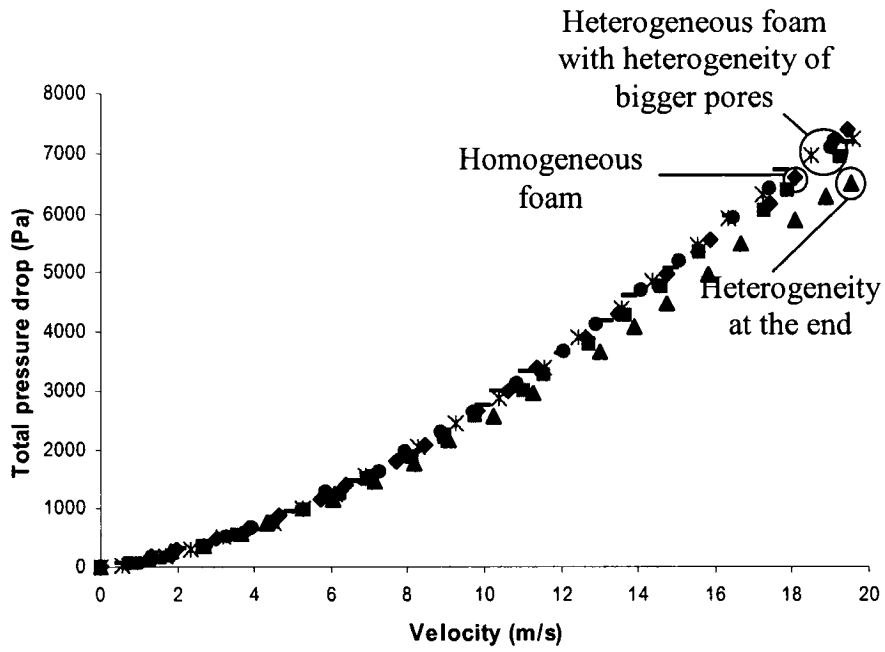

Figure 4.36: *Effect of heterogeneity with bigger pore size inside the foam on the total pressure drop of the porous media.*

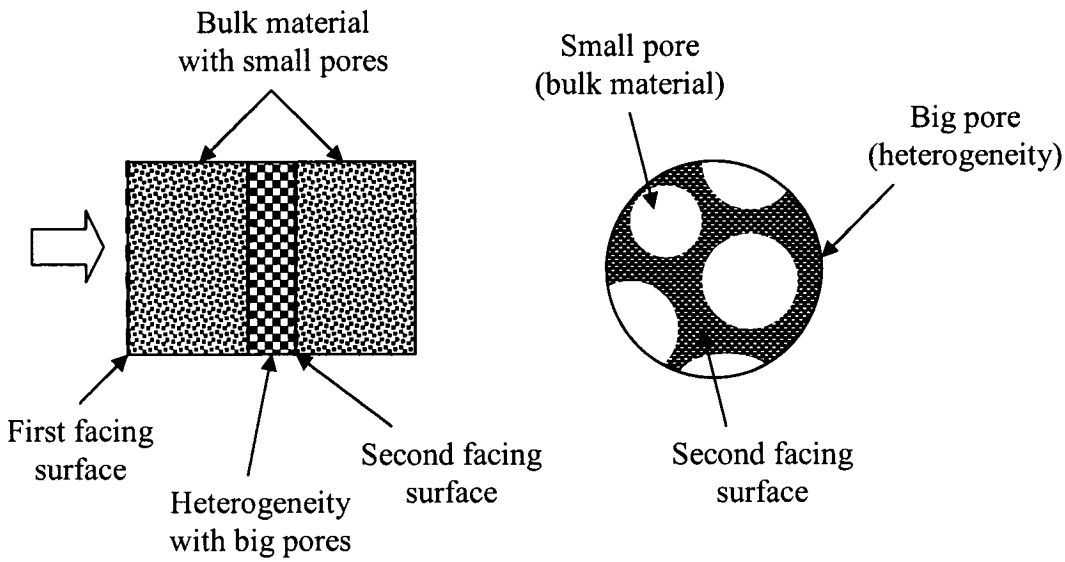

Figure 4.37: *Second facing surface demonstration.*

Several tests were performed in order to detect the thickness and location of heterogeneity inside the foams. As shown in Figure 4.38, increasing the heterogeneity thickness affects the total pressure drop slightly.

Detecting the location of heterogeneity was attempted in another set of experiments. The heterogeneity was placed inside the foam at different locations and found that there was no difference in the total pressure drop. So, this method cannot be used to detect the heterogeneity locations inside the foam. The results of this test are shown in Figure 4.39.

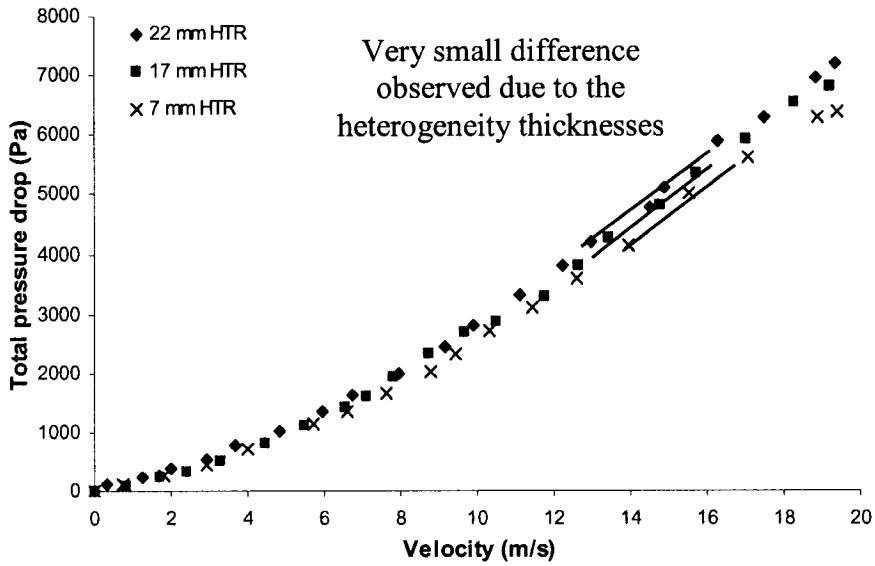

Figure 4.38: *Test results of foams having different heterogeneity thicknesses.*

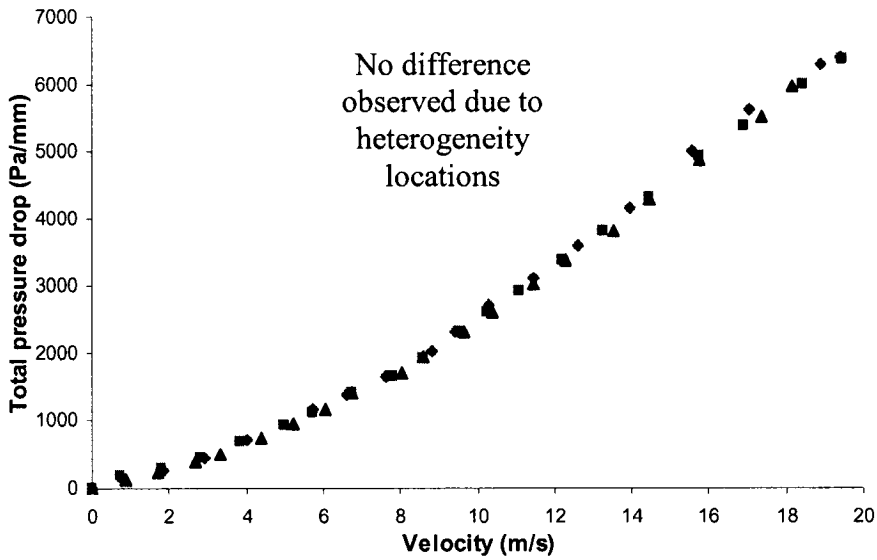

Figure 4.39: *Test results of foams having different heterogeneity locations.*

CHAPTER 5: SUMMARY AND CONCLUSIONS, CONTRIBUTIONS, AND RECOMMENDATIONS FOR FUTURE WORKS

5.1. Summary and Conclusions

Metallic foams are one of the recent developments in material science which are known for their special physical and mechanical properties, such as high stiffness in conjunction with very low specific weight or high gas permeability combined with high thermal conductivity. These properties make metallic foams to have diverse industrial applications such as light weight structures, filters, energy absorptions, and even medical applications.

Pressure drop of flow through metallic foams is an important parameter and should be evaluated and optimized. Pressure drop can be calculated knowing the permeability, the dimensions and geometry of the porous media, as well as the viscosity, flow rate and density of the fluid. Microstructure of the metallic foams which is characterized by parameters such as morphology of the ligaments that form the network of pores, pore size, pore shape and porosity make them difficult to model. Different analytical models have been suggested; however, these models are not in agreement with each others and that is why most of the studies have been directed towards the experimental measurements.

The test equipment had been built based on the experimental set-up of Paek *et al.* [78] and ISO4022-1987-10-01 standards. 46 nickel-chromium open cell Recemat metallic

foams from different grades having pore size of 0.4 to 2.3 mm, thickness of less than 2 to 63 mm, and porosities of about 83% to 91% were tested. Recemat foams are relatively homogeneous foams made through metallization of polyurethane foam by electro deposition technique.

Although classical models show that the pressure drop normalized by the medium thickness for a constant material depends only on the fluid velocity, our experiments show that for a given velocity, the normalized pressure drop reduces with increasing the thickness. Actually, this can result in different permeability coefficients for different thicknesses of the same material.

Several experiments were performed in order to study the effect of thickness on the pressure drop of metallic foams and observed that the foam facing surface, which the fluid encounters before entering the foam, affects the pressure drop of the porous media. It was also found that the total pressure drop can be divided into two components; entrance and bulk pressure drops. The bulk contribution can be normalized by the thickness, however, the entrance contribution effect cannot.

Entrance effect contributes more to the foam pressure drop at higher velocities and thinner foams, and after a critical thickness, bulk effect dominates the pressure drop. The critical thickness depends on the foam microstructure and increases by increasing the foam pore size. Experiments proved that, the entrance effect not only depends on the foam microstructure and its permeability, but also on the foam thickness and the fluid velocity. It showed that, increasing the material pore diameter at the facing surface decreases the entrance effect contribution. Increasing the fluid velocity furthermore was observed to increase the entrance effect contribution. And finally foam thickness was also

noticed to affect the entrance effect contribution and found that increasing the foam thickness, decreases the foam unit entrance effect. Based on these observations, it is suggested that Hazen-Dupuit-Darcy equation be modified to become responsible for the pressure drop caused at the foam entrance.

As stated before, increasing the thickness decreases the foam unit pressure drop. This results in the unit pressure drop curves for the foams of same grade approaching a unique curve at thicknesses higher than the critical thickness. This curve represents the unit pressure drop through a foam with no entrance effect or with unlimited thickness. In this case the pressure drop is mainly due to the bulk effect. This unique curve can be calculated based on the relations between the permeability constants and thickness for same grade foams having different thicknesses (i.e. the values that correspond to constants K and C versus thickness are used to calculate this curve).

Considering the entrance effect on the foam pressure drop, tests were performed on designed composite foams to explore the possibility of detecting the heterogeneity in the foam. The results showed that if the microstructure of a foam is dissimilar at different sides of the foam, this can be easily detected due to different entrance contribution to pressure drop. If the heterogeneity inside the foam is of smaller pore, its thickness can be detected, because the thicker heterogeneities contribute more to the total pressure drop. But if the heterogeneity is of bigger pores, due to the additional pressure drop caused by internal entrance effect, the thickness of this kind of heterogeneities cannot be distinguished. Tests on different composite foams having exactly the same heterogeneity at different locations inside the foams resulted in the same pressure drop curves.

Therefore, it is not possible to find the location of this kind of heterogeneities inside the foam using this technique.

5.2. Contributions

- Large range of homogeneous metallic foams from different grades and thicknesses were gathered. This collection along with the testing set-up which had already been developed provides a very good opportunity to study the air flow behavior through metallic foams.
- The entrance effect contribution to pressure drop of metallic foams was observed, demonstrated, analyzed and modeled in this work.
- Also a preliminary study to more rigorous non-destructive tests to find the heterogeneity of porous materials was performed and resulted in proposing the basic concepts of locating the side and some types of internal heterogeneities.

5.3. Recommendations for Future Work

The present work was performed on 46 different samples with different pore diameters and thicknesses. Although these samples provide a good opportunity to study the metallic foams, but not all the ranges are complete and tests cannot be done on high thicknesses of those grades. It is recommended to complete the sample sets for all the grades such as 0.5 and 2.3 mm and compare the results with the other grades. This will enable the validation of the results of this work for metallic foams with broader range of pore diameters.

Tests are suggested to be performed on higher thicknesses of metallic foams in order to check and modify the stated hypothesis and model.

It is also recommended to modify the experimental set-up to be capable of testing the foams with different sample diameters to study the lateral flow effect on the pressure drop of metallic foams.

Experimental techniques should be designed in order to determine the effect of internal surface to resolve the problem for inside heterogeneities with bigger pores, and also to locate more complex heterogeneities, i.e. mixed heterogeneities.

As well as the experimental investigations, it is suggested to use Computational Fluid Dynamics (CFD) techniques to model and study the flow behavior in light of the current experimental results.

In addition, it is highly recommended to perform the tests on different metallic foams, or in general, preferably, other homogeneous porous materials to validate the stated assumptions and findings.

REFERENCES

1. L.J. Gibson and M.F. Ashby: *Cellular Solids, Structure and Properties*, Pergamon Press Inc., New York, 1988, p. 1.
2. J. Banhart: Manufacturing routes for metallic foams, *Journal of Materials*, Vol. 52, No. 12, 2000, pp. 22-27.
3. J. Banhart: Foam Metal: The Recipe, *Europhysics News*, Vol. 30, No. 1, 1999, pp. 17-20.
4. National Industrial Research Institute of Nagoya (NIRIN) website, *http://www.nirin.go.jp*, as in Nov. 2005.
5. V. Gergely, H.P. Degischer and T.W. Clyne: Recycling of MMCs and production of metallic foams. In: Clyne TW, editor. *Comprehensive composite materials, Vol. 3: metal matrix composite*, Elsevier, Amsterdam, 2000, pp. 797–820.
6. The Metal Powder Industries Federation (MPIF) website, *http://www.mpif.org*, as in Nov. 2005.
7. D. Bellmann, H. Clements and J. Banhart: USANS investigation of early stages of metal foam formation, *Applied Physics A: Materials Science & Processing*, Vol. 74, Supplement 1, 2002, pp. 1136-1138.
8. J. Banhart, D. Bellmann and H. Clements: Investigation of metal foam formation microscopy and ultra small-angle neutron scattering, *Fraunhofer-Institute for Advanced Materials*, Vol. 49, No. 17, 2001, pp. 3409-3420.
9. H.N.G. Wadley: Cellular metals manufacturing, *Advanced Engineering Materials*, Vol. 4, No. 10, 2002, pp. 726-733.
10. C.Y. Yu, H.H. Eifert, J. Banhart and J. Baumeister: Metal foaming by a powder metallurgy method: production, properties and applications, *Materials Research Innovations*, Vol. 2, No. 3, 1998, pp. 181-188.
11. M.F. Ashby, A. Evans, N.A. Fleck, L.J. Gibson and H.N.G Wadley: *Metal Foams A Design Guide,* Butterworth-Heinemann, Boston, 2000.
12. J. Banhart: Manufacture, characterization and application of cellular metals and metal foams, *Progress in Materials Science*, Vol. 46, No. 6, 2001, pp. 559–632.
13. H. Sang, L.D. Kenny, I. Jin: Blowing process and apparatus for manufacture of shaped slabs from particle-stabilized foamed metal, International Patent WO 9221457, 10 Dec. 1992.
14. L.D. Kenny: Mechanical properties of particle stabilized aluminum foam, *Materials Science Forum*, Vol. 217-222, No. 3, 1996, pp. 1883-1890.
15. J.T. Wood: Production and applications of continuously cast, foamed aluminum, *Proceedings of the Symposium on Metal Foams*, Stanton, Delaware, Oct. 1997, editors: J. Banhart and H. Eifert, MIT Press–Verlag, Bremen, 1998, pp. 31-35.

16. S. Kleinheyer and G. Bilz: Method and apparatus for preparation of parts from metal foam in molds by using two interconnected vessels, German Patent 4326982, 9 Feb. 1995.

17. M. Linke, W. Jungk and E. Fisher: Method and apparatus for producing metallic foams, European Patent Application 544291, 26 Nov. 1992.

18. A.E. Simone and L.J. Gibson: Aluminum foams produced by liquid-state processes, *Acta Materialia*, Vol. 46, No. 9, 1998, pp. 3109-3125.

19. T. Miyoshi, M. Itoh, S. Akiyama and A. Kitahara: Aluminum foam, Alporas: the production process, properties and applications, *Proceedings of the Symposium on Porous and Cellular Materials for Structural Applications*, Vol. 521, editors: D.S. Schwartz, D.S. Shih, A.G. Evans and H.N.G. Wadley, MRS, San Francisco, California, 1998, pp. 133-137.

20. E. Andrews, J. Huang and L. Gibson: Creep behavior of a closed-cell aluminum foam, *Acta Materialia*, Vol. 47, No. 10, 1999, pp. 2927-2935.

21. Y. Yamada, K. Shimojima, Y. Sakaguchi, M. Mabuchi, M. Nakamura, T. Asahina, T. Mukai, H. Kanahashi and K. Higashi: Processing of cellular magnesium materials, *Advanced Engineering Materials*, Vol. 2, No. 4, 2000, pp.184-187.

22. A.G. Evans, J.W. Hutchinson, N.A. Fleck, M.F. Ashby and H.N.G. Wadley: The topological design of multifunctional cellular metals, *Progress in Materials Science*, Vol. 46, Issue 3&4, 2001, pp. 309-327.

23. P. Neumann: Porous metal structures made by sintering: processes and applications, *MetFoam 99: International Conference on Metal Foams and Porous Metal Structures*, Bremen, Germany, June 1999, editors: J. Banhart, M.F. Ashby and N.A. Fleck, MIT Press–Verlag, Bremen, 1999, pp. 167-170.

24. Y. Zhao and D. Sun: A novel sintering-dissolution process for manufacturing Al foams, *Scripta Materialia*, Vol. 44, No. 1, 2001, pp. 105-110.

25. M. Bram, C. Stiller, H.P. Buchkremer, D. Stöver and H. Baur: High-porosity titanium, stainless steel, and superalloy parts, *Advanced Engineering Materials*, Vol. 2, No. 4, 2000, pp. 196-199.

26. M. Gauthier, L. Lefebvre, Y. Thomas and M. Bureau: Production of metallic foams having open porosity using a powder metallurgy approach, *Material and Manufacturing Processes*, Vol. 19, No. 5, 2004, pp. 793-811.

27. L.P. Lefebvre, M. Gauthier, M.N. Bureau, M. LeRoux, R. Panneton and D. Pilon: Properties of nickel foams having different pore size distributions and densities, *MetFoam2003 conference*, June 2003.

28. B. Bernard, D. Doniat: Porous metallized structures and their applications, European Patent Application 151064, 18 Jan. 1985.

29. X. Badiche, S. Forest, T. Guibert, Y. Bienvenu, J.D. Bartout, P. Ienny, M. Croset and H. Bernet: Mechanical properties and non-homogeneous deformation of open-cell nickel foams: Application of the mechanics of cellular solids and of porous materials, *Materials Science and Engineering, A*, Vol. 289, Issue 1&2, 2000, pp. 276-288.

30. Product data sheet of ''Celmet'', Sumitomo Electric, Japan., 1986.

31. Recemat International website, *http://www.recemat.com*, as in April 2007.

32. M. Weber, J. Banhart, J. Baumeister: *Ullmann's Encyclopedia of Industrial Chemistry*, Sixth Edition, 2000 Electronic Release, Metallic Foams.

33. The Shelly Family website, *http://www.shelleys.demon.co.uk*, as in Nov. 2005.

34. Fraunhofer Institute Fertigungstechnik Materialforschung website, *http://www.ifam.fhg.de,* as in Nov. 2005.

35. A. Bhattacharya, R.L. Mahajan: Metal foam and finned metal foam heat sinks for electronics cooling in Buoyancy-Induced convection, *Journal of Electronic Packaging*, Vol. 128, Issue 3, 2006, pp. 259-266.

36. A. Bhattacharya, R.L. Mahajan: Finned metal foam heat sinks for electronics cooling in forced convection, *Journal of Electronic Packaging*, Vol. 124, Issue 3, 2002, pp. 155-163.

37. L. Mathieu, T. Mueller, P. Bourban, D. Pioletti, R. Müller and J. Manson: Architecture and properties of anisotropic polymer composite scaffolds for bone tissue engineering, *Biomaterials*, Vol. 27, No. 6, 2006, pp. 905-916.

38. Industrial Materials Institute of National Research Council of Canada website, *http://www.imi.cnrc-nrc.gc.ca*, as in Nov. 2005.

39. T. Miyoshi, M. Itoh, S. Akiyama and A. Kitahara: Alporas aluminum foam: production process, properties, and applications, *Advanced Engineering Materials*, Vol. 2, No. 4, 2000, pp. 179-183.

40. V. Loya: The effect of microstructure on the permeability of metal foams. M.A.Sc. thesis, Concordia University, Montreal, Canada, 2005.

41. J. Zhou, C. Mercer and W.O. Soboyejo: An investigation of the microstructure and strength of open-cell 6101 aluminum foams, *Metallurgical and Materials Transactions, A: Physical Metallurgy and Materials Science*, Vol. 33A, Issue 5, 2002, pp. 1413-1427.

42. J. Banhart, H. Stanzick, L. Helfen and T. Baumbach: Metal foam evolution studied by synchrotron radioscopy, *Applied Physics letters*, Vol. 78, No. 8, 2001, pp. 1152-1154.

43. J. Burzer, T. Bernard, H.W. Bergmann and O. Damm: Modeling of the mechanical properties of metallic foams based on X-ray analysis, *MetFoam 99: International Conference on Metal Foams and Porous Metal Structures*, Bremen, Germany, June 1999, editors: J. Banhart, M.F. Ashby and N.A. Fleck, MIT Press–Verlag, Bremen, 1999, pp. 277-282.

44. A.C Spowage, A.P Shacklock, A.A. Malcolm, S.L May, L. Tong and A.R. Kennedy: Development of characterization methodologies for macroporous materials, *Journal of Porous Materials*, Vol. 13, Issues 3&4, 2006, pp. 431-438.

45. Katholieke Universiteit Leuven website, *http://www.kuleuven.ac.be*, as in May 2007.

46. A. Sassov, E. Cornelis and D. Van Dyck: Non destructive 3-D investigation of metal foam microstructure, *Materialwissenschaft und Werkstofftechnik*, Vol. 31, No. 6, 2000, pp. 571-573.

47. E. Cornelis, A. Kottar, A. Sassov, D. Van Dyck: Desktop X-ray microtomography for studies of metal foams, *MetFoam 99: International Conference on Metal Foams and Porous Metal Structures*, Bremen, Germany, June 1999, editors: J. Banhart, M.F. Ashby and N.A. Fleck, MIT Press–Verlag, Bremen, 1999, pp. 233–234.

48. A. Sassov, E. Cornelis and D.V. Dyck: Nondestructive 3-D investigation of metal foam microstructure, *Materialwissenschaft und Werkstofftechnik*, Vol. 31, Issue 6, 2000, pp. 571-573.

49. D. Wildenschild, J.W. Hopmans, C.M.P. Vaz, M.L. Rivers, D. Rikard and B.S.B. Christensen: Using Xray computed tomography in hydrology: systems, resolutions, and limitations, *Journal of Hydrology*, Vol. 267, Issues 3&4, 2002, pp. 285-297.

50. B. Kriszt, B. Foroughi, A. Kottar, H.P. Degischer: Mechanical behavior of aluminum foam under uniaxial compression, *Materials Science and Technology*, Vol. 16, Issues 7&8, 2000, pp. 792-796.

51. Y. Nakashima and Y. Watanabe: Estimate of transport properties of porous media by microfocus X-ray computed tomography and random walk simulation, *Water Resources Research*, Vol. 38, No. 12, 2002, pp. 1272-1284.

52. P. Khayargoli, V. Loya, L.P. Lefebvre and M. Medraj: The impact of microstructure on the permeability of metal foams, *Proceedings of CSME Forum*, London, Canada, 2004, pp. 220-228.

53. A. Hazen: Some physical properties of sand and gravels with special reference to their use in filtration, *Massachusetts State Board of Health, Twenty-fourth Annual Report*, 1893, pp. 541.

54. J.L. Lage: The fundamental theory of flow through permeable media from Darcy to turbulence, in: *Transport Phenomena in Porous Media*, editor: B. D. Ingham and I. Pop, 1998, pp. 1-30.

55. D. Nield and A. Bejan: *Convection in Porous Media*, Springer, New York, 1999.

56. P.A. Davis, N.E. Olague: Application of a validation strategy to Darcy's experiment, *Advances in Water Resources*, Vol. 15, Issue 3, 1992, pp.175-180.

57. J.L Lage and B.V. Antohe: Darcy's experiments and the deviation to nonlinear flow regime, *Journal of Fluids Engineering*, Vol. 122, No. 3, 2000, pp. 619-625.

58. F. Cajori, Revised translation of "I. Newton, *Philosophiae Naturalis Principia Mathematica* by A. Motte", University of California Press, Berkeley, 1934.

59. J.L. Lage and P.S. Krueger: Protocol for measuring permeability and form coefficient of porous media, *Physics of Fluids*, Vol. 17, Issue 8, 2005, pp. 088101-088101-4.

60. S. Sorek, J. Bear, G. Ben-Dor and G. Mazor: Shock waves in saturated thermoelastic porous media, *Transport in Porous Media*, Vol. 9, No. 1&2, 1992, pp. 3-13.

61. J.C Ward: Turbulent flow in porous media, *Journal of Hydraulics, Division of ASCE*, Vol. 90, part HY5, 1964, pp. 1–12.

62. B.V. Antohe, J.L. Lage, D.C. Price and R.M. Weber: Experimental determination of permeability and inertia coefficients of mechanically compressed aluminum porous matrices, *Journal of Fluids Engineering*, Vol. 119, Issue 2, 1997, pp. 405-412.

63. G.S. Beavers and E.M. Sparrow: Compressible gas flow through a porous material, *International Journal of Heat and Mass Transfer*, Vol. 14, Issue 11, 1971, pp. 1855-1859.

64. R.M. Fand, B.Y.K Kim, A.C.C Lam and R.T. Phan: Resistance to the flow of fluids through simple and complex porous media whose matrixes are composed of randomly packed spheres, *Journal of Fluids Engineering*, Vol. 109, No. 3, 1987, pp. 268-74.

65. M. Firdaouss, J.L. Guermond, and P.L. Que´re´: Nonlinear corrections to Darcy's law at low Reynolds numbers, 1997, *Journal of Fluid Mechanics*, Vol. 343, pp. 331–350.

66. J.P.D. Plessis, A. Montillet, J. Comiti and J. Legrand: Pressure drop prediction for flow through high porosity metallic foams, *Chemical Engineering Science*, Vol. 49, No. 21, 1994, pp. 3545-3553.

67. A. Bhattacharya, V.V. Calmidi and R.L. Mahajan: Permeability and inertial coefficient of high porosity metal foams, *Proceedings of the 2001 National Heat Transfer Conference,* 2001, Ananheim, CA, pp. 1287-1298.

68. J.G. Fourie and J.P. Du Plessis: Effective and coupled thermal conductivities of isotropic open-cellular foams, *American Institute of Chemical Engineers (AIChE) Journal*, Vol. 50, No. 3 , 2004, pp. 547-556.

69. P.C. Huang and K. Vafai: Flow and heat transfer control over an external surface using a porous block array arrangement, *International Journal of Heat and Mass Transfer,* Vol. 36, No. 16 , 1993, pp. 4019-4032.

70. S.Y. Kim, J.W. Paek and B.H. Kang: Flow and heat transfer correlations for porous-fin heat exchangers, *Journal of Heat Transfer*, Vol. 122, No. 3, 2000, pp. 572-578.

71. A.F. Bastwros: Effectiveness of open cell metallic foams for high power electronic cooling, *Presented at the Symposium on the Thermal Management of Electronics, IMECE*, Anaheim, CA.1998, pp. 211-217.

72. L.W. Zhang, S. Balachandar, D.K. Tafti and F.M. Najjar: Heat transfer enhancement mechanisms in inline and staggered parallel-plate fin heat exchangers, *International Journal of Heat and Mass Transfer*, Vol. 40, Issue 10, 1997, pp. 2307-2325.

73. B.M. Liu, R.C. Xin and W.Q. Tao: Experimental and numerical investigations on flow resistance in porous medium composed of randomly packed spheres, *Transport Phenomena in Thermal Engineering 1*, Xi'an, China, editors: J.S. Lee, S.H. Chung, and K.Y. Kim, Begell House, New York, 1993, pp. 231-236.

74. J.J. Hwang, G.J. Hwang, R.H. Yeh and C.H. Chao: Measurements of interstitial convective heat transfer and frictional drag for flow across metal foams, *ASME Journal of Heat Transfer*, Vol. 124, No. 1, 2002, pp. 120-129.

75. M. Kaviany: *Principles of Heat Transfer in Porous Media,* Second edition, Springer-Verlag, New York, 1995, pp. 18-51.

76. J.L. Lage, B.V. Antohe and D.A. Nield: Two types of nonlinear pressure-drop versus flow-rate relation observed for saturated porous media, *ASME Journal of Fluids Engineering*, Vol. 119, No. 3, 1997, pp. 700-706.

77. D. Seguin, A. Montillet, J. Comiti and F. Huet: Experimental characterization of flow regimes in various porous media—II: Transition to turbulent regime, *Chemical Engineering Science*, Vol. 53, No. 22, 1998, pp. 3897-3909.

78. J.W. Paek, B.H. Kang, S.Y. Kim and J.M. Hyun: Effective thermal conductivity and permeability of aluminum foam materials, *International Journal of Thermophysics*, Vol. 21, No. 2, 2000, pp. 453-464.

79. K. Boomsma and D. Poulikakos: The effects of compression and pore size variations on the liquid flow characteristics in metal foams, *ASME Journal of Fluids Engineering*, Vol. 124, No. 1, 2002, pp.263-272.

80. A. Bhattacharya, V.V. Calmidi and R.L. Mahajan: Thermophysical properties of high porosity metal foams, *International Journal of Heat and Mass Transfer*, Vol. 45, No. 5 , 2002, pp. 1017-1031.

81. S. Crosnier, R. Riva, B. Bador and V. Blet: Modeling of gas flow through metallic foams, *First European Hydrogen Energy Conference*, Alpexpo-Alpes Congrés, Grenobel, France, 2003.

82. L. Tadrist, M. Miscevic, O. Rahli and F. Topin: About the use of fibrous materials in compact heat exchangers, *Experimental Thermal and Fluid Science,* Vol. 28, No. 2&3 , 2004, pp. 193-199.

83. L. Wilson, A. Narasimhan and S.P. Venkateshan: Permeability and form coefficient measurement of porous inserts with non-darcy model using non-plug flow experiments, *ASME Journal of Fluids Engineering*, Vol. 128, Issue 3, 2006, pp. 638-642.

84. E. A. Moreira, M. D. M. Innocentini and J. R. Coury: Permeability of ceramic foams to compressible and incompressible flow, *Journal of the European Ceramic Society*, Vol. 24, Issues 10&11, 2004, pp. 3209-3218.

85. K. Boomsma, D. Poulikakos, Y. Ventikos: Simulations of flow through open cell metal foams using an idealized periodic cell structure, *International Journal of Heat and Fluid Flow*, Vol. 24, No. 6, 2003, pp. 825-834.

86. M.D.M. Innocentini, V.R. Salvini, A. Masedo and V.C. Pandolfelli: Prediction of ceramic foams permeability using Ergun's equation, *Material Research*, Vol. 2, No. 4, 1999, pp. 283-289.

APPENDIX A

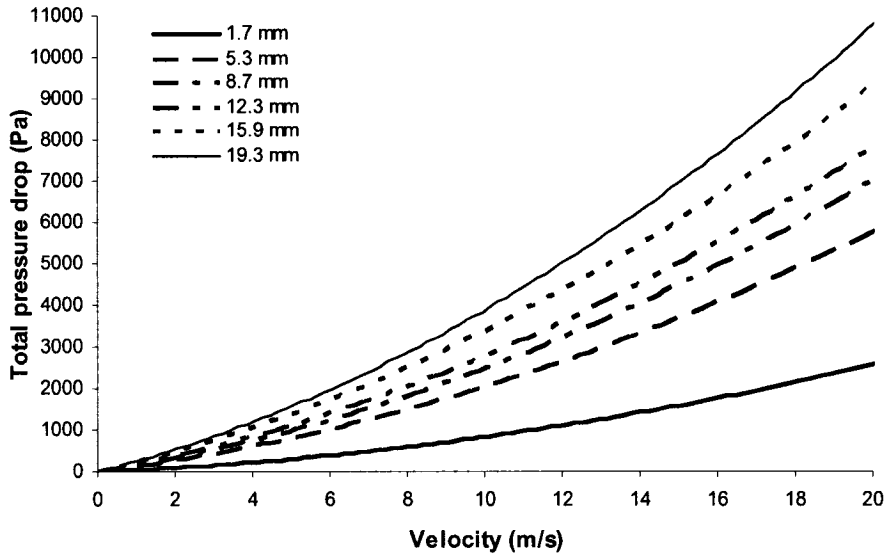

Figure A-1: Total pressure drop for NC 4753 (d=0.4mm).

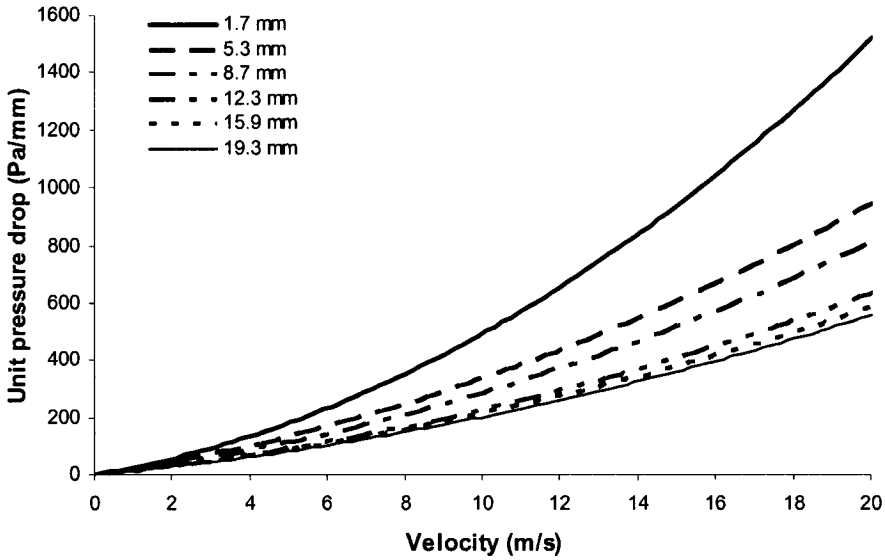

Figure A-2: Unit pressure drop for NC 4753 (d=0.4mm).

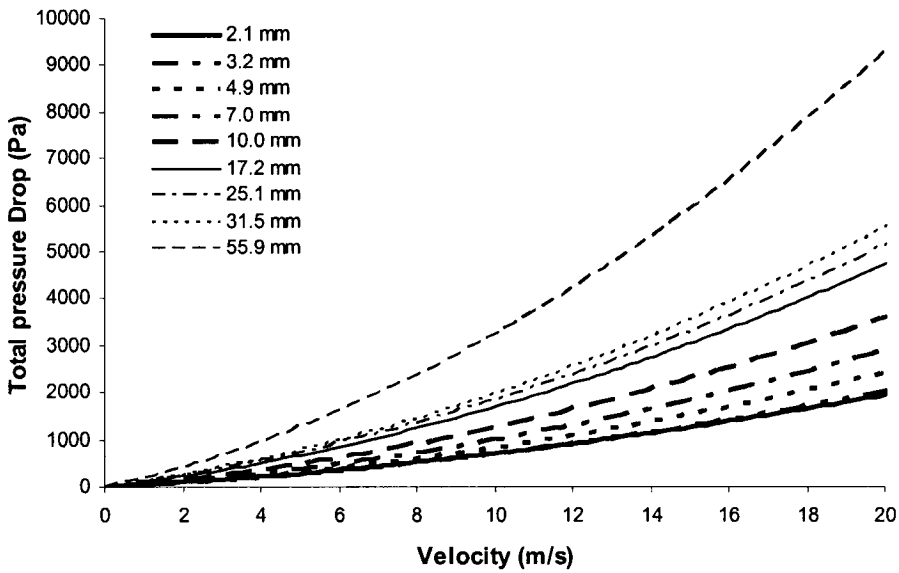

Figure A-3: Total pressure drop for NC 2733 (d=0.6mm).

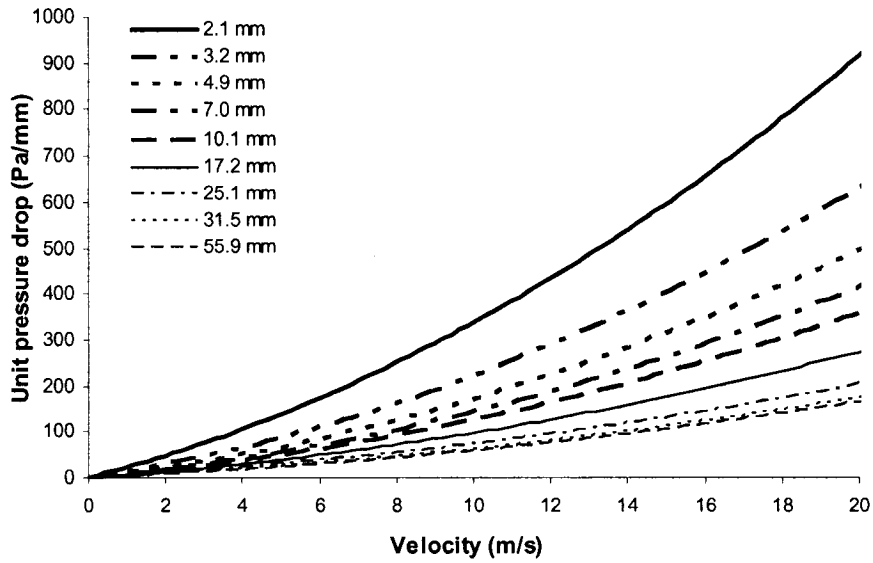

Figure A-4: Unit pressure drop for NC 2733 (d=0.6mm).

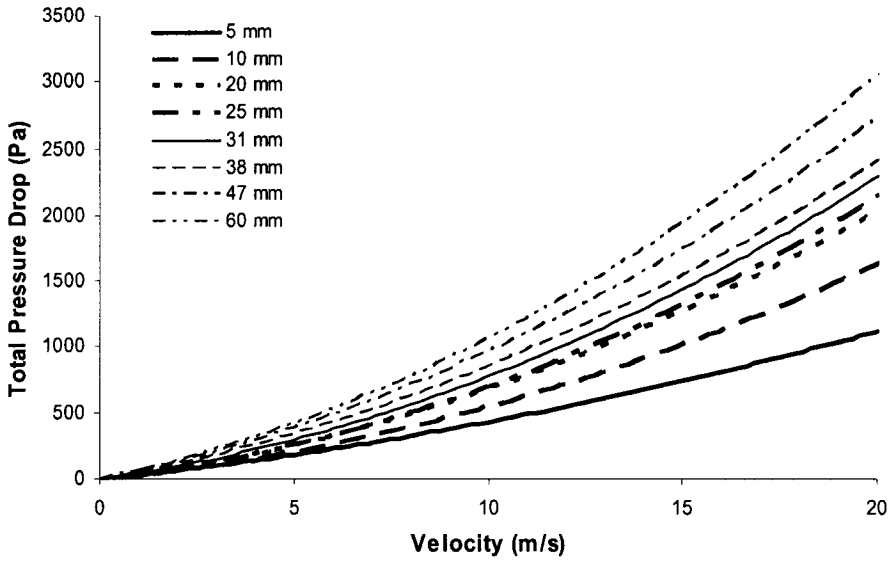

Figure A-5: Total pressure drop for NC 1116 (d=1.4mm).

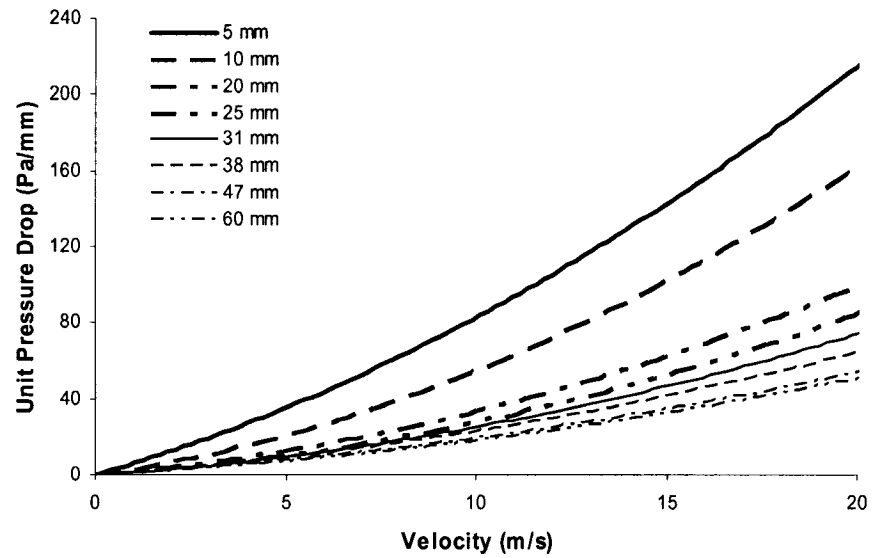

Figure A-6: Unit pressure drop for NC 1116 (d=1.4mm).